5-2013

METAMORPHISM, KINEMATIC EVOLUTION, AND TIMING CONSTRAINTS OF THE GREENBRIER FAULT AROUND THE ELA AND BRYSON CITY DOMES, NORTH CAROLINA

Remington M. Leger
University of Tennessee - Knoxville, rleger@utk.edu

To the Graduate Council:

I am submitting herewith a thesis written by Remington M. Leger entitled "METAMORPHISM, KINEMATIC EVOLUTION, AND TIMING CONSTRAINTS OF THE GREENBRIER FAULT AROUND THE ELA AND BRYSON CITY DOMES, NORTH CAROLINA." I have examined the final electronic copy of this thesis for form and content and recommend that it be accepted in partial fulfillment of the requirements for the degree of Master of Science, with a major in Geology.

Micah J. Jessup, Major Professor

We have read this thesis and recommend its acceptance:

Robert D. Hatcher, Jr., Theodore C. Labotka

Accepted for the Council:
Dixie L. Thompson

Vice Provost and Dean of the Graduate School

(Original signatures are on file with official student records.)

METAMORPHISM, KINEMATIC EVOLUTION, AND TIMING CONSTRAINTS OF THE GREENBRIER FAULT AROUND THE ELA AND BRYSON CITY DOMES, NORTH CAROLINA

A Thesis presented for the
Master of Science
Degree
The University of Tennessee, Knoxville

Remington M. Leger
May 2013

ACKNOWLEDGMENTS

First and foremost, I thank my family for their support throughout my educational career. My advisor, Dr. Micah Jessup, was a great mentor and provided funding to conduct my research. He helped to shape my mind and my project into this successful work. I acknowledge my committee members, Dr. Robert D. Hatcher, Jr., and Dr. Theodore Labotka, whose expertise and guidance helped strengthen this thesis. Donnie Hicks, Jackie Langille, Tim Diedesch, and Kyle White assisted with field work and numerous edits of my thesis. Finally, my fellow graduate students helped me progress through my graduate career.

ABSTRACT

Field mapping, microstructural analysis, and electron microprobe analysis were performed on rocks from the Bryson City and Ela domes, North Carolina, to help constrain the tectonic history of the region. The domes are *en echelon* northeast-trending antiformal structures formed by two perpendicular sets of folds. They are bounded by the Greenbrier fault, which forms a ductile shear zone that juxtaposes the Great Smoky Group in the hanging wall with Grenville basement in the footwall. Isoclinal folds (F2) and axial planar foliation (S2) characterize the regional deformation (D2). Inter- to syn-kinematic porphyroblasts (relative to D2) of kyanite, staurolite, and garnet grew during Taconic Barrovian metamorphism (M2). Compositional maps of garnet yield Ca and Mn zoning patterns that are consistent with multiple stages of garnet growth. Pressure-temperature estimates, calculated using THERMOCALC v3.33, indicate that the Great Smoky Group reached conditions of 667 degrees Celsius and 9.2 kbar. A high-strain mylonite zone (S2b) near the contact between the Great Smoky Group and the Greenville basement is parallel to the regional foliation (S2). Mineral stretching lineations trend northeast-southwest around the margins of both domes. Rotated porphyroblasts indicate that shear zone formation (S2b) post-dated Barrovian metamorphism. Quartz deformation mechanisms record shearing (D2) of the Greenbrier fault at 500-600 degrees Celsius. Shear sense indicators record top-to-the-northeast displacement that predates doming, consistent with orogen-parallel transport during this stage of deformation. A subsequent deformation event (D3) created open to tight isoclinal folds (F3) and a pervasive axial planar cleavage development (S3) that overprints earlier fabric. Brittle faults record the final stage of deformation (D4). Kyanite alteration to sericite or white mica and chlorite replacement of biotite and garnet is attributed to a post-kinematic, retrograde metamorphic event (M4). These data demonstrate that the ductile portion of the Greenbrier fault

around the Ela and Bryson City domes accommodated orogen-parallel transport during the late Taconic orogeny.

TABLE OF CONTENTS

LIST OF TABLES

LIST OF FIGURES

LIST OF ATTACHMENTS

File 1: Geologic map and cross sections of the Ela and Bryson City domes Swain County, North Carolina (PDF file) map_and_cross sestion.pdf

CHAPTER 1

INTRODUCTION

A frontier in modern geology begun in the second half of the 20th century involved the study of rocks exposed in mountain chains affected by multiple orogenic events. First in unraveling the tectonic history of a multiple-stage orogeny is a comprehensive understanding of the complications related to overprinting of numerous deformation and/or metamorphic events (e.g., Ramsay, 1962; Hobbs et al., 1976; Bell and Rubenach, 1983; Williams, 1985; Bell et al., 1998). Few places provide a better natural laboratory for such a study than the southern Appalachians (Fig. 1). This unique mountain chain, formed during the Paleozoic, was assembled through the combination of the Ordovician Taconic (465-450 Ma), Devonian-Mississippian Neoacadian (365-350 Ma), and Mississippian-Permian Alleghanian (335-260 Ma) orogenies (Hatcher, 1987; Hatcher et al., 2007; Merschat, 2009). The Alleghanian orogeny was followed by rifting of Pangea in the early Mesozoic. Distinctive structural and metamorphic fabrics preserved throughout each tectonic subdivision of the orogen record the complex interplay between these deformational events (Fig. 1).

The first step in unraveling the complex history of the Appalachians is characterization of the polyphase deformational and metamorphic events. These events, recorded by metamorphic assemblages and fabric development, can be characterized by estimating the pressure-temperature-time-deformation (P-T-t-D) paths during the evolution of the orogen. This study focuses on the P-T-t-D history of rocks in the Great Smoky Mountains to constrain the tectonic evolution of the Appalachians during the Taconic, Neoacadian, and Alleghanian orogenies.

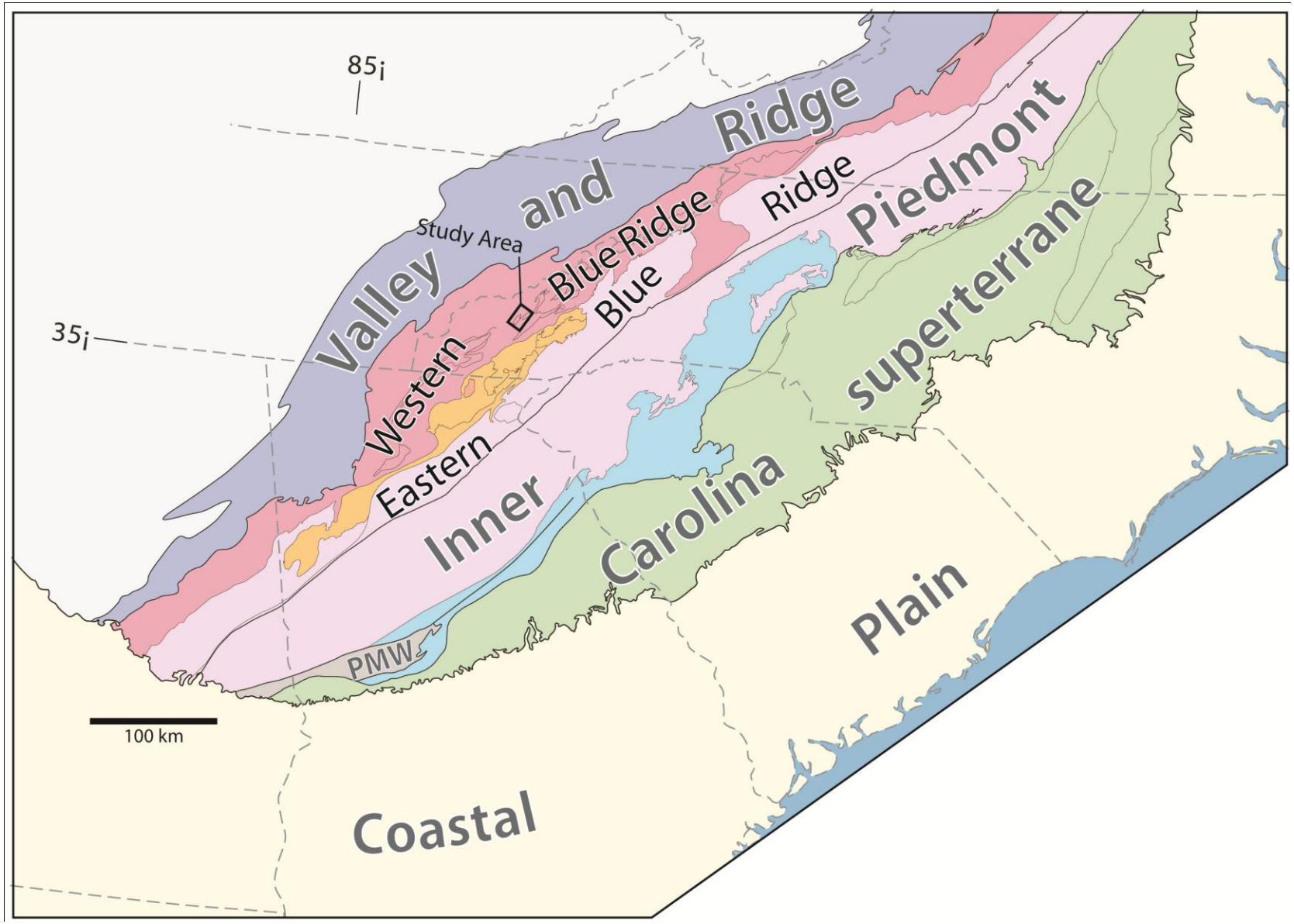

Figure 1. Lithotectonic map of the Appalachian Mountains. PMW, Pine Mountain window (after Huebner and Hatcher, 2013).

The Great Smoky Mountains comprise five thrust sheets whose timing of emplacement spans all three orogenies: the Dunn Creek, the Miller Cove, the Great Smoky, the Gatlinburg, and the Greenbrier thrust sheets (Fig. 2)(King et al., 1958; Hadley and Goldsmith, 1963; King et al., 1968; Connelly and Woodward, 1992). Major questions that still exist are: (1) what is the extent and style of strain localization in the hanging wall cover rocks, versus the basement rocks in the footwall; (2) what is the timing of metamorphic porphyroblast growth during Barrovian metamorphism relative to movement along the Greenbrier fault; and (3) what process led to the formation of domes that are cored by Greenville basement and mantled by the Great Smoky Group? Through an integration of meso- and microscale structural analysis and estimates of pressure and temperature, this investigation constrains the P-T-t-D history of rocks collected from the Greenbrier fault exposed near the Ela and Bryson City domes in the Great Smoky Mountains (Fig. 3). These data clarify some of the ambiguity about the timing and deformation style along the fault in locations throughout the western Blue Ridge as well as its role during the Taconic orogeny.

Throughout parts of the western Blue Ridge, the boundary between the pre-Taconic rifted-margin sediments of the Snowbird Group and the overlying Great Smoky Group is defined as the Greenbrier fault. Along the majority of its length, the Greenbrier fault contains the Great Smoky Group in the hanging wall and the Snowbird Group in the footwall. However, around the Ela and Bryson City domes and the Ravensford anticlinorium, the fault juxtaposes the Great Smoky Group in the hanging wall with the Grenville basement in the footwall (Fig. 3). Despite the range of rock types in the hanging wall and footwall of the Greenbrier fault, the larger-scale structural relationships in the Great Smoky Mountains and cross-section reconstructions indicate these faults are part of the same system (Hadley and Goldsmith, 1963; Connelly and

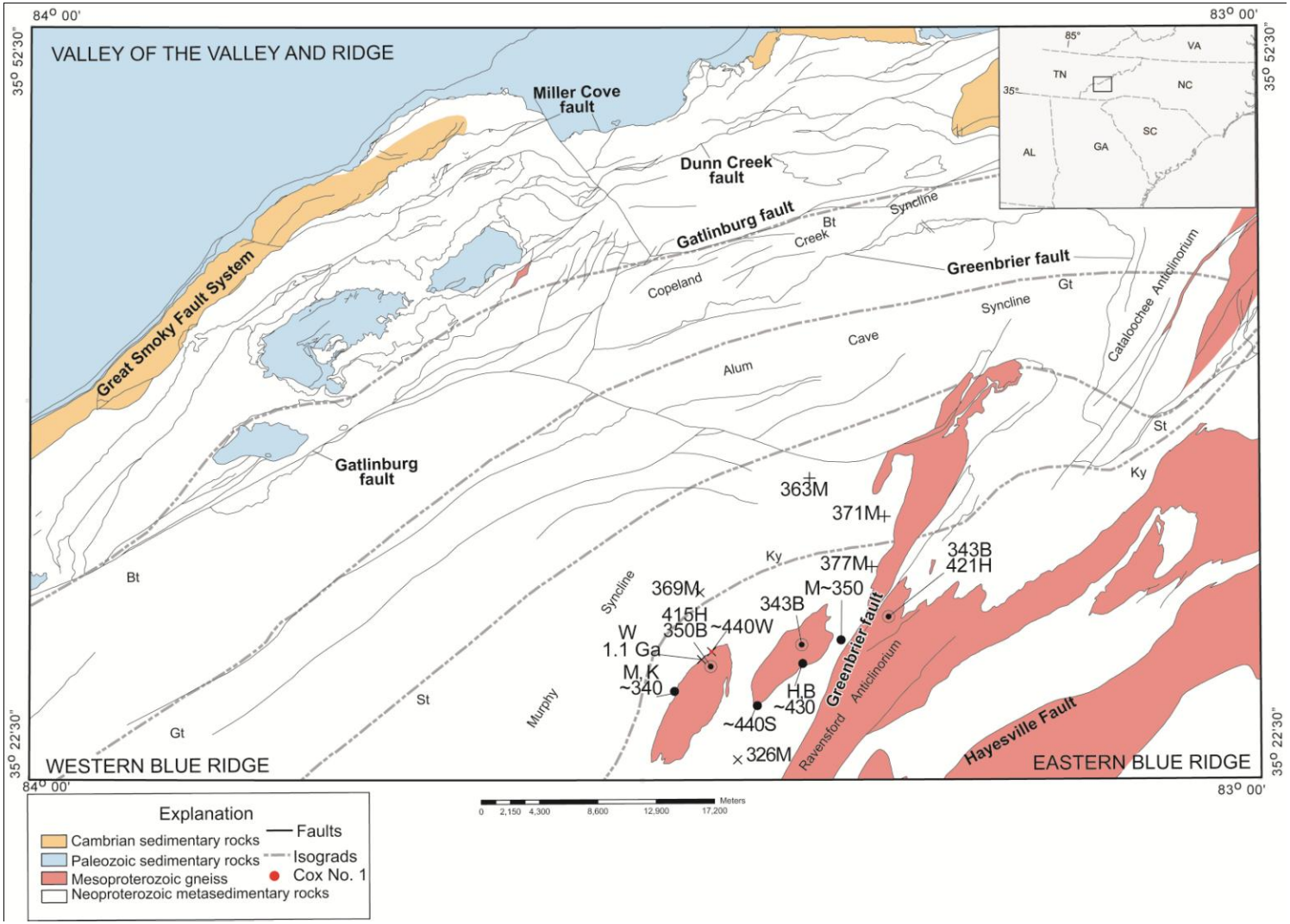

Figure 2. Simplified geologic map of the eastern Great Smoky Mountains showing isograds and mineral ages surrounding the Ela and Bryson City domes. Dallmeyer (1975) (circled dot), Kish (1991) (x), Connelly and Dallmeyer (1993) (+), and Southworth et al (2005b) (dot). The monazite samples of Kohn and Malloy (2004) are near Connelly and Dallmeyer (1993) sample locations. All ages are Ma unless otherwise stated. Hornblende (H), biotite (B), muscovite (M), sphene (S), biotite (Bt), garnet (Gt), staurolite (St), kyanite, (Ky)(modified after Southworth et al., 2005a) (structural and metamorphic data after Hadley and Goldsmith, 1963).

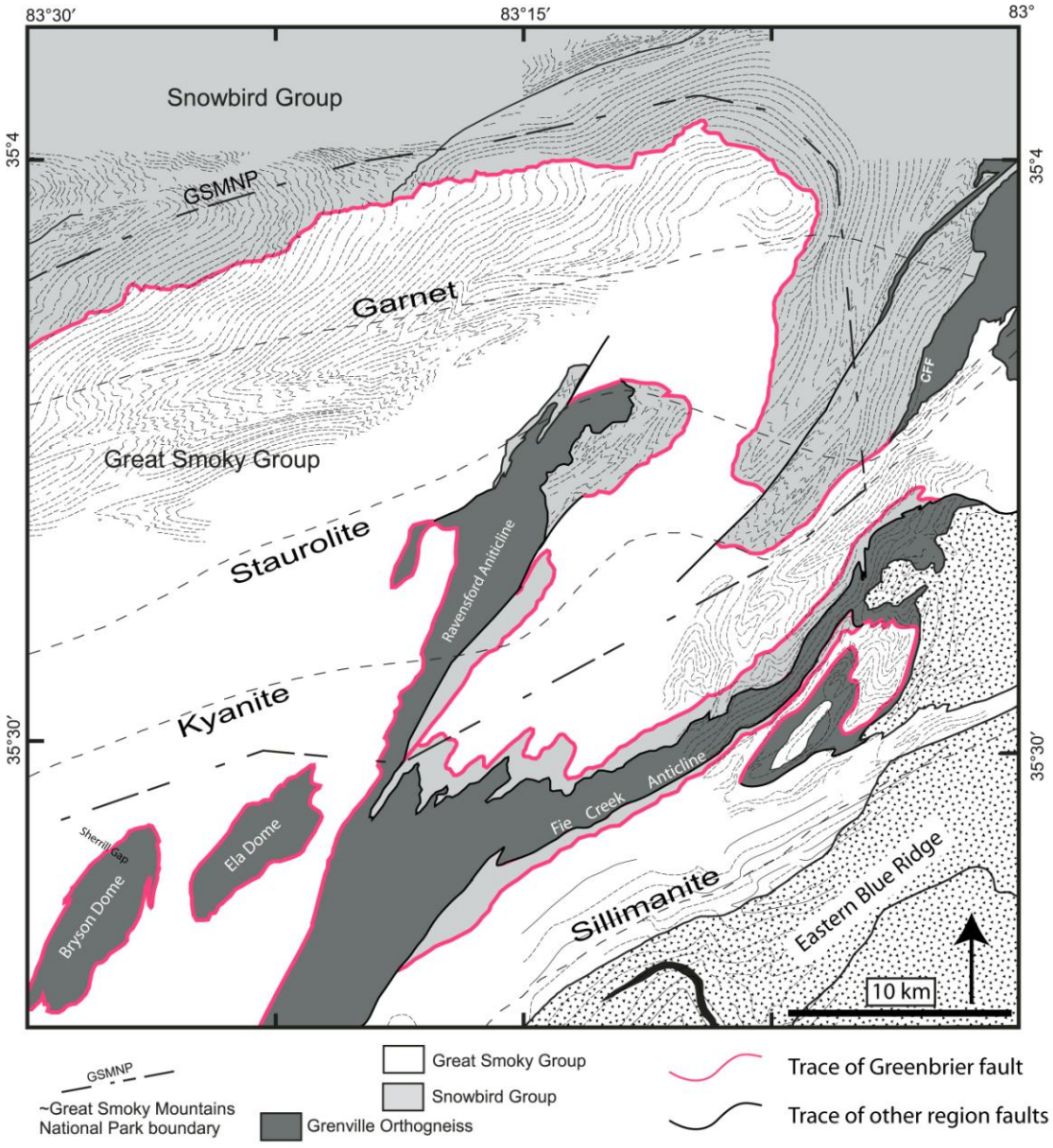

Figure 3. Schematic geologic map of the eastern Great Smoky Mountains highlighting the trace of the Greenbrier fault and regional foliations indicated by dashed lines (modified after Plate 3 of Hadley and Goldsmith, 1963).

Woodward, 1992; Southworth et al., 2006).

Several models have been proposed for the evolution of the Greenbrier fault. In one model, the Greenbrier fault is a pre-metamorphic thrust that accommodated shortening during the early phases of the Taconic orogeny (Hadley and Goldsmith, 1963). Cross-section reconstructions of the Greenbrier and Dunn Creek faults, suggest these faults originated as ramps and flats within a foreland fold-thrust belt during the early Taconic orogeny (Connelly and Woodward, 1992). In contrast, the Greenbrier fault could have originated as a stratigraphic contact (Clemons, 2006) and post-dates Taconic metamorphism. Previous studies, referenced above, largely focused on the main trace of the Greenbrier fault where it juxtaposes pre-Taconic sediments deposited in adjacent rift basins. Less research has been conducted farther to the southeast where the Greenbrier fault juxtaposes the Great Smoky Group directly on Grenville basement (Southworth et al., 2006; Thigpen and Hatcher, 2009; Cattanach and Bozdog, 2010).

This work addresses the structural and metamorphic evolution (P-T-t-D) of the rocks contained in and around the Ela and Bryson City domes to understand the nature of the contact between the Great Smoky Group in the hanging wall and Grenville basement in the footwall. Based on previous work, the contact exhibits one of three possible relationships: (1) predominantly pre-metamorphic slip typical of Greenbrier fault interpretations farther northwest (e.g., Hadley and Goldsmith, 1963; Connelly and Woodward, 1992; Montes, 1997); (2) predominantly post-metamorphic slip similar to the interpretation by Clemons and Moecher (2010); or (3) a polyphase deformational history involving pre- and post-metamorphic slip, consistent with interpretations 1 and 2.

I tested these hypotheses by conducting detailed petrologic descriptions and structural analysis of the Greenbrier fault surrounding the Ela and Bryson City domes. Metamorphic

conditions for the region were estimated by conducting thermobarometric calculations on samples from the Great Smoky Group. Since publication of the pioneering work on the Greenbrier fault (e.g., Hadley and Goldsmith, 1963; King et al., 1968), the structural geology and tectonics community has created a more sophisticated understanding of mid-crustal deformation, shear zones, and mylonites (Lister and Williams, 1979; Lister and Hobbs, 1980; Lister and Snoke, 1984; Law, 1987; Hirth and Tullis, 1992; Simpson and De Paor, 1993; Stipp et al., 2002). New detailed structural analysis is warranted in this region to update the kinematic history of the Greenbrier fault. These P-T-t-D estimates also constrain the regional tectonic framework of the Greenbrier fault in the southern Appalachians, while addressing process-oriented questions about the thermal and kinematic evolution of large thrust faults during orogenesis.

CHAPTER 2

BACKGROUND

2.1. Regional geology

The western Blue Ridge represents the eastern margin of Laurentia that was later affected by episodic collision and accretion during the Paleozoic following the breakup of Rodinia in the Neoproterozoic (Hatcher et al., 2004; Hatcher et al., 2007; Hatcher, 2010). The western Blue Ridge consists of Laurentian basement rocks, unconformably overlain by syn-rift deposits of the Ocoee Supergroup and Catoctin, Mount Rogers, and Grandfather Mountain Formations (Rankin, 1975; Wehr and Glover, 1985; Hatcher, 1987, 1989; Thomas, 1991). The Valley and Ridge province is the foreland fold-thrust belt of the Alleghanian orogeny and lies west of the Blue Ridge. The eastern boundary of the western Blue Ridge is separated from the central Blue Ridge by the Hayesville-Soque River fault system and the eastern Blue Ridge by the Chattahoochee-Holland Mountain fault system (Hatcher, 1987). In the southern Appalachians, the Great Smoky Mountains of Tennessee and North Carolina make up about one-fourth of the western Blue Ridge.

Rocks of the Great Smoky Mountains are dominated by the Precambrian metasedimentary Ocoee Supergroup that is divided into the Snowbird Group, Great Smoky Group, and Walden Creek Group (King et al., 1958; Table 1). The Ocoee Supergroup was deposited along the rifted margin of the Laurentia during the Neoproterozoic and was deformed by subsequent orogenies. The units consist mainly of siliciclastic sedimentary rocks with minor limestone and dolomite components. The stratigraphic and structural relationship between the units that comprise the Ocoee Supergroup is complex and few

Table 1. Stratigraphy of the Great Smoky Mountains (after King et al., 1958).

Age	Succession A: Northwest of and below the Greenbrier Fault			Succession B: Southeast of and above the Greenbrier fault		
Middle Cambrian through Middle Ordovician	Knox Group Conasauga Group Rome Formation			Murphy Group		
Early Cambrian	Chilhowee Group					
Late Precambrian	Ocoee Supergroup	Walden Creek Group	Sandsuck Formation Wilhite Formation Shields Formation Licklog Formation	Ocoee Supergroup	Great Smoky Group	Anakeesta Formation Thunderhead Sandstone Elkmont Sandstone
		Unclassified Formations	Sandstones of Webb Mountain and Big Ridge Cades Sandstone Rich Butt Sandstone		Snowbird Group	Roaring Fork Sandstone Longarm Quartzite Wading Branch Formation
		Snowbird Group	Metcalf Phyllite Pigeon Siltstone Roaring Fork Sandstone Longarm Quartize Wading Branch Formation			
Earlier Precambrian	Grenville basement					

*Successions A and B can be cross-correlated only at the level of Snowbird Group

locations contain a complete stratigraphic sequence (Costello and Hatcher, 1991). The relationships among the three units of the Ocoee Supergroup have major implications for the tectonic evolution of the southern Appalachians. For example, the Snowbird Group and Great Smoky Group may have been deposited in adjacent basins divided by a horst and then later overthrust by the Greenbrier fault (Rast and Kohles, 1986).

The combination of the Paleozoic deformations divided the western Blue Ridge into five major thrust sheets: Dunn Creek, Miller Cove, Great Smoky, Gatlinburg, and Greenbrier (King et al., 1958; Hadley and Goldsmith, 1963; King et al., 1968; Connelly and Woodward, 1992). Although interpreted to be one of the oldest structures in the region, the Greenbrier fault was preceded by, or was coeval with, a generation of east-northeast trending folds (e.g., Copeland Creek-Cartertown anticlines,)(Hadley and Goldsmith, 1963; King et., 1968). After

emplacement of the Greenbrier fault, it was deformed by a generation of southeast-trending folds (i.e., Ravensford and Cataloochee anticlinoria)(Fig. 2)(Hadley and Goldsmith, 1963; King et al., 1968; Southworth et al., 2005b). These later folds are coeval with deformation of the Great Smoky Mountain thrust that was emplaced during the Alleghanian orogeny (Hadley and Goldsmith, 1963; King et al., 1968).

The metamorphic isograds (Fig. 2) originally mapped for the Great Smoky Mountains record metamorphism during the Taconic orogeny (Hadley and Goldsmith, 1963; Carpenter, 1970; Hadley and Neslon, 1971). The isograds record a Barrovian-style metamorphism across the Great Smoky Mountains so that greenschist facies rocks in the northwest progressively increase in metamorphic grade to amphibolite facies rocks in the southeast. Regional cleavage and foliation development are correlated with this phase of metamorphism.

2.2. Geology of the Ela and Bryson City domes

The Ela and Bryson City domes are two *en echelon* northeast-trending antiforms that expose Grenvillian basement rocks in western North Carolina. Here, the Greenbrier fault placed Great Smoky Group rocks directly over the Grenville basement (Fig. 3). The two domes are similar in outcrop pattern and size; both occur as exposures of granitic gneiss bodies ~8.9 km long by ~2.4 km wide (Hadley and Goldsmith, 1963). Rocks of the Ocoee Supergroup are in faulted contact with both gneiss bodies and are mapped as the Copperhill Formation, a member of the Great Smoky Group (Southworth et al., 2005b; Thigpen and Hatcher, 2009; Cattanach and Bozdog, 2010). The Copperhill Formation is characterized as predominantly feldspathic metagraywacke and mica schist with lesser interbeds of metaconglomerate, quartzite, and metaarkose (Hurst, 1955). Rocks surrounding the domes are lower-amphibolite facies and occur wholly within the kyanite-staurolite zone. A mylonitic shear zone separates the overlying

metasedimentary rocks from rocks in the core of the domes, although the contact between the units is sharp where exposed. On the northern half of the Bryson City dome, the shear zone is mapped as a 16-60 m-wide zone consisting of mylonitic orthogneiss and augen protomylonite with sheared feldspars ranging in length from 0.3 cm to 3.8 cm (Cameron, 1951). Stretching lineations are variably developed in the mylonite zone. Rocks of a similar nature are found on the southern half of the dome but do not form a mappable unit. The core of the Bryson City dome is dominated by orthogneiss with compositions ranging from granite to granodiorite (Cameron, 1951). Foliation in both metasedimentary rocks in the hanging wall and orthogneiss in the footwall is parallel to the mylonitic shear zone foliation. Gneissic banding is variably developed throughout the dome and the gneiss is intruded by several large bodies of weakly foliated quartz monzonite. Metagabbro, hornblende schist, and biotite schist are also exposed in the Bryson City dome in gradational contact with the gneissic rocks (Cameron, 1951). Locally, brittle faults cut the hanging wall rocks both oblique and parallel to the foliation.

Rocks of the Ela dome are dominated by migmatitic biotite paragneiss that is more typical of regional Grenville basement. Ela dome rocks are correlated with rocks of the Mars Hill terrane based on lithology and age (Southworth et al., 2005b). Leucosomes in the paragneiss are parallel to the regional foliation, characteristic of stromatic migmatites, and do not penetrate the overlying Great Smoky Group, suggesting migmatization occurred during the Grenville metamorphic event (Kish et al., 1975). A zone of granitic mylonite is common near the core-cover contact of the Ela dome and a zone of S-C mylonitic exist in the hanging wall schist.

2.3. Previous work on the Greenbrier fault

Hadley and Goldsmith (1963) first defined the Greenbrier fault as a younger over older pre-metamorphic thrust that juxtaposes the Neoproterozoic rocks of the Great Smoky Group in the hanging wall with either the Neoproterozoic Snowbird Group or the Mesoproterozoic Grenville basement in the footwall. This interpretation is based on the observation that neither slaty cleavage nor regional metamorphic isograds are disturbed or offset by the fault. Additionally, fault gouge found at two exposures is recrystallized to fine-grained mica. Furthermore, broader structural relationships suggest that the Greenbrier fault must be present along the northeast side of the Straight Fork window and around the Ela and Bryson City domes (Hadley and Goldsmith, 1963). Older maps of the Ela and Bryson City domes (e.g., Cameron 1951; Hadley and Goldsmith, 1963) show an unfaulted contact between the Great Smoky Group and Grenville basement, whereas more recent maps show the contact as the Greenbrier fault (Southworth et al., 2005a; Thigpen and Hatcher, 2009; Cattanach and Bozdog, 2010). An estimated 23 km of slip was reported for the Greenbrier fault based on comparison of the thickness of the Snowbird Group above and below the fault (Hadley and Goldsmith, 1963). This estimate is tenuous since it assumes that the formation maintains a constant thickness and did not experience any significant erosion prior to faulting (Hadley and Goldsmith, 1963). Connelly and Woodward (1992) used the relationship of the Dunn Creek and Greenbrier fault geometries, along with concordant and discordant relationships across the fault surfaces, to suggest that these faults once exhibited a ramp-flat geometry. Based on this interpretation, cross-section restorations of the Greenbrier fault yield a similar displacement estimate of ~23 km (Woodward et al., 1991; Connelly and Woodward, 1992). In contrast, slip estimates based on stratigraphic piercing points across the fault demonstrate a minimum displacement of 40 km (Montes, 1997).

This evidence, along with the interpretation that the fault is pre-metamorphic, suggests it formed during Taconic foreland-style folding and thrusting. This is potentially the only evidence that exists for this style of Taconic deformation in the southern Appalachians, which is characterized by predominantly folded and thrusted sedimentary strata with little to no deformation accumulated in the basement rocks. Recent critical assessments of the Greenbrier fault have produced alternative interpretations for its tectonic history. Clemons and Moecher (2008, 2010) interpreted the Greenbrier fault to be a faulted stratigraphic contact with predominantly post-metamorphic slip.

Field mapping, geochronology, thermobarometry, and microstructural analyses conducted on the Greenbrier fault between the Snowbird Group and Great Smoky Group have not generated a unique solution to the history of the fault (e.g., Cameron, 1951; Hadley and Goldsmith, 1963; Kish et al., 1975; Connelly and Woodward, 1992; Montes, 1997; Southworth et al., 2005b; Clemons, 2006). The younger over older stratigraphic relationship (Hadley and Goldsmith, 1963) is contradictory to common assumptions about thrust faults. Several interpretations have therefore been suggested to explain this observation. Southworth et al., (2006) suggested Neoproterozoic extension between 580 and 560 Ma along the Greenbrier fault as a solution to this unique relationship, whereas Clemons and Moecher (2010) suggested that the fault was originally a conformable stratigraphic contact that was subsequently faulted with less displacement than the width of the faulted stratigraphy. The latter interpretation is problematic for the Greenbrier fault because it cuts both up and down section. For example, at an exposure east of Harmon Den Mountain, the Greenbrier fault rises from basement rocks through the Snowbird Group into the Great Smoky Group and down again through 2048 m of the Great Smoky Group (Hadley and Goldsmith, 1963).

2.4. Timing constraints

The complex metamorphic history of the Great Smoky Mountains is represented by the diverse radiometric ages published for the region (Fig. 2). Although many studies conclude that peak metamorphism in the region occurred during the Taconic orogeny, ^{40}Ar / ^{39}Ar cooling ages and U-Th-Pb monazite geochronology indicate thermal overprinting occurred during the Acadian and Alleghanian orogenies (Dallmeyer, 1975; Connelly and Dallmeyer, 1993; Moecher et al., 2003; 2004; Kohn and Malloy, 2004; Southworth et al., 2005b). Sm-Nd and Rb-Sr garnet ages from Mesoproterozoic metagrabbros (Goldberg and Dallmeyer, 1997) farther to the northeast of the study area record two discrete metamorphic age domains at 460-450 Ma (Taconic) and 393-386 Ma (Acadian). Hornblende Sm-Nd and Rb-Sr ages from the same location record similar discrete tectonothermal events at 472-451 Ma (Taconic) and 398-279 Ma (Acadian) (Goldberg and Dallmeyer, 1997).

Numerous radiometric age studies have been derived from the Ela and Bryson City domes, the Copperhill Formation surrounding the domes, and from the Greenbrier fault (Fig. 2). $^{40}Ar/^{39}Ar$ hornblende plateau ages from Grenville basement rocks from the Ravensford anticlinorium and from within the Bryson City dome record ages of 421 ± 15 Ma and 415 ± 15 Ma, respectively (Dallmeyer, 1975). Grenville basement rocks in the Ela dome record similar $^{40}Ar/^{39}Ar$ hornblende plateau ages of ~430 Ma (Southworth et al., 2005b). These rocks, which reside in the kyanite-staurolite zone, reached conditions exceeding the closure temperature of hornblende (~500° C) and record Ordovician (Taconic) Barrovian metamorphism. Biotite $^{40}Ar/^{39}Ar$ age of ~430 Ma and an U-Pb sphene age of ~440 Ma obtained from Grenville rocks in the Ela dome are consistent with Taconic peak metamorphism (Southworth et al., 2005b). Muscovite $^{40}Ar/^{39}Ar$ plateau ages from the Copperhill Formation surrounding both domes range

from 377-326 Ma (Kish, 1991; Connelly and Dallmeyer, 1993) and ~350 Ma (Southworth et al., 2005b). Muscovite and potassium feldspar plateau ages of ~340 Ma $^{40}Ar/^{39}Ar$ were obtained from the Greenbrier fault surrounding the Bryson City dome. U-Pb TIMS monazite ages and U-Th-Pb monazite chemical ages from the Great Smoky Mountains record discrete thermal events between 480-440 Ma (Taconic) (Moecher et al., 2003; 2004) and ~400 Ma (Kohn and Malloy, 2004). Recent monazite and zircon chronology from southern Appalachian alluvium record Ordovician metamorphism at 463 Ma and 450 Ma, respectively (Moecher et al., 2011).

CHAPTER 3

STRUCTURAL FRAMEWORK

3.1. Mesoscale structures

Bryson City dome

Compositional layering (S_1), variably overprinted by metamorphism and deformation, is preserved in such locations around the Bryson City dome as near Sherrill Gap on the northeast side of the dome (Fig. 3; Fig. 4a). Here, alternating layers of schist and quartzite are interpreted as original compositional layering. Overprinting during deformation and/or transposition removed evidence of sedimentary structures such as cross-beds or graded-bedding that are required to define original bedding. Because the field area lacks primary structures that can be used to define an original surface, this investigation defines S_1 as the youngest compositional surfaces; however S_1 is not intended to define primary depositional contacts.

Two generations of mesoscale folds occur in the hanging wall and footwall of the Greenbrier fault in the map area. First generation folds (F_2) deform compositional layering (S_1) into upright to recumbent isoclinal passive flow folds with axial surfaces parallel to S_2 (Fig. 4b). Although these are the first generation of observable folds in the field, their axial planar relationship to S_2 indicates that they formed during D_2 deformation. S_1 has been transposed into the main foliation of the region (S_2), but is observed locally in F_2 fold hinges in both the metagraywacke units of the metasedimentary unit (Fig. 4b) and as gneissic banding in the core rocks. In the hanging wall, S_2 is defined by aligned aggregates of fine- to coarse-grained biotite and muscovite with subordinate hornblende, kyanite, and staurolite. When present in local areas, kyanite and staurolite blades are aligned parallel to S_2, but they do not define a lineation.

Figure 4. Field observations from the Bryson City dome. (A) Compositional layering (S_1) preserved as alternating layers of mica-rich units and quartz-rich units. S_2 is parallel to S_1. (B) Open F_3 fold deforming isoclinal F_2 in metagraywacke unit.

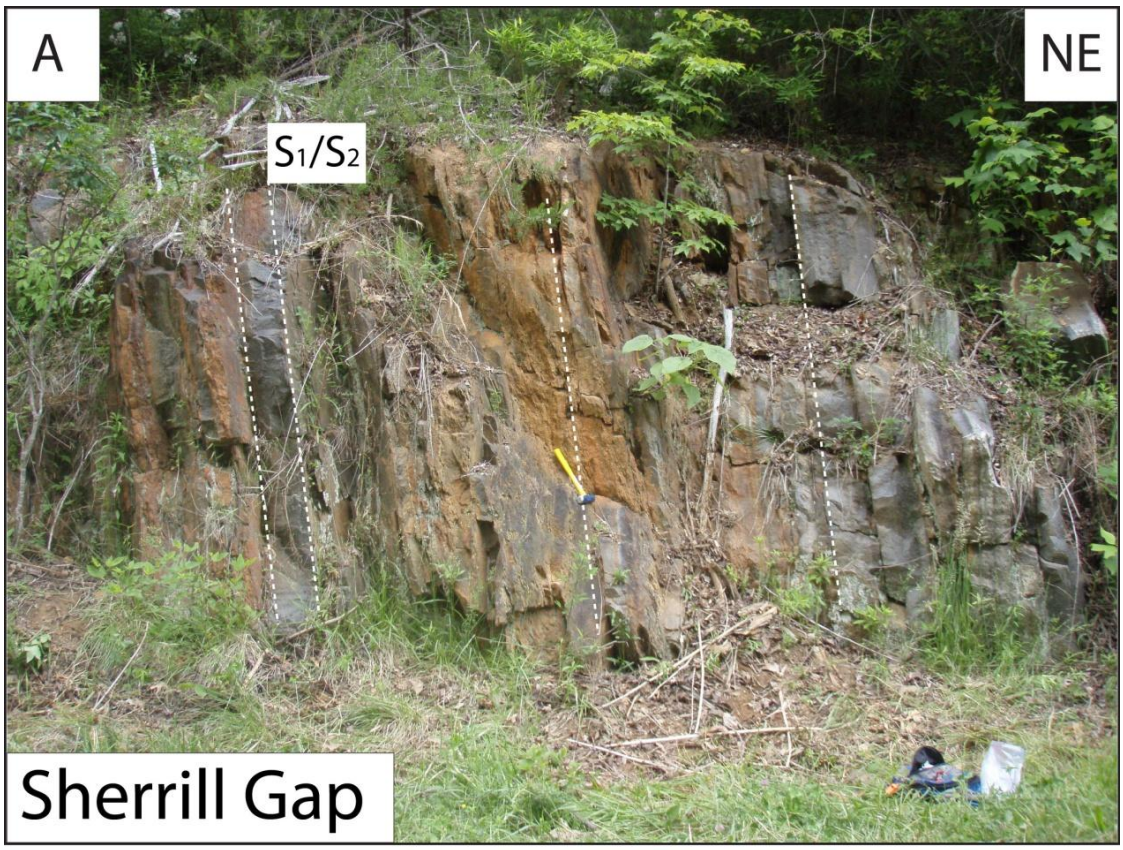
A
NE
S1/S2
Sherrill Gap

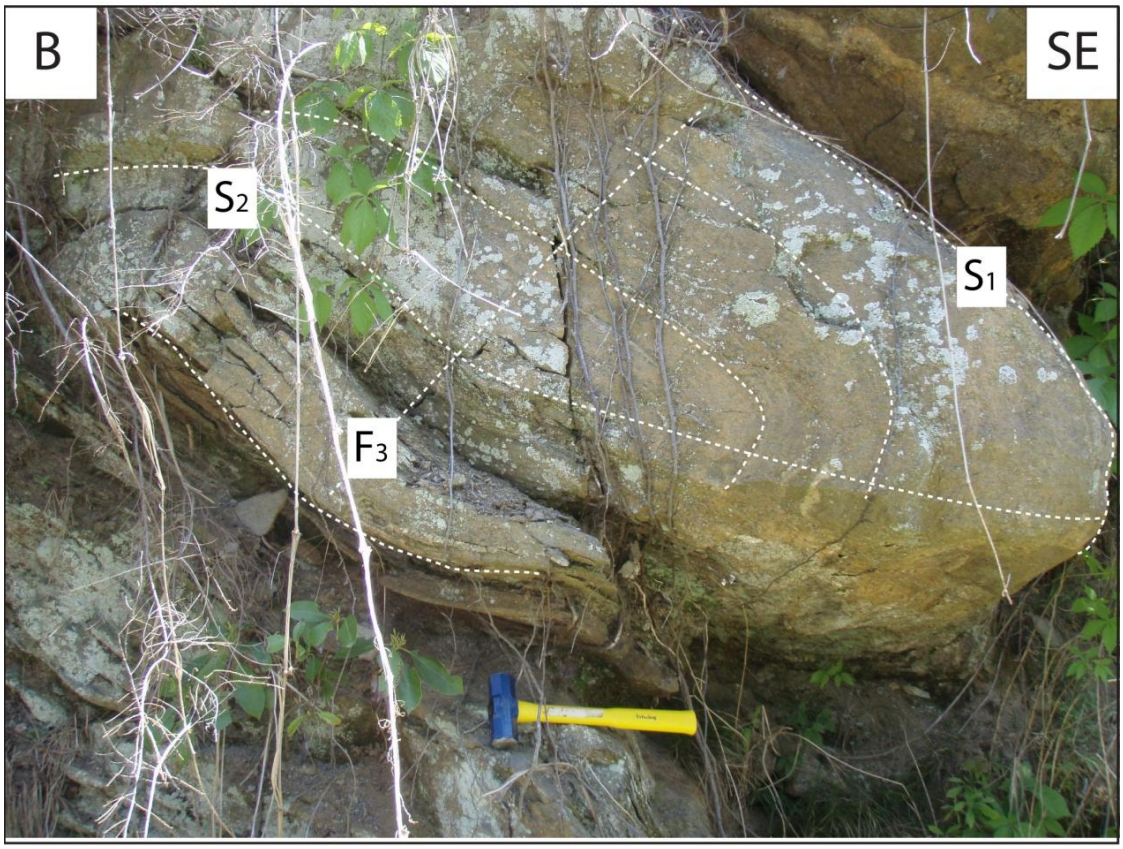
B
SE
S2
S1
F3

Orientation of the foliations and the lineations follows the general elongate shape of the Bryson City dome (Fig. 5a, b; Plate 1). At the northeastern tip of the dome, S_2 dips gently to the northeast (i.e., in the same direction as the plunge of the dome). Elsewhere around the dome, the strike of S_2 foliation is subparallel to the trace of the core-cover contact, and it dips steeply away from the contact with a few overturned layers dipping toward the dome (Plate 1). On the west and southwest portions of the dome, S_2 strikes northeast-southwest and dips southeast. The gneissic foliation in the granitic core of the dome similarly parallels the core-cover contact. Second generation folds (F_3) are gentle warps and flexures that deform F_2/S_2 into open to tight passive flow folds (Fig. 4b). The fold axes of F_3 folds trend NE-SW and dip ~50° SE or NW (F_3: 190, 40°NW) (Fig. 5b). Orientation of the fold axes are similar to the long axis of the dome, which suggests they developed during the same deformation event (Hadley and Goldsmith, 1963; Kish et al., 1975). Crenulation fold axes are parallel to F_3 fold axes and define an S_3 foliation in both the hanging wall schist and footwall gneiss layers (Fig. 6a). These northeast-trending F_3 crenulation axes define the dominant lineation. An undeformed pegmatite dike (Cox Number 1)(Fig. 2)(e.g., Cameron, 1951) on the northeast side of the Bryson City dome that crosscuts D_2 structural features yields a Rb-Sr whole rock age of 440 Ma, establishing a minimum age of the D_2 event as Taconic (Kish, 1991). At the southernmost part of the dome, crenulations increase in amplitude and S_3 becomes subparallel to S_2. The Greenbrier is the most prominent fault in the study, occurring as a mylonitic shear zone (S_{2b}) whose fabric parallels S_2. My new mapping confirmed that mineral lineations (defined by elongate mineral grains or aggregates of grains that trend northeast; Fig. 5b) are related to shearing along the Greenbrier (Cameron, 1951). Kinematic indicators sampled along the north side of the dome include C and C'- type shear bands and record top-to-the-northeast shear sense (Fig. 6b; Table 2).

Figure 5. Lower hemisphere equal-area stereograms showing foliation and lineations of the Ela and Bryson City domes. The domes have been divided into domains based on the trend of the strike and dip to better show the domal geometry. (A) Bryson City dome poles to S_2 foliation. Mean orientation = 120/83°SW. β=030°→ 08. (B) Lineations are undifferentiated mineral lineation related to Greenbrier movement and F_3 crenulations lineations. (C) Ela dome poles to S_2 foliation. Mean orientation = 125/82°SW. β=035°→ 08.

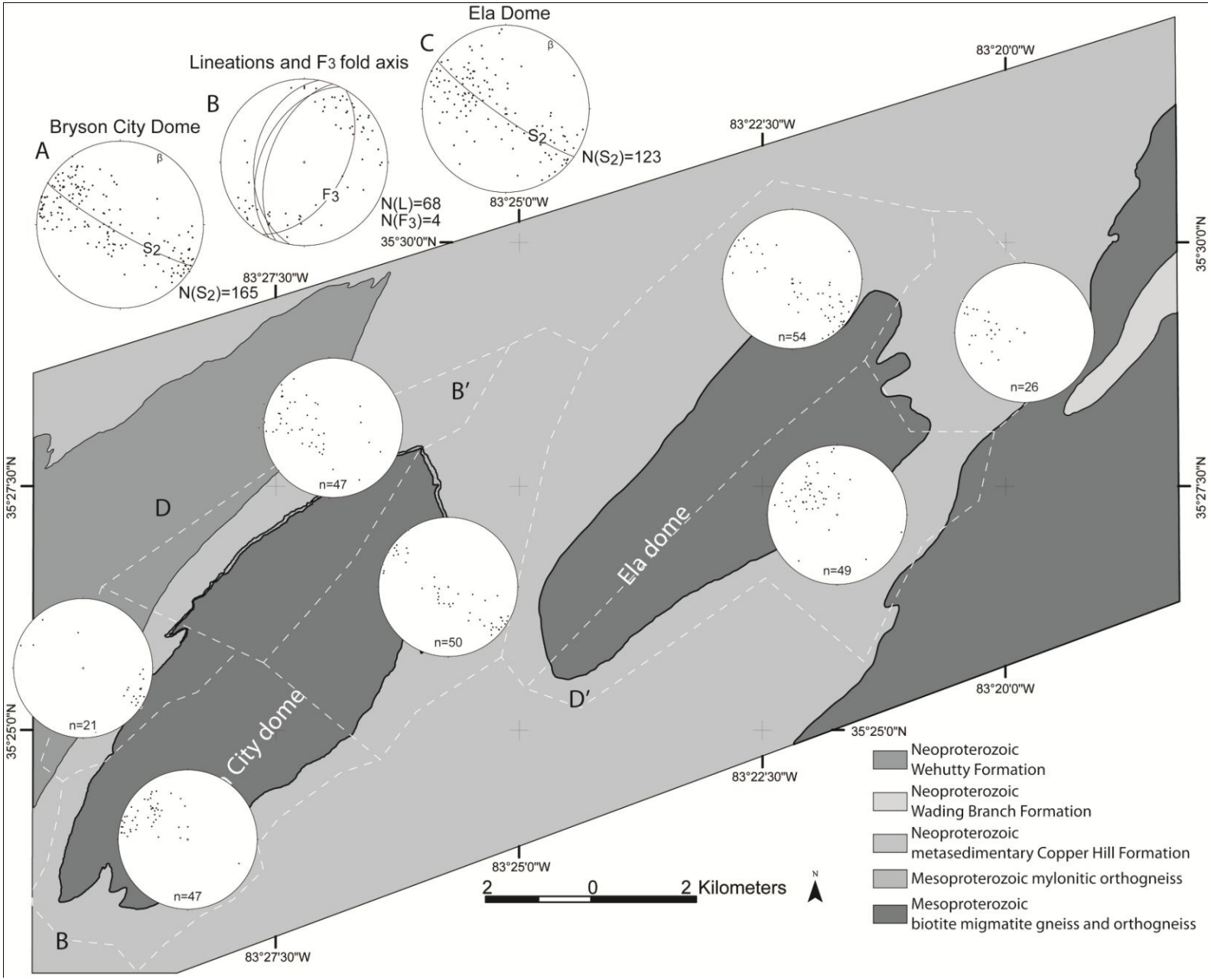
Ela Dome
C
β
S2
N(S2)=123
Lineations and F3 fold axis
B
F3
N(L)=68
N(F3)=4
Bryson City Dome
A
β
S2
N(S2)=165
83°20'0"W
83°22'30"W
83°25'0"W
83°27'30"W
35°30'0"N
35°27'30"N
35°25'0"N
n=54
n=26
n=47
n=49
n=50
n=21
n=47
B′
D
D′
Ela dome
City dome
B
2 0 2 Kilometers
N
Neoproterozoic
Wehutty Formation
Neoproterozoic
Wading Branch Formation
Neoproterozoic
metasedimentary Copper Hill Formation
Mesoproterozoic mylonitic orthogneiss
Mesoproterozoic
biotite migmatite gneiss and orthogneiss

Figure 6. Field observations from the Bryson City dome. (A) Crenulations in schist deform S_2 foliation. (B) S-C mylonite in Grenville basement on the northern side of the Bryson City dome showing top-down-to-the-northeast shear sense.

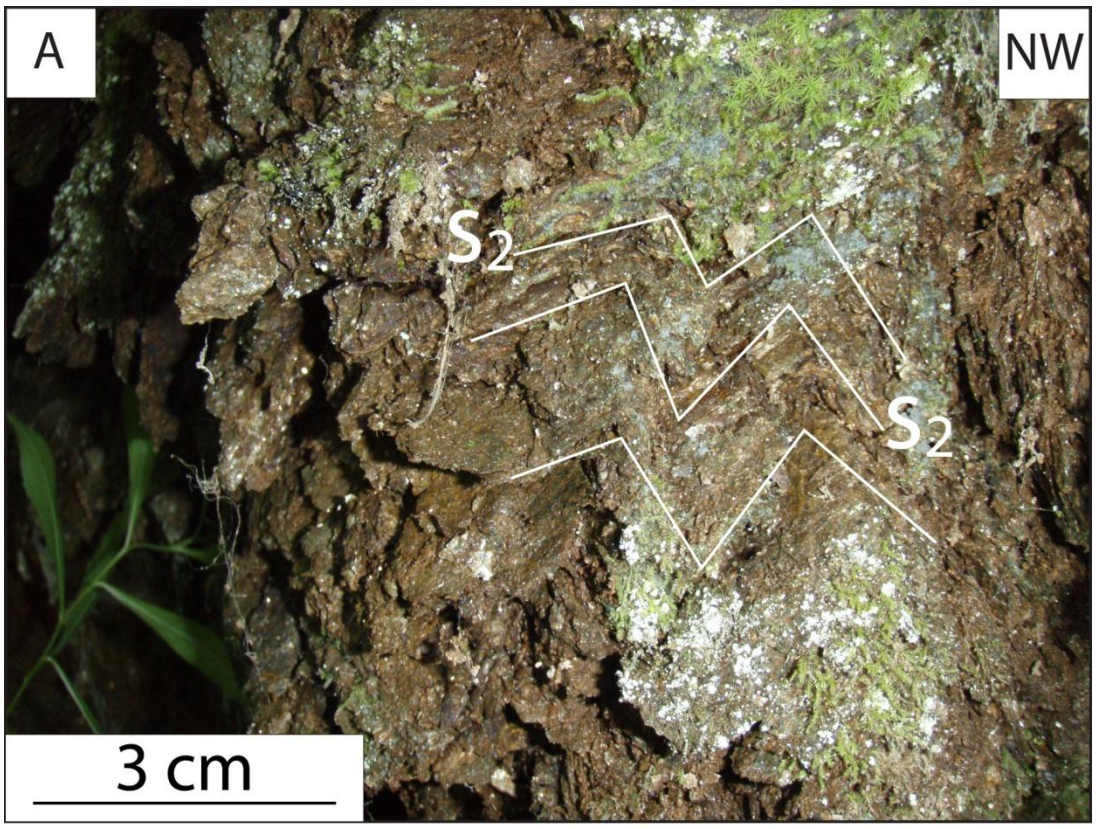
A
NW
S_2
S_2
3 cm

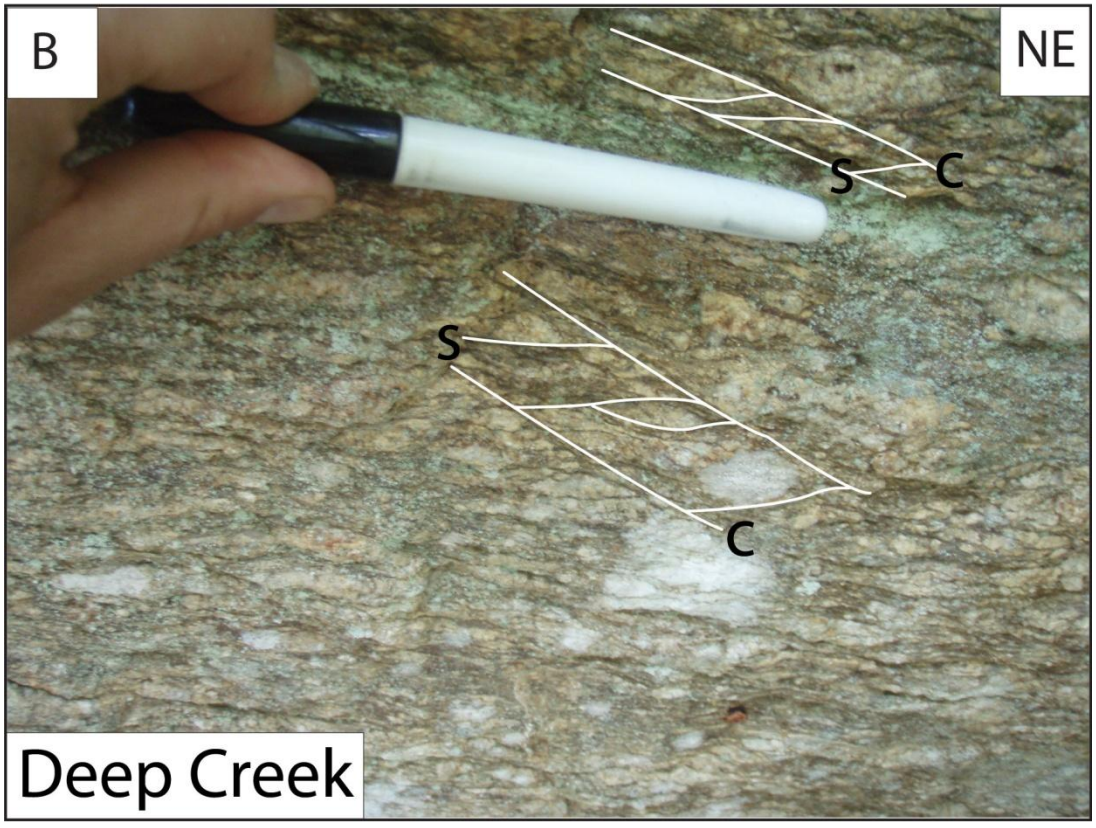
B
NE
S
C
S
C
Deep Creek

Table 2.
Summary of Greenbrier fault shear sense and deformation temperature data.

Sample	Rock type	Shear sense	Deformation Temperature (° C)	Temperature indicator
Greenbrier fault-Bryson City dome				
11BC-A	grt schist	top-d-NE	500-650	GBM
11BC-B	augen gneiss	top-NE	500-650	GBM
11BC-1	ms schist	top-NE	500-650	GBM
11BC-3A	bt shist	top-NE	500-650	GBM
11BC-3B	metagraywacke	top-up-NE	500-650	GBM
11BC-5	augen gneiss	top-NE	500-650	GBM
11BC-6	augen gneiss	top-up-NE	500-650	GBM
11BC-7	augen gneiss	top-NE	500-650	GBM
	mylonite	top-NE		
11BC-8	orthogneiss		500-650	GBM
	mylonite	top-up-NE		
11BC-9	orthogneiss		500-650	GBM
	mylonite	top-up-NE		
11BC-10	orthogneiss		500-650	GBM
Greenbrier fault–Ela dome				
	mylonite			
11ED-2	paragneiss	top-d-S	500-650	GBM
11ED-3	grt schist	top-d-NE	500-650	GBM
11ED-4A	bt schist	top-NE	500-650	GBM
11ED-6	bt schist	top-d-NE	500-650	GBM
11ED-8	bt schist	top-NE	500-650	GBM

Abbreviations: bt, biotite; ms, muscovite; grt, garnet; top-d-NE, top-down-to-the northeast; top-NE, top-to-the-northeast; top-up-NE, top-up-to-the-northeast; top-d-S, top-down-to-the-south. GBM Grain-boundary migration recrystallization

Deformation temperatures and indicators are based on quartz deformation textures.

Although the granitic mylonite described above forms a mappable unit around the northern side of the dome, rocks of similar type create a window through the Greenbrier fault around the entire structure. At most outcrops, metasedimentary rocks adjacent to the mylonitic granite (aka "border gneiss" of Cameron, 1951) do not appear to be sheared on the mesoscale, but contain rotated porphyroclasts (e.g., garnet and feldspar) and shear bands on the microscale that record top-to-the-northeast shear sense (see Chapter 3). Reverse faults and high-angle normal faults in hanging wall exposures created F_4 drag folds during a final stage of brittle deformation (D_4).

Ela dome

The overall mesoscale fabrics of the Ela dome are similar to those of the Bryson City dome. Compositional layering between mica-rich units and quartz-rich units, interpreted to reflect original compositional variations (S_1), is variably preserved in the hanging wall. The main foliation (S_2) is parallel to S_1 where compositional layering is preserved. S_2 is axial planar to F_2 generation folds that occur as isoclinal flexural flow folds. The main foliation (S_2) in the metasedimentary rocks is parallel to the cover-core contact and dips away from the dome's center. (Fig. 5c; Plate 1). The mylonitic foliation (S_{2b}) is parallel to S_2 foliation as well as to the foliation developed in the gneiss within the dome. A transition between protomylonite in the core to mylonitic fabric (S_{2b}) near the contact records an increase in strain. Unlike the Bryson City dome, mesoscale shear bands occur in metasedimentary units (Fig. 7a). Mineral and stretching lineations defined by elongated grains or aggregates of grains in the Greenbrier fault have a dominant northeast-southwest trend (Fig. 5b). It is unclear whether S_2 developed into the mylonitic foliation due to localized shear near the contact or if the mylonitic foliation developed parallel to S_2 during a subsequent event.

F_2 folds are affected by a later generation of F_3 passive flow folds (Fig. 7b). Type 3 fold interference patterns indicate a low angle between the F_2 and the F_3 fold axes (Fig. 7c). An S_3 crenulation cleavage developed axial planar to the F_3 generation folds. Toward the southeastern flank of the dome, S_3 becomes subparallel to S_2 due to transposition of the foliation. Crenulation lineations associated with D_3 deformation trend northeast-southwest similar to the long axis of the Ela dome. A northeast-striking, southeast-dipping brittle normal fault cuts the Great Smoky Group at the southern end of the Ela dome and S_2 layering is deflected into the fault surface about an F_4 generation fold axis (Fig. 7d).

Figure 7. Field observations from the Ela dome. (A) S-C mylonitic schist on the south side of the Ela dome. (B) F_3 open to tight folds deforming pegmatite dike on the south side of the Ela dome. (C) Type 3 fold interference pattern in metagraywacke unit. (D) Brittle normal fault in Great Smoky Group with top-down-to-the-north shear.


A
SW
SW
IN
Grain Size Scale
3
4
5
mm


B
SW

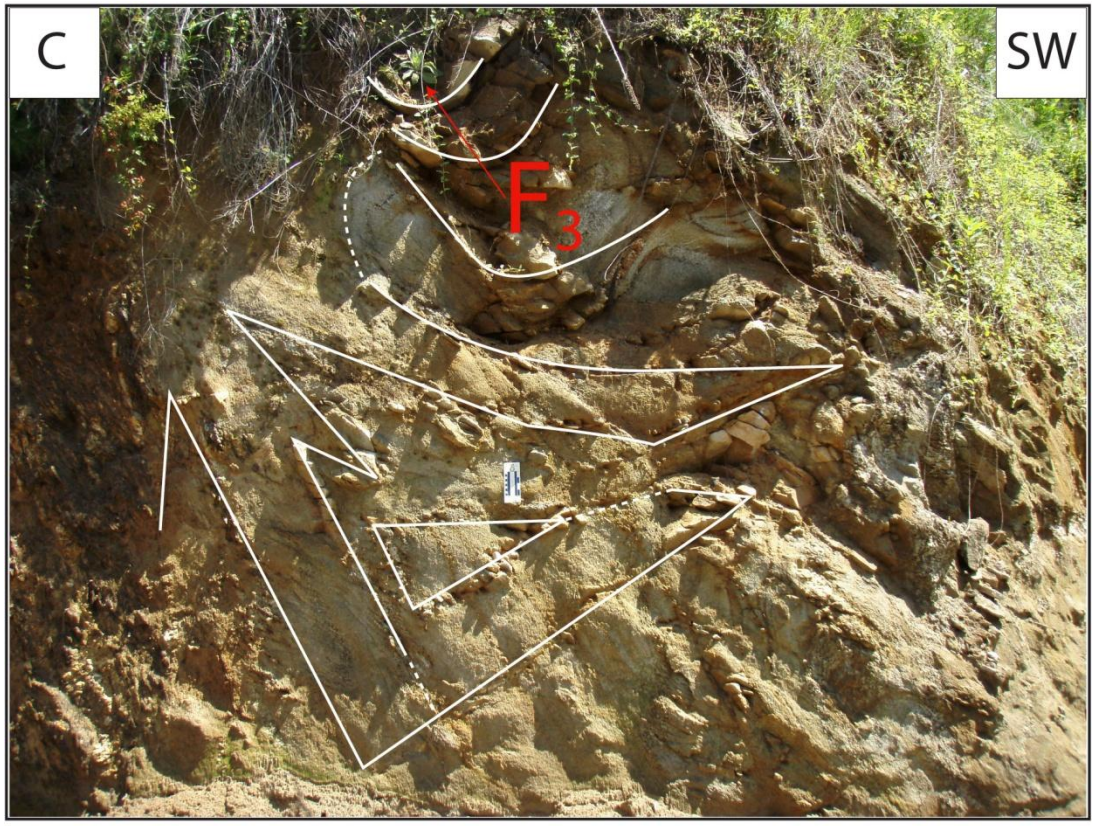
C
SW
F3


D
S

3.2. Microscale structures

Great Smoky Group of the Bryson City dome (11BC-A and 11BC-38)

Sample 11BC-A (35.4692°, -83.4296°) collected from the Greenbrier fault on the northern flank of the Bryson City dome is a pelitic schist with subhedral garnets and anhedral kyanite porphyroblasts (Fig. 8; Table 3). Additionally, staurolite occurs in the sample as randomly oriented ~10-µm-long needles arranged in bundles and clusters that nucleated at feldspar grain boundaries. Their composition was confirmed by electron microprobe analysis (EMPA). Kyanite is mostly altered to randomly oriented fine-grained white micas. The porphyroblasts lie in a foliated matrix (265°, 23° NW) defined by the parallel alignment of muscovite and biotite. Subhedral quartz and plagioclase are interlayered with the mica grains. Accessory minerals occurring throughout the matrix include graphite, tourmaline, apatite, monazite, zircon, and various opaque minerals. Garnet grains typically contain an inclusion-rich inner core of parallel trails (S_{1i}) oblique to the main foliation (S_2), an inclusion-poor outer core, and an inclusion-rich outer rim with trails that are tangent to the crystal faces of the garnet (Fig. 9a). The textural zoning at the rim of the garnet is recognized as growth inclusions that formed from the nucleation of new grains at the growing crystal faces (Passchier and Trouw, 2005). Garnet inclusions consist predominantly of quartz and ilmenite, with subordinate amounts of biotite, sulfides, plagioclase, apatite, tourmaline, monazite, and xenotime. Garnet sigma structures and S-C type shear sense indicators record top-down-to-the-northeast shear sense (Fig. 9b; Table 2). Quartz grains have lobate grain boundaries characteristic of grain-boundary migration recrystallization (GBM). Furthermore, internal deformation in plagioclase grains has created elongate grains that are parallel to the main foliation. Deformation mechanisms suggest temperatures of 500-600° C (Table 2)(Stipp et al., 2002).

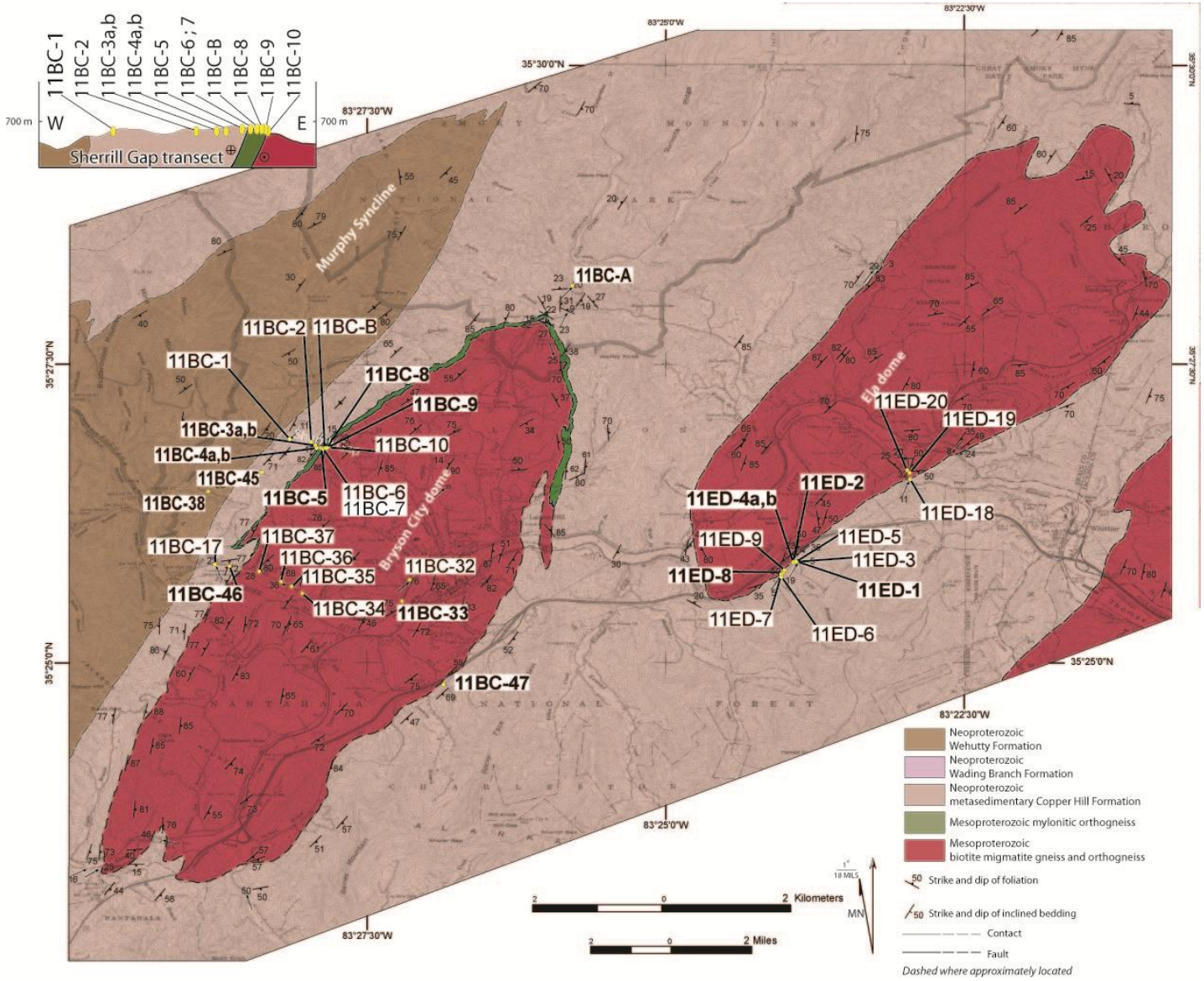

Figure 8. (A) Geologic map of the Ela and Bryson City domes showing sample locations. (B) Cross section excerpt of the Bryson city dome from profile D (Plate 1) with sample locations. Map and cross-section are different scales. Bolded labels are samples described in text.

Figure 9. Photomicrographs from the Bryson City dome. The orientation marks define trend and plunge of the lineation for each section where present; otherwise, the samples were cut parallel to the prevailing lineation of the outcrop. (A) Inclusion trails (S_{1i}) in inter-kinematic garnet. (B) S-C shear bands with top-to-the-northeast shear sense. Plag, plagioclase; Bt, biotite; Ms, muscovite; Grt, garnet; Qtz, quartz.

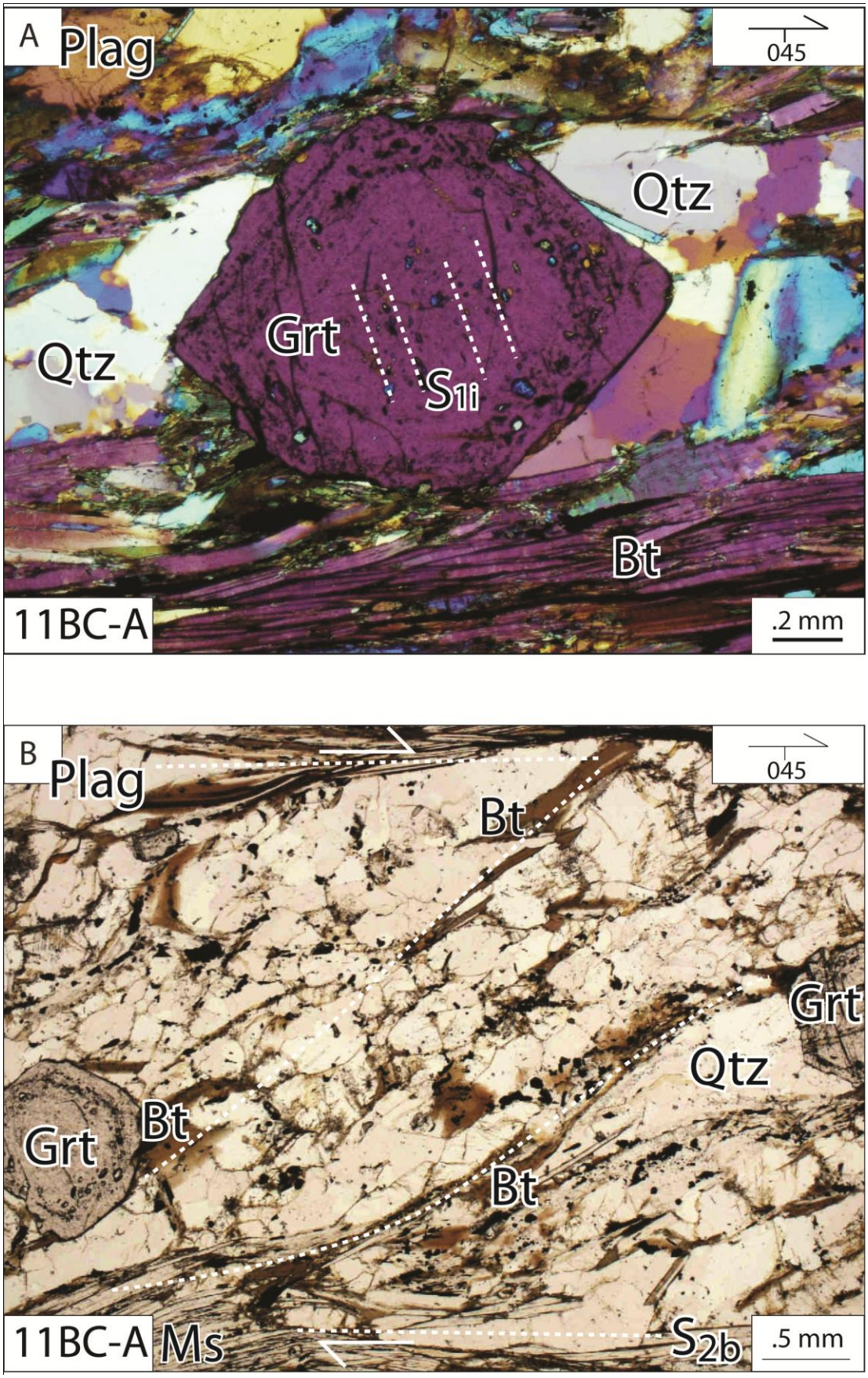
A
Plag
045
Qtz
Grt
Qtz
S1i
Bt
11BC-A
.2 mm
B
Plag
045
Bt
Grt
Qtz
Grt
Bt
Bt
11BC-A
Ms
S2b
.5 mm

Table 3. Major mineral assemblage for pelitic samples discussed in text

Sample	Grt	Ky	St	Ksp	Ilm	Rutile
11BC-A	X	X	-	-	X	-
11BC-38	X	X	X	-	X	-
11BC-4B	X	-	-	-	X	-
11BC-3A	X	-	-	-	X	-
11BC-45	X	X	X	-	X	-
11ED-4A	-	-	-	-	X	-
11ED-8	X	-	-	-	X	-

(X) indicates presence of mineral; (-) indicates absence of mineral.
All sample contain quartz, biotite, muscovite, and plagioclase; for a full list of accessory mineral see appendix III.
Abbreviations: Grt, garnet; Ky, kyanite; St, staurolite; Ilm, ilmenite.

Sample 11BC-38 (35.4405°, -83.4805°) is a pelitic schist from the Anakeesta Formation of the Great Smoky Group containing quartz, biotite, muscovite, plagioclase, staurolite, kyanite, and garnet (Fig. 8). Accessory minerals include graphite, tourmaline, apatite, monazite, zircon, xenotime, and opaque minerals. The sample displays a continuous S_2 foliation (035°, 80° SW) defined by aligned, interlayered sheaths of muscovite and biotite, kyanite blades, and elongate staurolite porphyroblasts. The mica grains deflect around porphyroblasts of kyanite, staurolite, and garnet. Subhedral poikiloblastic staurolite grew up to 3 cm by 1.5 cm and contain linear inclusion trails of primarily quartz that are aligned at an oblique angle to the long axes of the staurolite (S_{1i}). The trails are discontinuous with the main foliation and thus did not nucleate during D_2 deformation. Other inclusions are subhedral to anhedral garnet, biotite, and opaque minerals. The staurolite porphyroblasts contain abundant inclusions of graphite; however, around the inclusion garnets, graphite-free zones occur and mimic the crystal shape of garnet (Fig. 10). The kyanite porphyroblasts contain inclusions of quartz and opaque minerals aligned

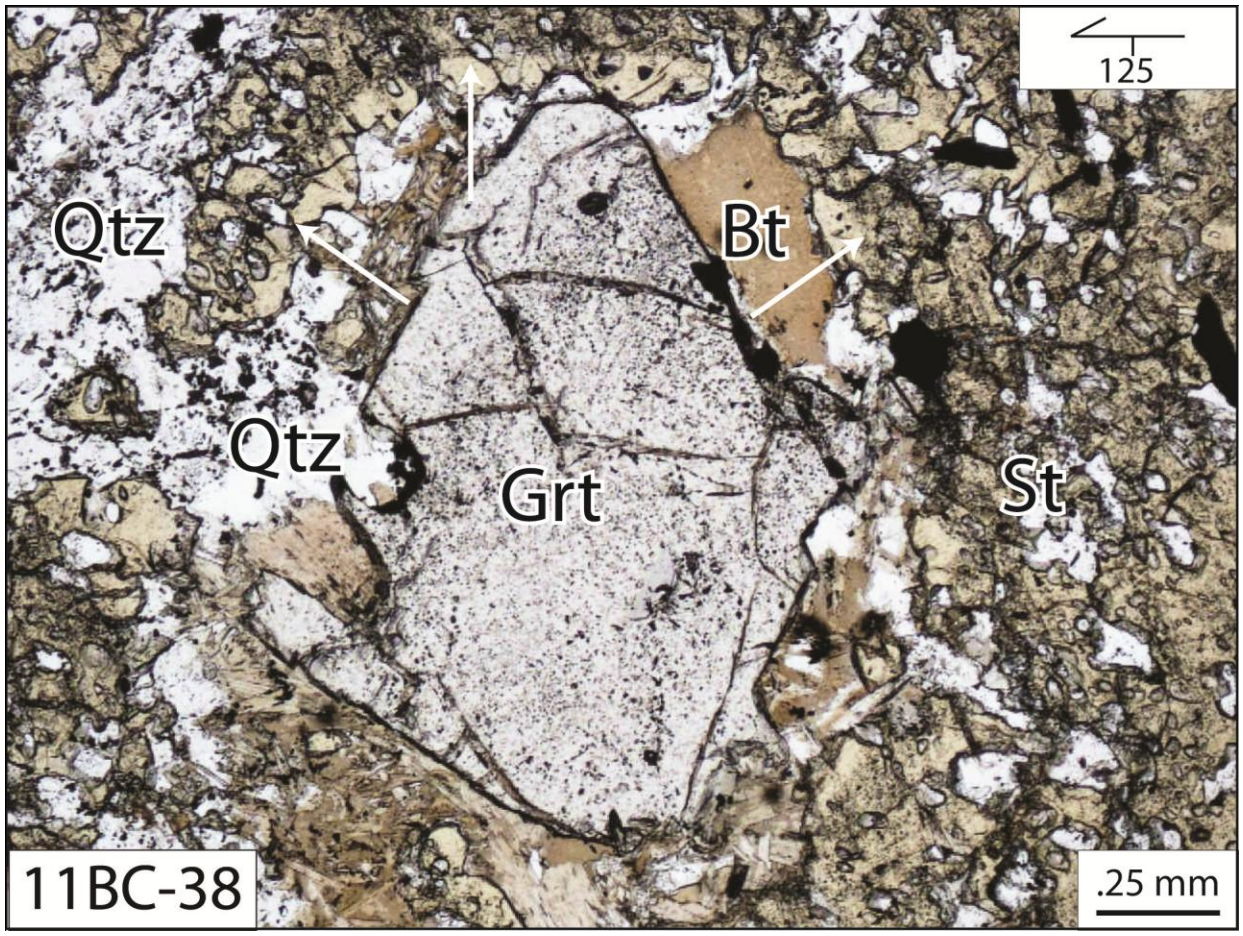

Figure 10. Photomicrograph from the Bryson City dome. The orientation marks define trend and plunge of the lineation for each section where present; otherwise, the samples were cut parallel to the prevailing lineation of the outcrop. Garnet included in staurolite. Notice inclusion-poor portion of staurolite in the shape of garnet. Bt, biotite; Grt, garnet; Qtz, quartz; St, staurolite.

in a similar pattern to the staurolite inclusion trails. Kyanite grains are commonly bent and sometimes display deformation kinks likely related to D_3 deformation (Massey and Moecher, 2005). Anhedral garnet porphyroblasts in the matrix contain inclusions of graphite, quartz, biotite, and opaque minerals with similar inclusion trails to those of sample 11BC-A. No shear-sense indicators were observed in this sample. Quartz grains have lobate grain boundaries and undulose and patchy extinction indicating deformation temperature of 500-600° C (Table 2)(Stipp et al., 2002). Nondescript, randomly oriented needles ~10 μm long mainly concentrated at plagioclase grain boundaries may be sillimanite or staurolite. Observable retrograde reactions include the breakdown of biotite and kyanite to sericite.

Great Smoky Group of the Bryson City dome near Sherrill Gap (11BC-4B, 11BC-3A, and11BC-45)

Sample 11BC-4B (35.4468°, -83.4656°) was collected ~12 m structurally above the contact with the granitic orthogneiss and is a pelitic schist containing anhedral garnet porphyroblasts (Fig. 8). Compositional segregation between a mica-rich schistose portion and a quartz/plagioclase-rich portion is interpreted as compositional variation (S_1) and is parallel to S_2. The S_2 foliation (217°, 85° NW and 17° →237°) is defined by muscovite, biotite, and elongate plagioclase grains. The width to length ratio of flattened plagioclase grains range from 5:1 to 10:1 (Kish et al., 1975). Accessory minerals include apatite, monazite, zircon, and various opaque minerals. The sample is cut by a micro-brittle normal fault (Fig. 11). A brecciated fault surface of quartz and plagioclase 0.24 to 2.84 mm wide cuts oblique to S_2. Mica grains near the fault are deflected toward the fault surface. A single garnet porphyroclast has been cleaved in two along the fault surface and is heavily fractured as a result. Some muscovite and biotite grains in the mica-rich portion are kinked, which appears to be related to the brittle deformation in the sample. No ductile shear sense indicators were observed in this sample. Quartz grains

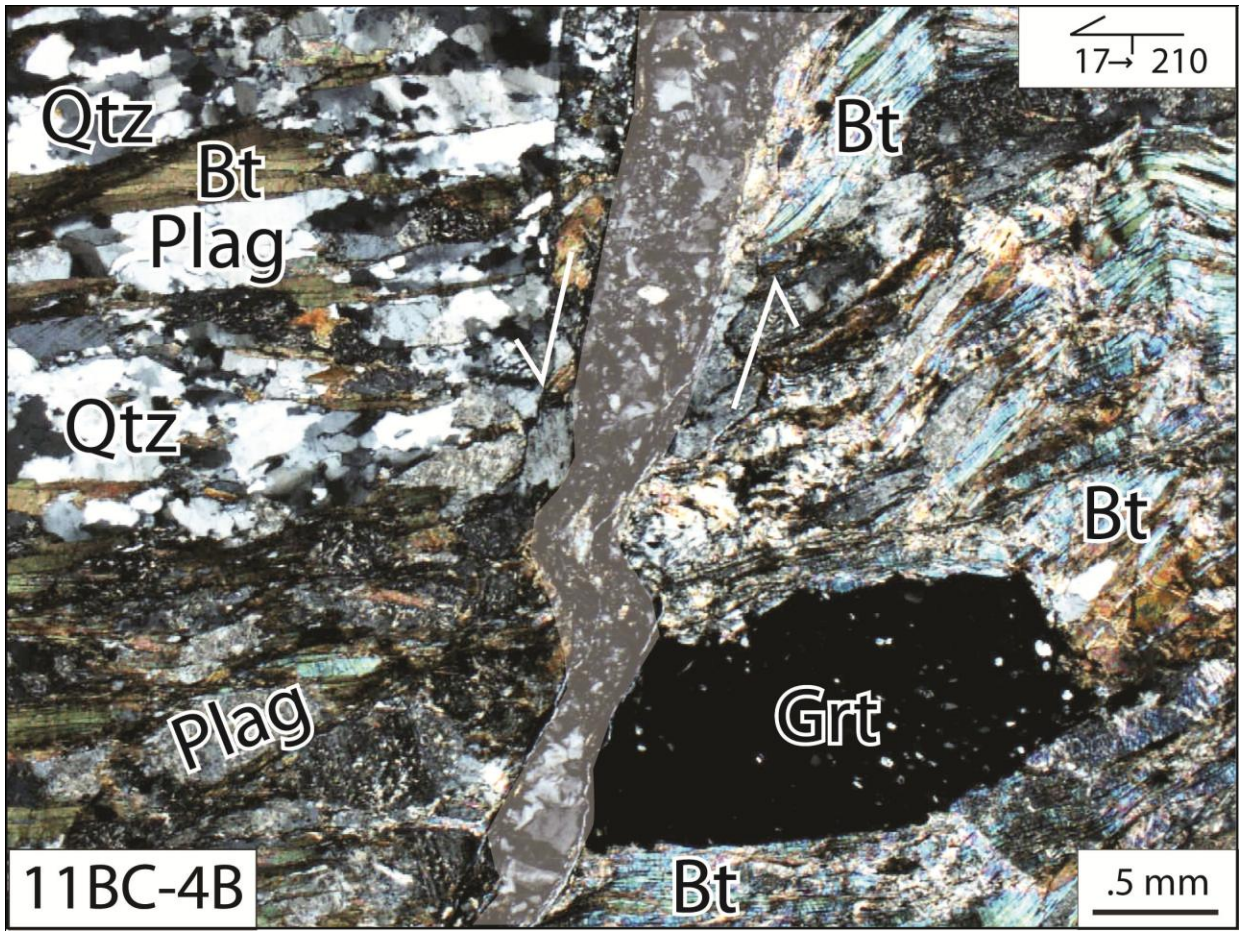

Figure 11. Photomicrograph from the Bryson City dome. The orientation marks define trend and plunge of the lineation for each section where present; otherwise, the samples were cut parallel to the prevailing lineation of the outcrop. Cataclasite vein from a brittle normal fault. Garnet has been faulted. Plag, plagioclase, Bt, biotite; Grt, garnet; Qtz, quartz.

have lobate boundaries characteristic of GBM, which indicate deformation temperatures of 500-600° C (Stipp et al., 2002)(Table 2). Retrograde reactions in the sample include chloritization of biotite, mainly near the fault surface; and plagioclase grains are partially to completely altered to fine-grained white mica.

Sample 11BC-3A (35.4468°, -83.4656°), collected from the Greenbrier fault, is a pelitic schist with subhedral garnet porphyroblasts (Fig. 8). It was sampled ~23 m structurally above the contact with the granitic orthogneiss. Garnet porphyroblasts are set in a foliated matrix (S_2) (212°, 81° NW and 11° → 242°) defined by muscovite, biotite, and flattened plagioclase grains. Accessory minerals are graphite, tourmaline, apatite, monazite, zircon, and various opaque minerals. Garnet porphyroblasts contain an inclusion-rich inner core, an inclusion-poor outer core, and an outer rim of inclusions aligned tangent to the garnet faces. Relict S_{1i} is preserved as linear inclusion trails of quartz and opaque grains in the inner core of garnet porphyroblasts. In the matrix, S_1 is deformed into isoclinal microfolds defined by biotite and muscovite with fold axes that are parallel to S_2 (Fig. 12a). Chlorite occurs throughout the sample as retrograde replacement of biotite, and plagioclase cores are commonly altered to fine-grained white mica. Top-to-the-northeast shear sense is defined by garnet sigma structures, C'-type shear-sense indicators, and mica fish (Fig. 12b; Table 2). Quartz grains have undulose extinction and lobate grain boundaries indicating deformation temperatures of 500-600° C (Table 2)(Stipp et al., 2002).

Sample 11BC-45 (35.4431°, -83.4731°) is a pelitic schist with porphyroblasts of garnet, kyanite, and staurolite set in a foliated (043°, 71° SE) matrix of biotite and muscovite interlayered with plagioclase and quartz (Fig. 8). Kyanite and staurolite are aligned parallel to the main foliation (S_2) but do not define a lineation in the sample. A younger S_3 foliation (210°,

Figure 12. Photomicrographs from the Bryson City dome. The orientation marks define trend and plunge of the lineation for each section where present; otherwise, the samples were cut parallel to the prevailing lineation of the outcrop. (A) Isoclinal micro-folds that define S_2 in schist. (B) Garnet sigma structure with top-to-the northeast shear sense. Plag, plagioclase, Bt, biotite; Grt, garnet; Qtz, quartz.

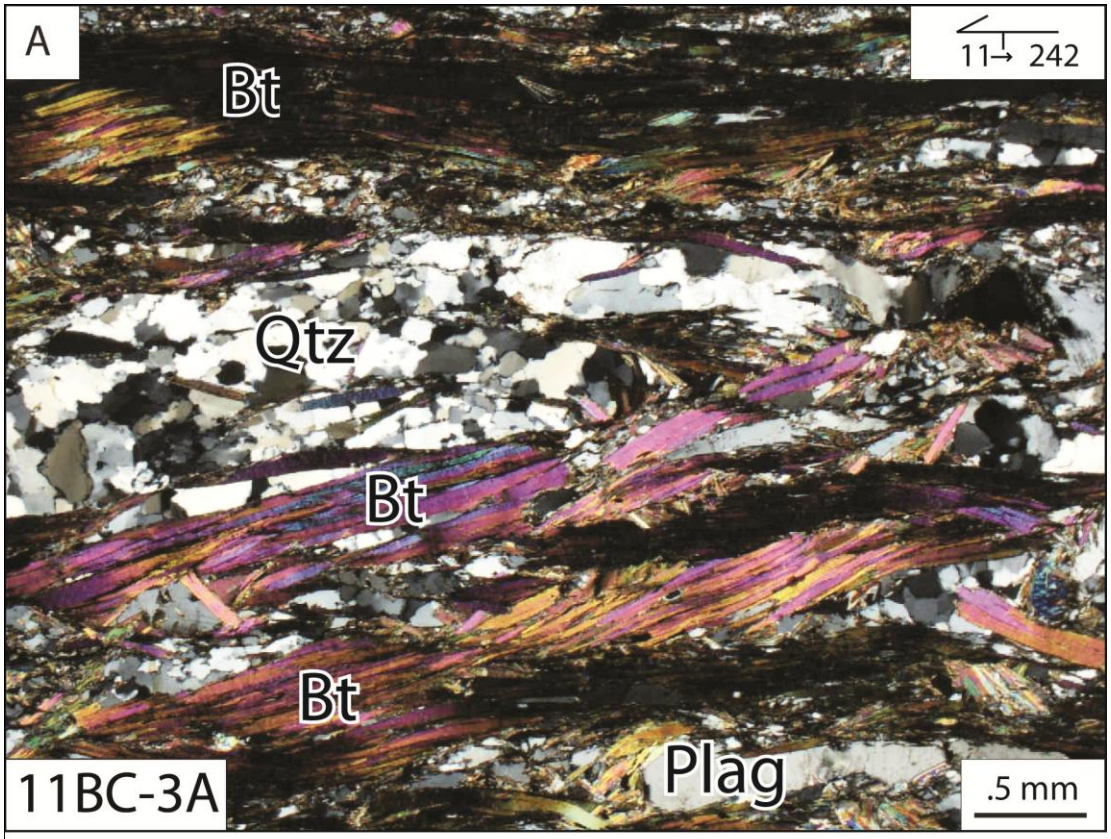
A
11→ 242
Bt
Qtz
Bt
Bt
Plag
11BC-3A
.5 mm

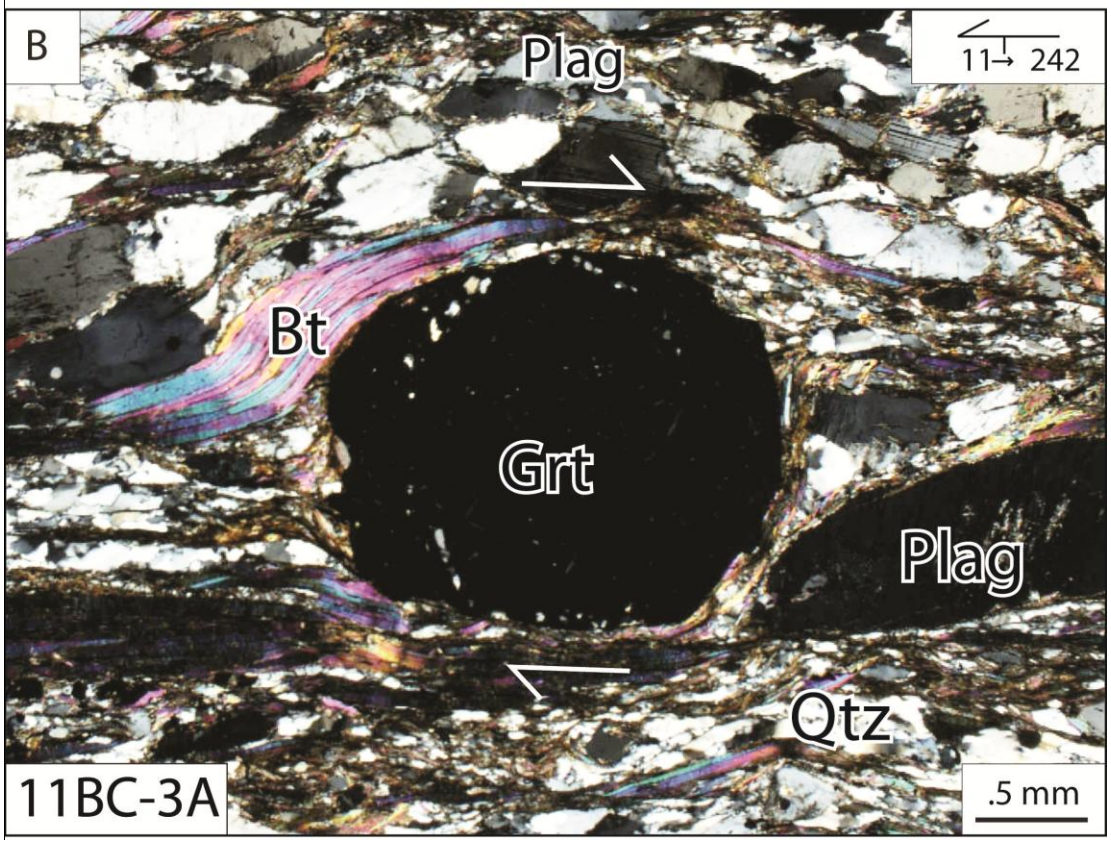
B
11→ 242
Plag
Bt
Grt
Plag
Qtz
11BC-3A
.5 mm

31° NW) overprints S_2 and is associated with a crenulation lineation (9° → 030°). Garnet porphyroblasts are observed in the matrix and as inclusions within kyanite blades. The porphyroblasts lack strain shadows and the foliation is weakly deflected around the grains. Although the porphyroblasts are commonly less inclusion-rich than observed in other samples collected around Bryson City, their trails conform to those observed in other samples. Graphite, apatite, monazite, zircon, and opaque minerals occur throughout the sample. Kyanite grains are partially altered to fine-grained mica as is commonly observed in kyanite-bearing samples from the study area. Randomly oriented, ~10 μm long needles that nucleated at plagioclase grain boundaries may be sillimanite or staurolite. No shear-sense indicators were observed in this sample. Quartz and plagioclase grains exhibit lobate grain boundaries both intergranularly and intragranularly. Quartz also displays sweeping and checkerboard extinction, which has been attributed to the combination of basal <a> and prism <c> slip or the α-β transition in quartz, suggesting deformation temperatures >650° C (Fig. 13; Table 2)(Kruhl, 1996; Stipp et al., 2002).

Grenville rocks collected from the Greenbrier fault around Bryson City near Sherrill Gap (11BC-5, 11BC-8, 11BC-9, 11BC-33)

Sample 11BC-5 (35.4465°, -83.4648°) is a granitic protomylonite collected ~56 m structurally below the contact between the Grenville basement and the Great Smoky Group (Fig. 8). The sample contains augen of k-feldspar up to 2 cm long with an aspect ratio of 2:1. Symmetric augen are flattened parallel to the dominant mylonitic foliation and lineation (210°, 76° NW and 21°→ 225°), which is defined by biotite set in a matrix of quartz, plagioclase, microcline, and epidote. Although the k-feldspar augen appear to be single grains, petrographic analysis reveals the augen to be made up of numerous crystallized anhedral grains. K-feldspar grains range in size from 0.26-1 mm, with the largest grains concentrated in the augen.

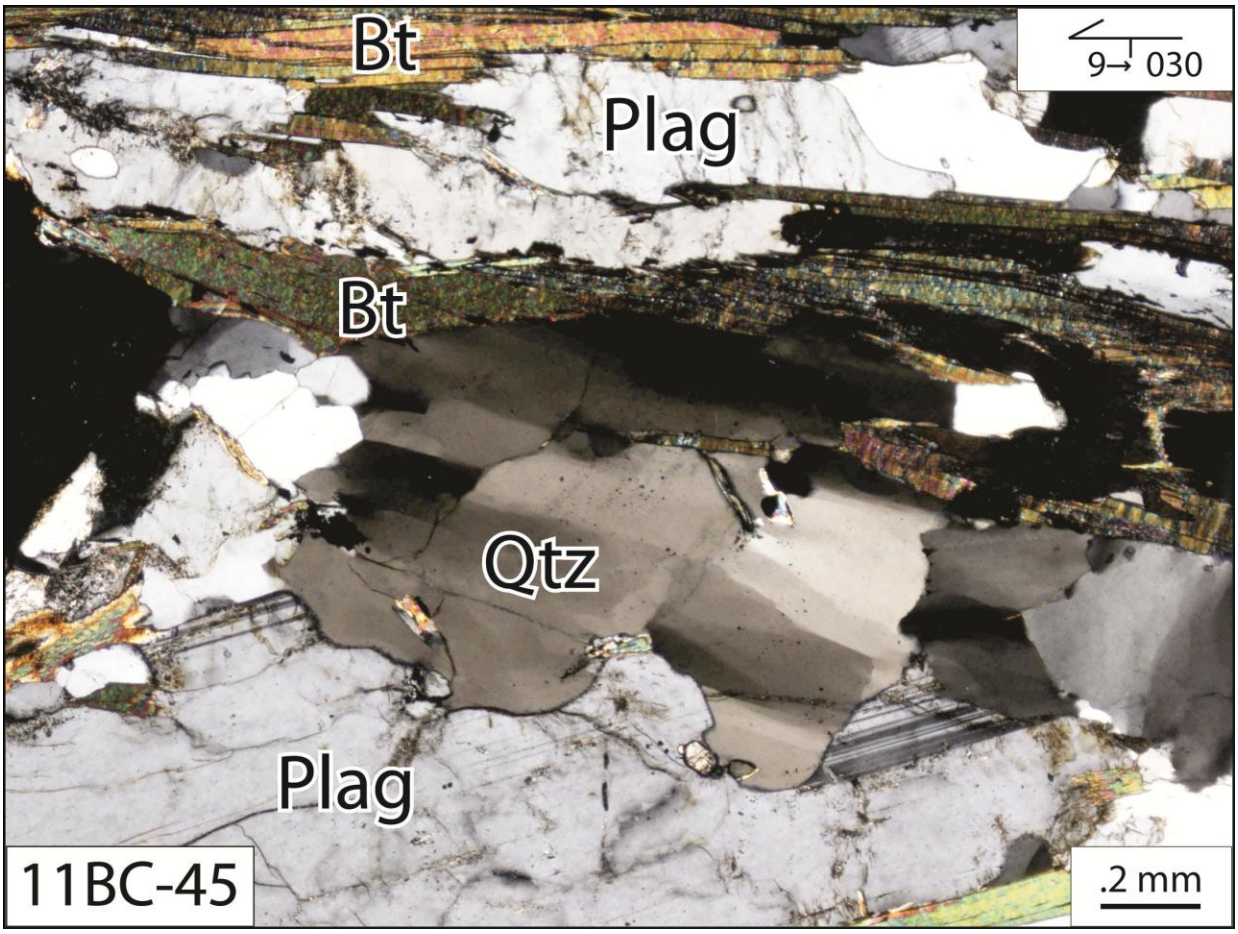

Figure 13. Photomicrograph from the Bryson City dome. The orientation marks define trend and plunge of the lineation for each section where present; otherwise, the samples were cut parallel to the prevailing lineation of the outcrop. Dynamically recrystallized quartz displaying checkerboard extinction. Plag, plagioclase, Bt, biotite; Qtz, quartz.

Perthite is rare but present in the sample. Similar to the pelitic samples, quartz grains exhibit lobate grain boundaries consistent with deformation temperatures of 500-600° C (Table 2)(Stipp et al., 2002). Quartz grains are seriate in size ranging from 0.14–1.27 mm, and they have an average diameter of 0.52 mm. Sigma-type shear-sense indicators of epidote aggregates define a top-to-the-northeast shear sense (Fig. 14a; Table 2). Feldspar grains in the sample are commonly altered to fine-grained white micas.

Sample 11BC-8 (35.4465° - 83.4641°) is a granitic mylonite sample collected ~92 m from the contact with the Great Smoky Group (Fig. 8). The paragenesis of the sample is quartz, biotite, muscovite, plagioclase, K-feldspar, and epidote. Perthitic textures are rare but present in the sample. A mylonitic foliation (220°, 79° NW and 20° → 230°) is defined by aligned muscovite and plagioclase grains. K-feldspar and quartz grains are seriate in size, ranging from 0.7-1.6 mm and 0.03-0.60 mm, respectively. The average quartz grain size is 0.20 mm in diameter. Quartz grain boundaries are irregular, commonly exhibiting lobate shapes with limited subgrains and sweeping undulose extinction (Fig. 14b). This indicates the sample is at the transition between recrystallization mechanisms of subgrain rotation and grain-boundary migration. The presence of subgrains is likely due to higher strain partitioning in the sample at similar temperatures to adjacent samples (Hirth and Tullis, 1992). The dominant deformation mechanism for the sample is GBM, indicating temperatures >500°C)(Table 2)(Stipp et al., 2002). Asymmetric strain shadows formed around aggregates of epidote show top-to-the-northeast shear sense (Table 2).

Sample 11BC-9 (35.4464° -83.4640°) is a granitic mylonite sampled ~100 m into the basement rocks (Fig. 8). The mylonitic foliation and lineation (230°, 73 NW° and 30° → 250°) is defined by biotite and muscovite interlayered with quartz, plagioclase, K-feldspar, epidote, and

Figure 14. Photomicrographs from the Bryson City dome. The orientation marks define trend and plunge of the lineation for each section where present; otherwise, the samples were cut parallel to the prevailing lineation of the outcrop. (A) Aggregate of epidote in deformed granitic protomylonite with top-to-the-northeast shear sense. (B) Dynamically recrystallized quartz from a granitic mylonite with lobate grain boundaries and sweeping undulose extinction. Plag, plagioclase; Ksp, K-feldspar; Ep, epidote.

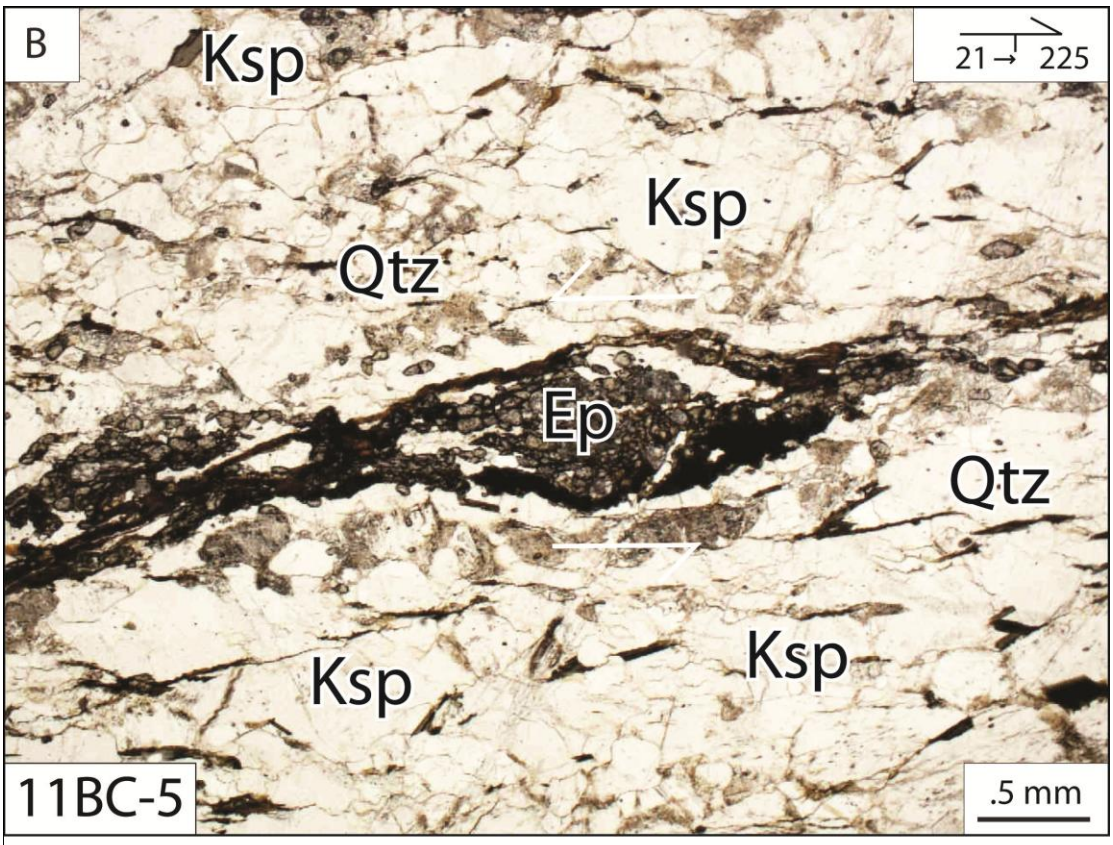
B
Ksp
21→ 225
Ksp
Qtz
Ep
Qtz
Ksp
Ksp
11BC-5
.5 mm

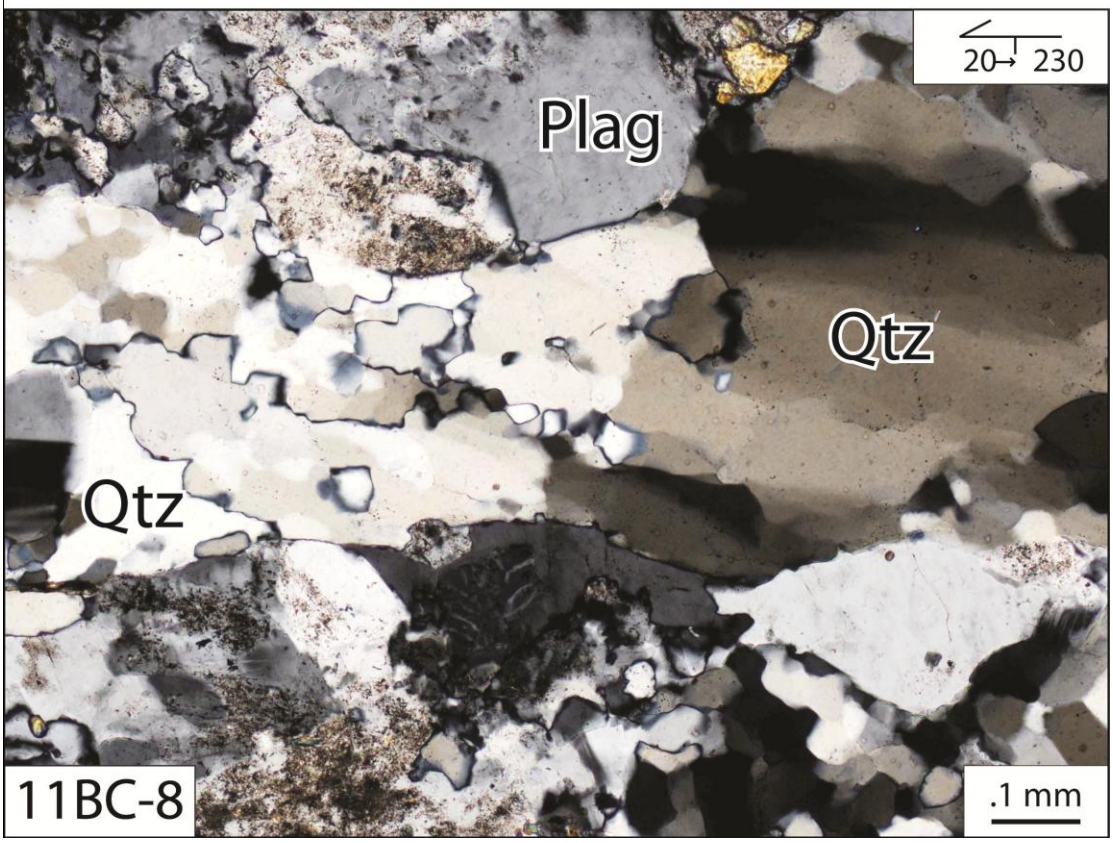
20→ 230
Plag
Qtz
Qtz
11BC-8
.1 mm

sphene. K-feldspar grains are typically mantled by finer grains of quartz and feldspar, and perthite is commonly observed throughout the sample. Quartz grains are elongated parallel to the foliation and commonly exhibit lobate grain boundaries indicating deformation temperatures of 500-600° C (Stipp et al., 2002). C'-type shear bands record top-up-to-the-northeast shear sense (Table 2).

Sample 11BC-33 (35.4251°, -83.4535°) is a deformed quartz monzonite sampled from the core of the Bryson City dome (Fig. 8). Despite the weakly deformed nature of the sample, its mineralogy is similar to the granitic rocks within the Greenbrier fault near Sherrill Gap. The sample contains a weak foliation (240°, 75° NW) defined by biotite laths set in a matrix of quartz, plagioclase, K-feldspar, epidote, rare perthite, and sphene. Both quartz and feldspar grains are inequigranular and commonly exhibit lobate grain boundaries, suggesting deformation temperatures of 500-600° C (Stipp et al., 2002) (Table 2). Quartz grains exhibit sweeping undulose extinction. Euhedral to subhedral imbricated K-feldspar grains are common in the sample and are typical of granitic texture (Fig. 15). Myrmekite is also common throughout the sample.

Great Smoky Group rocks of the Ela dome (11ED-4A, 11ED-8)

Sample 11ED-4A (35.4306°, -83.3989°) was collected from an outcrop of the Greenbrier fault along the southwestern tip of the Ela dome (Fig. 8). The sample is a pelitic S-C mylonitic schist containing the mineral assemblage quartz, biotite, muscovite, and plagioclase. Biotite and muscovite are the main foliation-defining minerals (055°, 23° SE and 5° → 054°). The mylonite foliation is parallel to S_2 as well as to the contact between the metasedimentary Great Smoky Group and the granitic core of the Ela dome. Apatite, monazite, and opaque minerals occur throughout the matrix. S-C, C', and mica fish record top-to-the-northeast shear sense (Table 2).

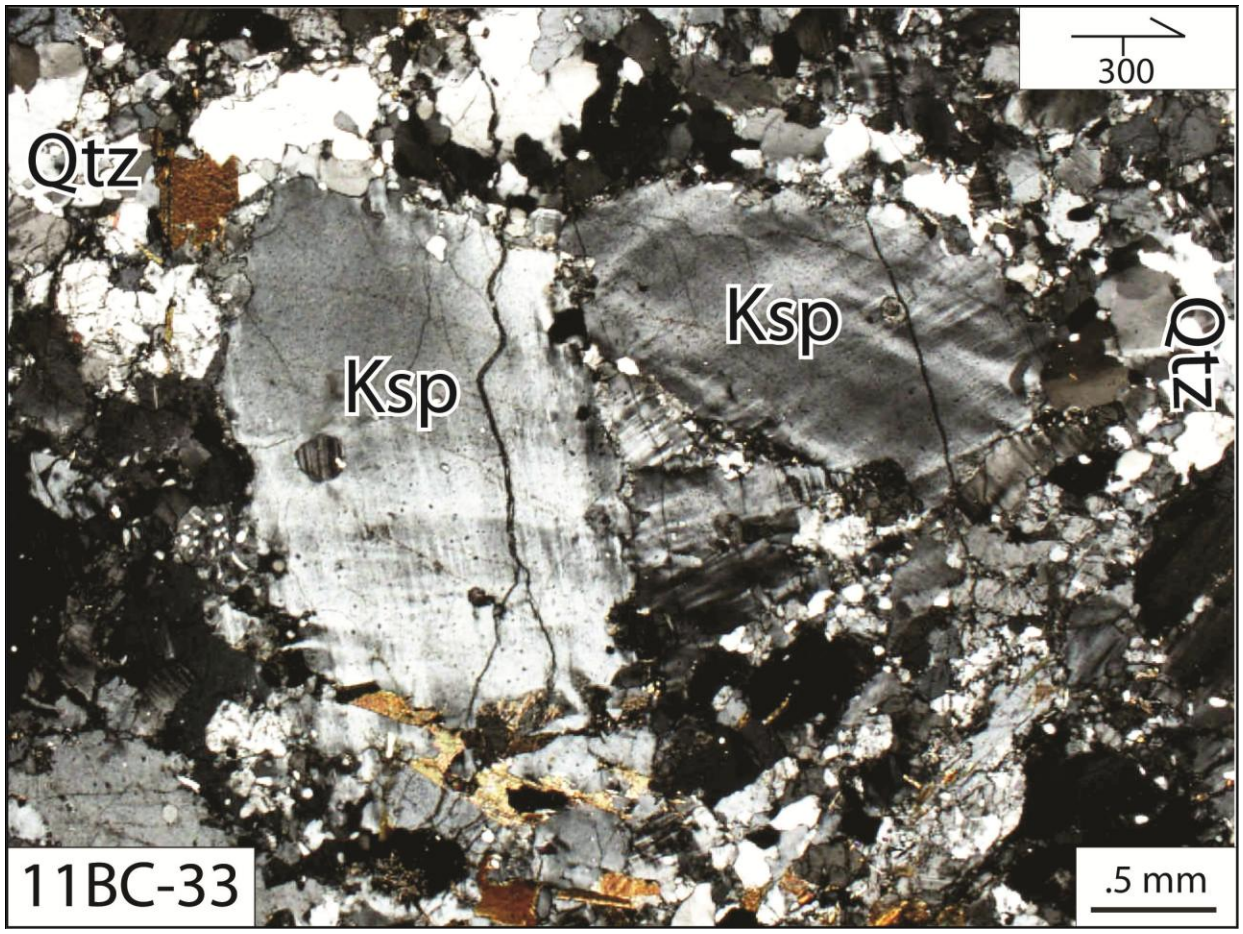

Figure 15. Photomicrograph from the Bryson City dome. The orientation marks define trend and plunge of the lineation for each section where present; otherwise, the samples were cut parallel to the prevailing lineation of the outcrop. Subhedral imbricated K-feldspar grains in weakly deformed granite. Qtz, quartz; Ksp, K-feldspar.

Quartz grains have lobate grain boundaries, and some grains have sweeping undulose extinction. The sample is cut by a 0.67 mm-wide vein of micro-breccia and pseudotachylite that parallels the main foliation (Fig. 16a). The vein is opaque in cross-nicols; stained yellow in plane polarized light; contains angular to semi-rounded quartz and feldspar grains less than 100 μm in size; and along its length grades into a fine breccia. No mesoscale fault related to the vein is observed in the field. Unlike the brittle structure in sample 11BC-4B, no deflection of the foliation occurs in the sample.

Sample 11ED-8 (35. 4291° -83.4005°) is a pelitic schist with subhedral garnet porphyroblasts set in a foliated matrix (041°, 54 SE°) defined by biotite, muscovite, and flattened feldspars interlayered with anhedral quartz and plagioclase (Fig. 8). The sample was collected from the S-C schist portion of the Greenbrier fault in the Great Smoky Group on the southern edge of the Ela dome. Accessory minerals occurring throughout the matrix include apatite, monazite, zircon, and opaque minerals. Additionally, sillimanite occurs in the sample as randomly oriented, ~10 μm-long needles arranged in bundles and clusters that nucleated at feldspar grain boundaries. Their composition was confirmed by EMPA. Crenulation folds related to D_3 deformation define a second foliation (S_3) that is subparallel to the mylonitic foliation (010°, 45°). Garnet porphyroblasts contain inclusion patterns similar to those observed in garnet-bearing samples around the Bryson City dome. An inclusion-rich inner core is surrounded by an inclusion-poor outer core and an inclusion-rich rim. Garnet inclusions are quartz, apatite, monazite, and opaque grains. S-C and C' type shear bands record top-to-the-northeast shear sense. Porphyroblasts of garnet and porphyroclasts of plagioclase are mantled by asymmetric strain shadows that record top-to-the-northeast shear (Fig. 16b; Table 2).

Figure 16. Photomicrographs from the Ela dome. The orientation marks define trend and plunge of the lineation for each section where present; otherwise, the samples were cut parallel to the prevailing lineation of the outcrop. (A) Vein of pseudotachylite from small brittle faults in the Greenbrier fault hanging wall. (B) Garnet sigma structure with top-to-the-northeast shear sense. Plag, plagioclase; Bt, biotite; Grt, garnet; Qtz, quartz.

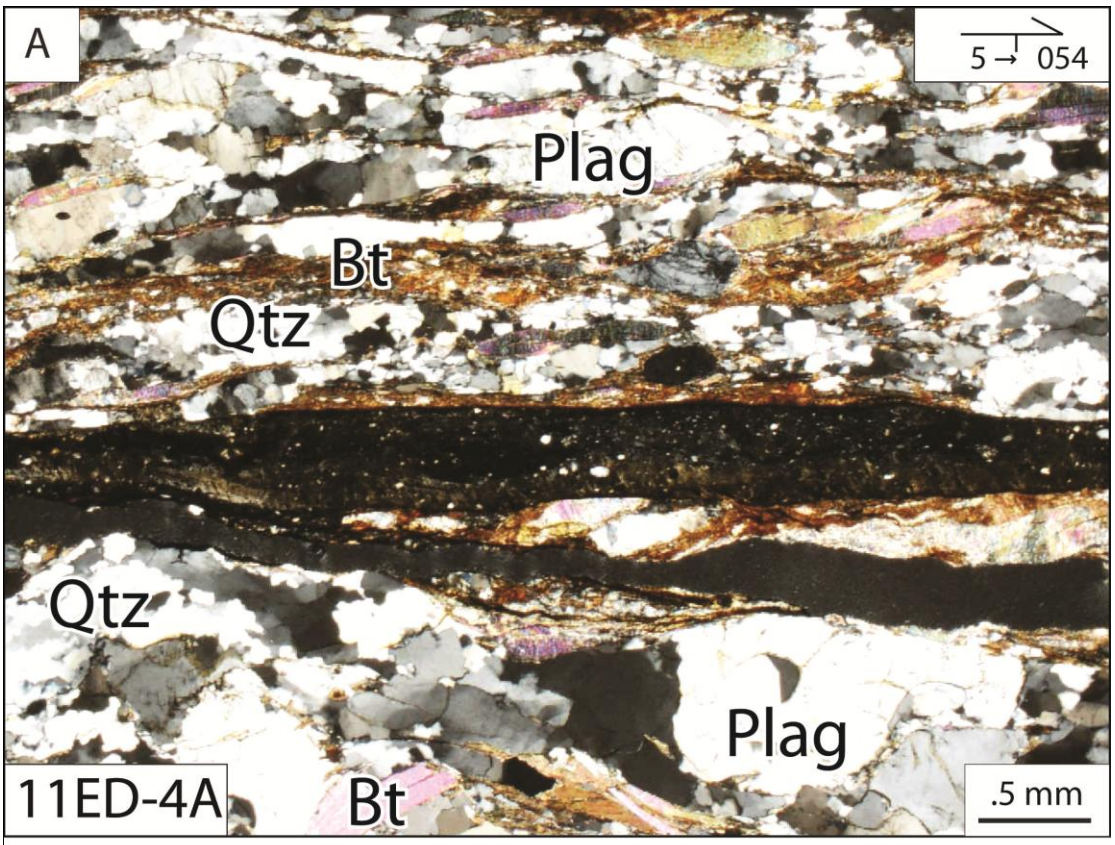
A
5 → 054
Plag
Bt
Qtz
Qtz
Plag
11ED-4A
Bt
.5 mm

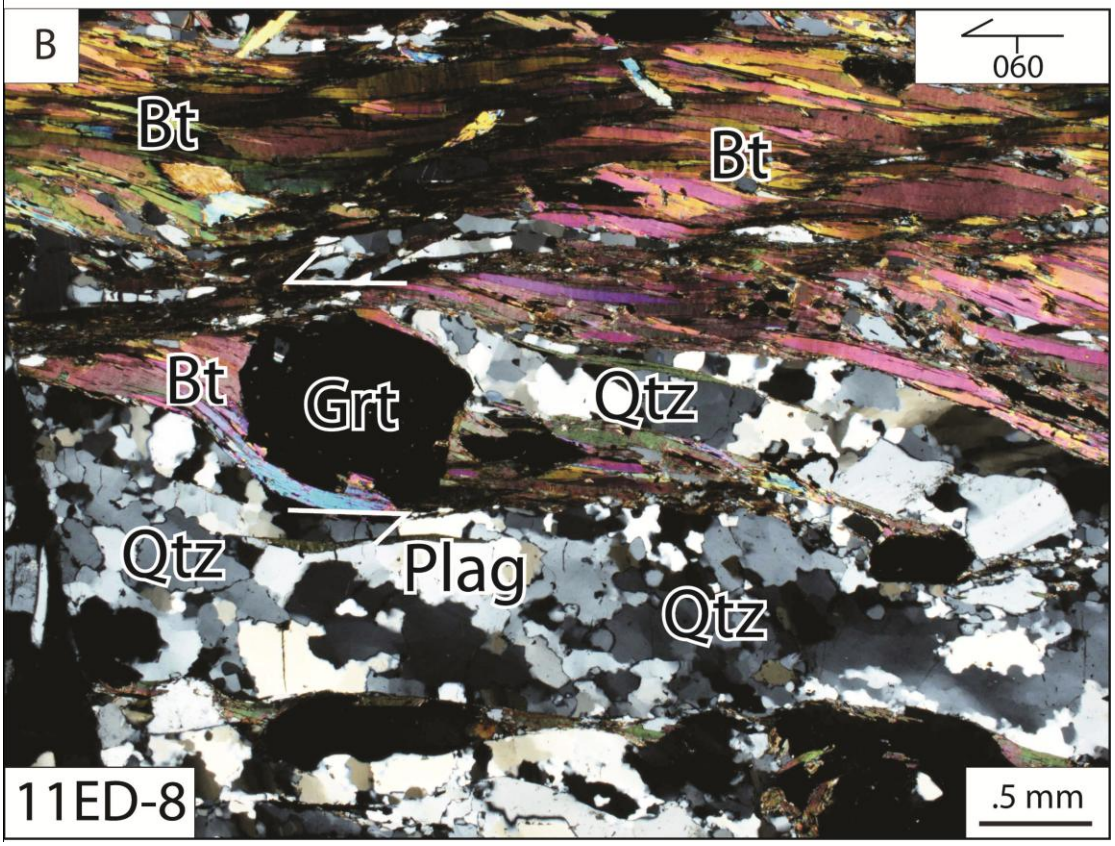
B
060
Bt
Bt
Bt
Grt
Qtz
Qtz
Plag
Qtz
11ED-8
.5 mm

Quartz grains have lobate grain boundaries, indicating deformation temperatures of 500-600° C (Table 2)(Stipp et al., 2002).

Grenville rocks collected from the Greenbrier fault around the Ela dome (11ED-2)

Sample 11ED-2 (35.4307°, -83.3989°) is a paragneiss collected from the Greenbrier fault ~1 m below the contact between the Great Smoky Group and the Grenville basement (Fig. 8). The mylonitic foliation (039°, 50 SE° and 35° → 184°) in the sample is defined by muscovite and biotite grains set in a fine-grained matrix of quartz, plagioclase, and K-feldspar. K-feldspar commonly exhibits myrmekite development in the high-strain regions at the grain edges. Garnet grains in the sample are highly fractured, resorbed, and distributed along the foliation. Epidote and sphene occur as accessory minerals. Quartz grains are seriate in size and commonly exhibit lobate boundaries, although some grains display triple junctions, suggesting partial annealing of the sample. Shear bands record top-down-to-the south shear sense (Table 2).

CHAPTER 4

METAMORPHISM AND THERMOBAROMETRY

Methods

Polished thin sections were prepared by cutting samples perpendicular to the foliation and parallel to the stretching lineation when present. Petrographic descriptions (Chapter 3) were conducted on an optical microscope, and opaque minerals were identified using reflected light. A Cameca SX-100 electron microprobe at The University of Tennessee, Knoxville, was used for quantitative spot analyses of select grains (e.g., garnet, biotite, muscovite, staurolite, and plagioclase) and qualitative X-ray imaging of garnet grains to characterize compositional variations and zoning patterns. All data were collected using an excitation voltage of 15kV. Point analysis of feldspar grains were obtained using a beam current of 10 nA and all other phases were analyzed using a beam current of 20nA. Garnet and staurolite grains were analyzed with a 1 μm spot size, while biotite, muscovite, and feldspar grain analyzes were performed at 5 μm. Peak and background counting times were 20 s for all elements except Ti and Y, which were 40 s. Natural and synthetic standards were used for calibration and ZAF corrections were performed according to the PAP procedure. X-ray maps of Mg, Y, Mn, and Ca were made for select garnet grains using a beam current of 40nA, 5 μm step size, and 100 ms dwell time. To test for compositional variations in other phases, EMP spot analyses were performed on grains adjacent to garnet porphyroblasts and on grains within the matrix located away from garnet porphyroblast. To avoid complications related to retrograde net transfer reactions with garnet, garnet compositions just inside the retrograde rim were used for P-T estimates (Kohn and Spear, 2000). Euhedral to subhedral garnet porphyroclasts with the least evidence of resorption were selected for analysis. In order to calculate P-T conditions, garnet analyses were combined with

analyses from biotite, muscovite, staurolite, and plagioclase grains that appeared to be in textural and chemical equilibrium.

The activity coefficients for each mineral phase were calculated by inputting quantitative chemical data from three samples into the AX software. Activities were then entered into the average P-T mode (Holland and Powell, 1998) of THERMOCALC v. 3.33, and P-T calculations were made using the updated Powell et al., (1998) data set (tc-ds55.txt).

4.1. Discussion of P-T estimates (results)

Sample 11BC-38 is a staurolite-kyanite schist sampled from the western side of the Bryson City dome (Fig. 8). It contains the prograde mineral assemblage quartz + biotite + muscovite + plagioclase + staurolite + kyanite (see Chapter 2). The sample exhibits textural relationships indicative of prograde metamorphism such as garnet inclusions in staurolite and garnet breakdown to biotite. Compositional X-ray maps and elemental zoning profiles were made for two select garnet grains from sample 11BC-38, one from the matrix (11BC-38m) and one included in staurolite (11BC-38i), in order to compare their growth histories (Fig. 17a,b).

The matrix garnet (Fig. 17a) displays a prograde growth zonation pattern characterized by a decrease in X_{Spss} and X_{Gross} and an increase in X_{Alm}, X_{Prp}, and Fe/(Fe+Mg) (Fe#) from the core to rim. A sharp decrease in X_{Spess} and X_{Gross} and an increase in X_{Alm} and X_{Prp} occur in the vicinity of an included biotite grain. A resorption rind, indicated by an increase in X_{Spss}, occurs within 150 μm of the garnet's rim. The anhedral nature and truncation of compositional zoning at the top and bottom of the garnet indicate partial resorption of the grain.

The inclusion garnet (Fig. 17b) has a low X_{Spss} and X_{Gross} interior that increases to within ~700 μm of the rim and then decreases towards the rim. X_{Alm} and X_{Prp} decrease from the core to the ~700 μm inversion point, at which point they increase toward the garnet rim.

Figure 17. X-ray composition maps and profiles of garnet grains of samples used to estimate pressure and temperature (P-T) conditions. Arrows on garnet profiles indicate the data point used in P-T estimates.

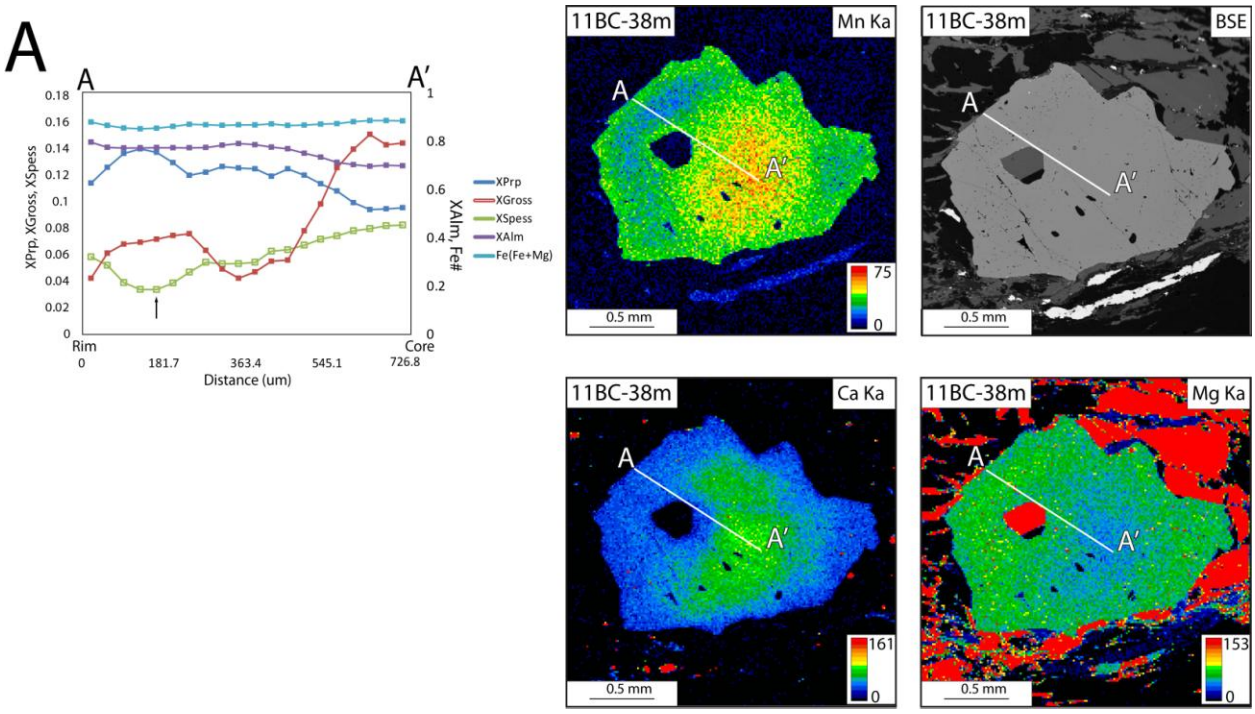
A
A
A′
0.18
0.16
0.14
0.12
0.1
0.08
0.06
0.04
0.02
0
XPrp, XGross, XSpess
1
0.8
0.6
0.4
0.2
0
XAlm, Fe#
XPrp
XGross
XSpess
XAlm
Fe(Fe+Mg)
Rim
Core
0
181.7
363.4
545.1
726.8
Distance (um)
11BC-38m
Mn Ka
A
A′
75
0
0.5 mm
11BC-38m
BSE
A
A′
0.5 mm
11BC-38m
Ca Ka
A
A′
161
0
0.5 mm
11BC-38m
Mg Ka
A
A′
153
0
0.5 mm

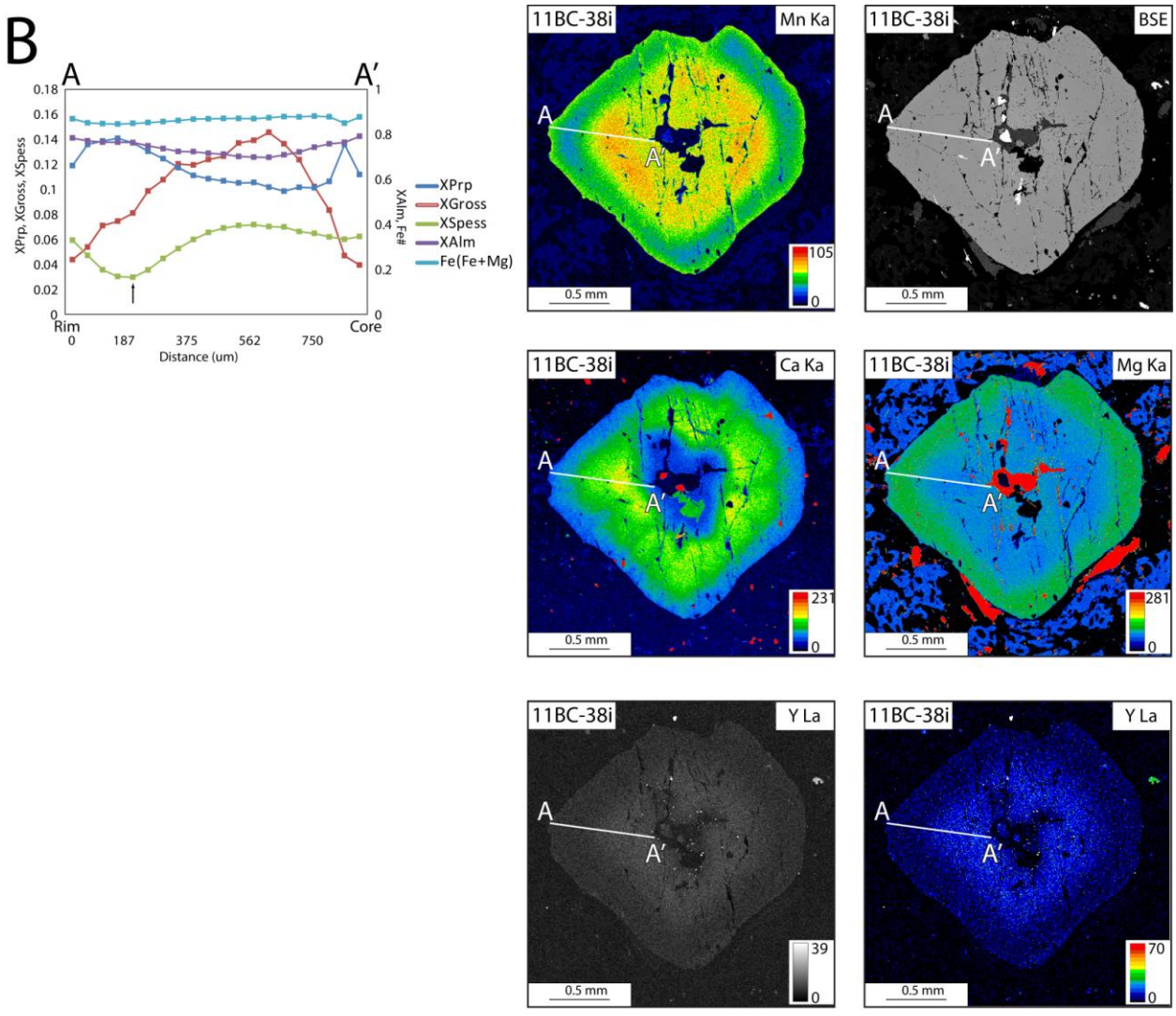
B
A
A′
0.18
0.16
0.14
0.12
0.1
0.08
0.06
0.04
0.02
0
XPrp, XGross, XSpess
1
0.8
0.6
0.4
0.2
0
XAlm, Fe#
XPrp
XGross
XSpess
XAlm
Fe(Fe+Mg)
Rim
Core
0
187
375
562
750
Distance (um)
11BC-38i
Mn Ka
105
0
0.5 mm
11BC-38i
BSE
0.5 mm
11BC-38i
Ca Ka
231
0
0.5 mm
11BC-38i
Mg Ka
281
0
0.5 mm
11BC-38i
Y La
39
0
0.5 mm
11BC-38i
Y La
70
0
0.5 mm

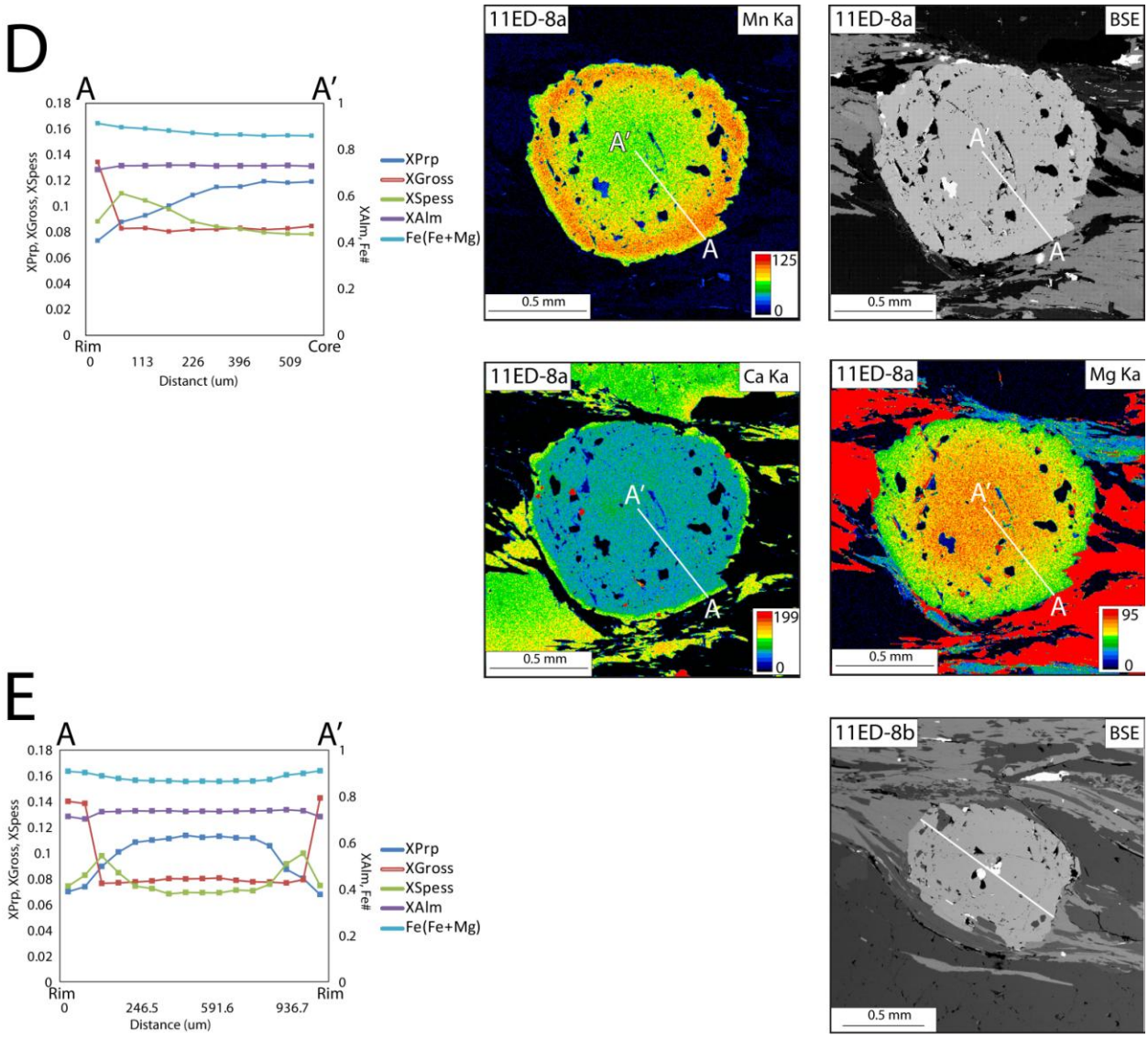
D
A
A′
XPrp, XGross, XSpess
XAlm, Fe#
XPrp
XGross
XSpess
XAlm
Fe(Fe+Mg)
Rim
Core
0
113
226
396
509
Distanct (um)
11ED-8a
Mn Ka
11ED-8a
BSE
11ED-8a
Ca Ka
11ED-8a
Mg Ka
0.5 mm
125
199
95
E
246.5
591.6
936.7
Distance (um)
11ED-8b
BSE

The garnet are characterized by a 150 μm post-peak metamorphic retrograde rind. The low X_{Spss} / X_{Gross} and high X_{Alm} / X_{Prp} interior of the garnet is interpreted as modifications of an originally prograde zoning pattern by diffusion of Mn, Ca, Fe, and Mg near biotite and plagioclase inclusions via the fractures that permeate the grain. The resulting composition is similar to the final stage of garnet growth. This interpretation is supported by the similarity between the composition of plagioclase and biotite inclusions to the composition of the matrix grains. A similar process likely caused the lower X_{Gross} values and higher X_{Alm} values observed near the biotite inclusion in the other garnet (11BC-38m; Fig. 17a). Biotite and muscovite throughout sample 11BC-38 show little chemical variation between grains, but biotite inclusions have lower Ti content. A transect across staurolite revealed little variation in chemistry. Plagioclase inclusions in garnet, plagioclase inclusions in staurolite, and matrix plagioclase all exhibit notable variation in An content from An1 to An31. Assuming plagioclase increased An content with increasing metamorphic conditions, the highest An value from a grain proximal to garnet was chosen for the P-T calculations. Since there were few chemical variations for matrix biotite, muscovite, and staurolite grains, an average of all analyses from these phases was used for thermobarometric calculations along with the lowest X_{spess} analysis from the matrix garnet (Appendix I). The combination of these data yields conditions of 654 ± 68 °C and 9.6 ± 1.2 kbar (Fig. 18; Table 4).

Since both garnets have similar zoning patterns, the phases inside staurolite grains should not have developed in an isolated system and should record similar P-T conditions to the matrix phases. To test this, a second P-T estimate for sample 11BC-38 was calculated using only biotite, muscovite, and plagioclase grains near the garnet inclusion in staurolite (11BC-38i) (Appendix I) and yielded pressure and temperature conditions of 606 ± 92 °C and 11.7 ± 1.8

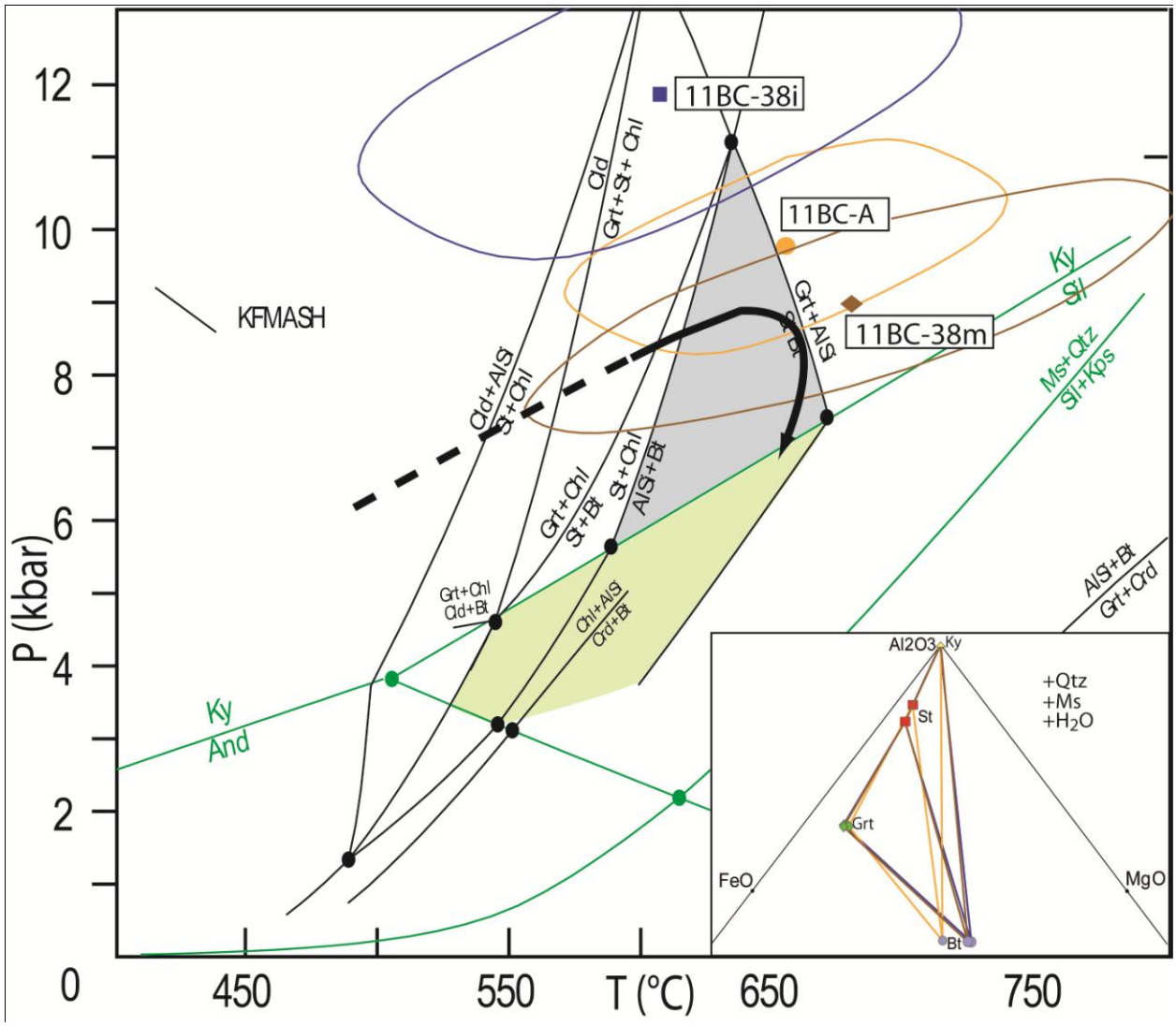

Figure 18. P-T estimates plotted against a petrogenetic grid for pelitic rocks in the KFMASH system (Holland and Powell, 1998). Grey indicates the kyanite-staurolite stability field. Green indicates the staurolite-sillimanite stability field. The P-T path is noted by the arrow. AFM diagram inset shows compositions of phases from samples 11BC-38m, 11BC-38i, and 11BC-A projected from muscovite. Ky, kyanite; And, andalusite; Sil, sillimanite; Grt, garnet; Cld, chloritoid; Chl, chlorite; Bt, biotite; Ms, muscovite; Qtz, quartz; Kps, K-feldspar; St, staurolite.

Table 4. Pressure-temperature estimates for Barrovian metamorphism

	THERMOCALC					
Sample	T (°C)	P (kbar)	Assemblage	Cor.	Fit	No. rxn
11BC-A	679 ± 101	8.8 ± 1.4	grt + ky + bt + ms + plag + qtz	.766	.69	5
11BC-38m	654 ± 68	9.6 ± 1.2	grt + st + ky + bt + ms + plag + qtz	.527	1.04	7
11BC-38i	606 ± 92	11.7 ± 1.8	grt + st + ky + bt + ms + plag + qtz	.538	1.55	7

THERMOCALC results calculated using the average P-T mode.
(Cor.) correlation coefficient; (Fit) standard deviation at 1σ; (No. rxn) number reactions used for P-T estimate.
Abbreviations: grt, garnet; st, staurolite; ky, kyanite; bt, biotite; ms, muscovite; plag, plagioclase; qtz, quartz.

kbar (Fig. 18). 11.7 kbar is likely an overestimate of pressure attributed to the absorbed nature of the plagioclase grains used in the calculations. An content of these grains is < XAn=10%, which suggests chemical disequilibrium of the phase with the surrounding minerals. This composition is consistent with all plagioclase grains included in staurolite.

Sample 11BC-A is a pelitic schist sampled from the northern flank of the Bryson City dome (Fig. 8). The sample contains the prograde mineral assemblage quartz + biotite + muscovite + plagioclase + kyanite (see Chapter 2). 11BC-A was chosen because of the following attributes: 1) its location relative to the Bryson City dome; 2) the presence of kinematic indicators; and 3) a mineral assemblage that records chemical equilibrium with minimal retrograde effects. Compositional X-ray maps and elemental zoning profiles of garnet from sample 11BC-A show a typical prograde zoning pattern for garnet porphyroblasts from the kyanite-staurolite Barrovian metamorphic zone (Figures 17c)(Tracy et al., 1976). X_{Spess} and X_{Gross} decrease from core to rim and X_{Spess} displays a bell-shaped curve (Spear, 1993). X_{Alm}, X_{Prp} and Fe# increase from core to rim. An increase in the X_{Spess} composition and a decrease in the X_{Prp} composition ~100 μm from the edge of the grain indicate late-stage retrograde diffusive modification (Kohn and Spear, 2000). There is no observable relationship between compositional zonation and the three distinct inclusion regions observed in the garnet. Little chemical variation was observed in biotite throughout the matrix grains. A single biotite grain

contained significantly lower Ti than all other grains, so the average value used in P-T calculations excluded the low Ti biotite grain. Similarly, muscovite grains showed little compositional variations throughout the sample with the exception of a few muscovite gains near a single garnet that had significantly higher Al contents. The Al values are considered anomalously high, and were excluded from the average chosen for P-T calculations. Transects across larger plagioclase grains demonstrated small compositional zonation characterized by an increase in An content from core (An_{23}) to rim (An_{27}), typical for rocks of this grade. Assuming the plagioclase grew during prograde metamorphism with increasing An content, the highest An value from the rim of a near-garnet plagioclase was used in the P-T calculations. These data were chosen in conjunction with the lowest Mg garnet composition to calculate P-T conditions (Appendix I). The data yielded P-T calculations of 679 ± 101° C and 8.8 ± 1.3 kbar (Fig. 18).

Sample 11ED-8 is a pelitic schist sampled within meters of the cover-core contact on the southwestern tip of the Ela dome (Fig. 8). It contains the prograde mineral assemblage quartz + biotite + muscovite + plagioclase + garnet. The sample is in the mylonite zone as indicated by the presence of asymmetrical tails on garnet (Fig. 16) and mica fish (see Chapter 2). The prograde mineral assemblage appears to be in textural equilibrium and is little affected by retrograde disequilibrium. Compositional X-ray maps (11ED-8a) and elemental zoning profiles (11ED-8a,b) of garnet from sample 11ED-8 show similar increases in X_{Spess} from the core to near the rim. This pattern is reverse to typical prograde growth zoning (Fig. 17d, e). Fe# increases from core to rim, typical of growth zoning. Both X_{Gross} and X_{Alm} show a generally flat unzoned interior interpreted as diffusion homogenization of the core at higher metamorphic conditions (Spear, 1991). A post-peak 50-100 μm retrograde rind is present as indicated by an inflection in zoning of X_{Spess}, X_{Prp}, X_{Alm}, and X_{Gross}. Again, no zoning variation is observed to coincide with

the three inclusion domains observed in the garnet grain. Compared with the other samples analyzed, the garnets from sample 11ED-8 have a distinctly different zoning pattern. This indicates that the sample experienced a different metamorphic history or reached conditions at which cation diffusion rates became significantly high enough to modify original growth zoning patterns (Yardley, 1977; Tracy, 1982; Spear, 1991). The zoning pattern of these garnets indicates that thermobarometric calculations on this sample could potentially be erroneous.

Textural evidence from a staurolite-kyanite schist sample (11BC-38) indicates a clockwise P-T path during prograde metamorphism. Following prograde garnet growth, the appearance of staurolite likely appeared via the reaction:

1) $Grt + Chl \pm Ms \rightarrow St + Bt$

The absorbed nature of most garnets and the presence of porphyroblastic biotite near the garnets support this interpretation. Renewed garnet growth and staurolite consumption likely occurred together with kyanite growth by the reaction:

2) $St + Bt \rightarrow As + Grt$

Reactions (1) and (2), along with the kyanite-sillimanite univariant line, bracket the peak metamorphic conditions for kyanite-grade rocks to 600-675° C and 6-12 kbar. The calculated P-T conditions for these rocks are in good agreement with the petrogenetic grid for schist in the KFMASH system (Fig. 18)(Spear et al., 1999).

4.2. *Metamorphic observations of the Great Smoky Group surrounding the Ela and Bryson City domes*

I used the metamorphic events outlined by previous authors to calibrate our investigation of the study area and to establish comparative events using 19 metapelitic and metagraywacke samples from around the Ela and Bryson City dome. These data make new contributions to the metamorphic evolution of the western Blue Ridge that began after a geologic map of the area

was produced (Hadley and Goldsmith, 1963). The chronology of deformation and metamorphic events established in this study correlates with the sequence and terminology established by Massey and Moecher (2005). M_1, which only affects the basement rocks, correlates to the Grenville metamorphic event and reached granulite facies as indicated by the presence of leucosomes. Correlative events include: inter-kinematic to syn-kinematic M_2 peak metamorphism, which lead to anatexis in the southern portion of the western Blue Ridge; a M_3 event represented by a post-kinematic event relative to S_2 occurring during D_3 deformation; and followed by a final static retrograde M_4 event.

M_2

In order to maintain consistency with previous investigations (Massey and Moecher, 2005), the earliest thermal event is referred to as M_2 metamorphism because of its temporal relationship to D_2. M_2 is a regional event that affected the western Blue Ridge and locally correlates to the kyanite-staurolite isograd. Pelitic rocks contain the prograde mineral assemblage biotite + muscovite + garnet + kyanite + staurolite. Eight of the 17 garnet-bearing schist samples (e.g., 11BC-45;46;47 and 11ED-1;3;6;9;18) show two-stage garnet growth indicated by a second generation of smaller, inclusion-free garnets (Fig. 19a). The larger garnets commonly exhibit strain shadows, while the smaller grains do not exhibit strain shadows, indicating growth occurred post-S_2 development. S_2 wraps around index minerals of staurolite, kyanite, and garnet. A few kyanite-staurolite bearing samples contain garnet as inclusions in larger kyanite and staurolite blades (Fig. 19b,c). Additionally, kyanite and staurolite grains are randomly aligned when viewed on the foliation surface (Fig. 19d). Since the rocks around the Ela and Bryson City domes did not reach sillimanite grade, development of fibrolite and tabular prismatic sillimanite consistent with the M_{2B} event described by Massey and Moecher (2005) is

Figure 19. Photomicrographs from the Ela and Bryson City domes. The orientation markers define the trend and the plunge of the lineation for each section where present; otherwise, the samples were cut toward the prevailing lineation of the outcrop. (A) Two generations of garnet, with one larger inclusion-rich grain and one smaller inclusion-poor grain. (B) Garnet included in kyanite blade. Kyanite shows deformation kink bands. (C) Garnet included in staurolite. (D) Random aligned kyanite in the plane of S_2 foliation. Bt, biotite; Ms, muscovite; Grt, garnet; Qtz, quartz; St, staurolite.

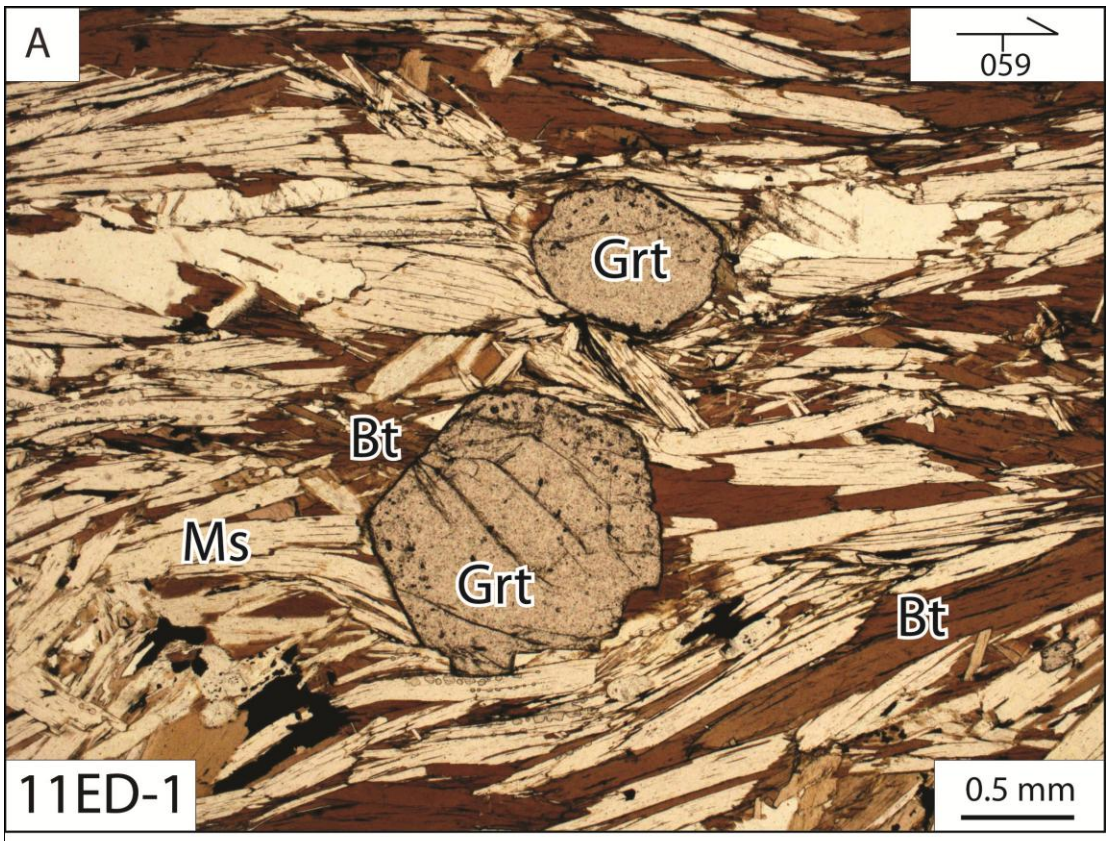
A
059
Grt
Bt
Ms
Grt
Bt
11ED-1
0.5 mm

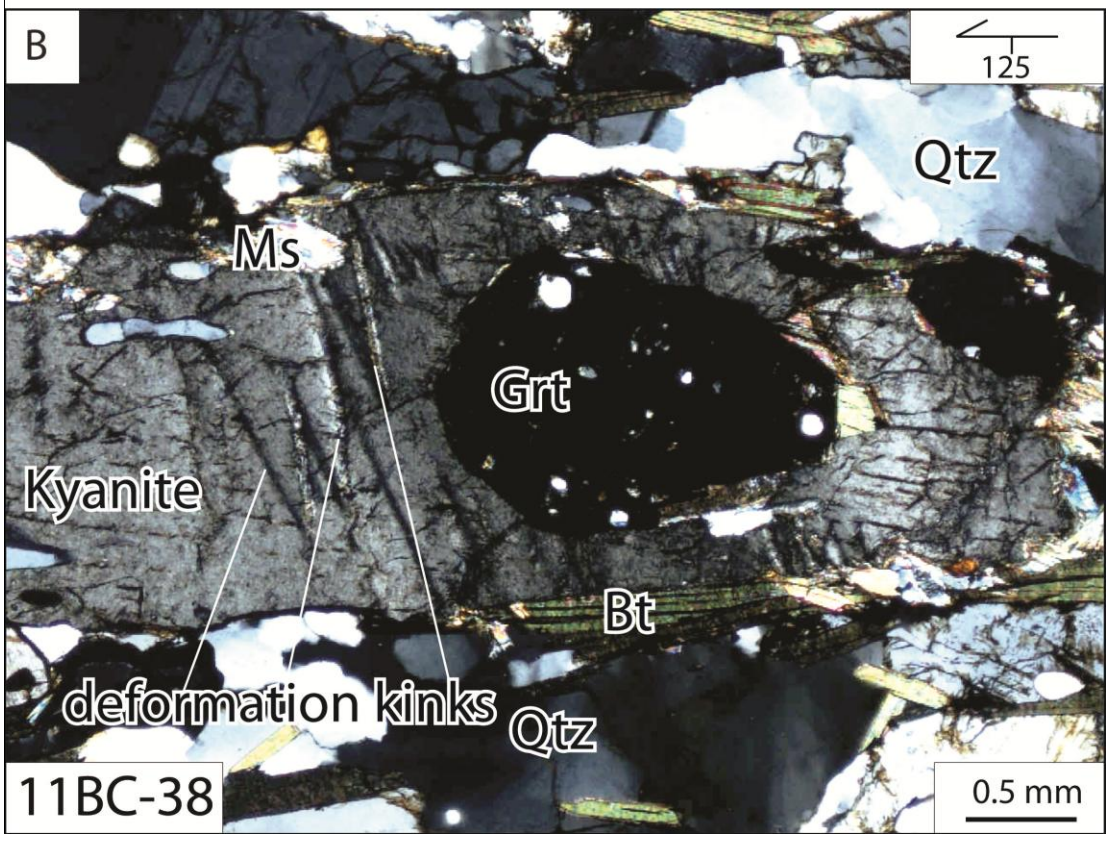
B
125
Qtz
Ms
Grt
Kyanite
Bt
deformation kinks
Qtz
11BC-38
0.5 mm

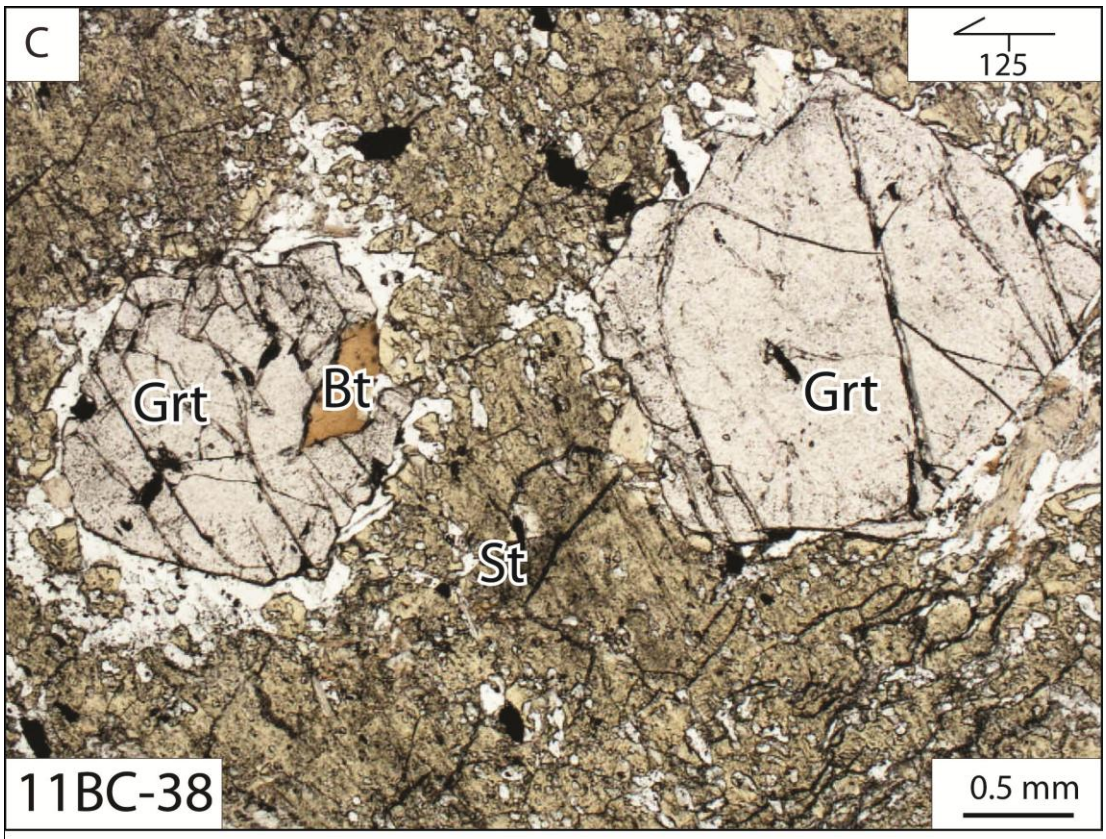
C
125
Grt
Bt
Grt
St
11BC-38
0.5 mm

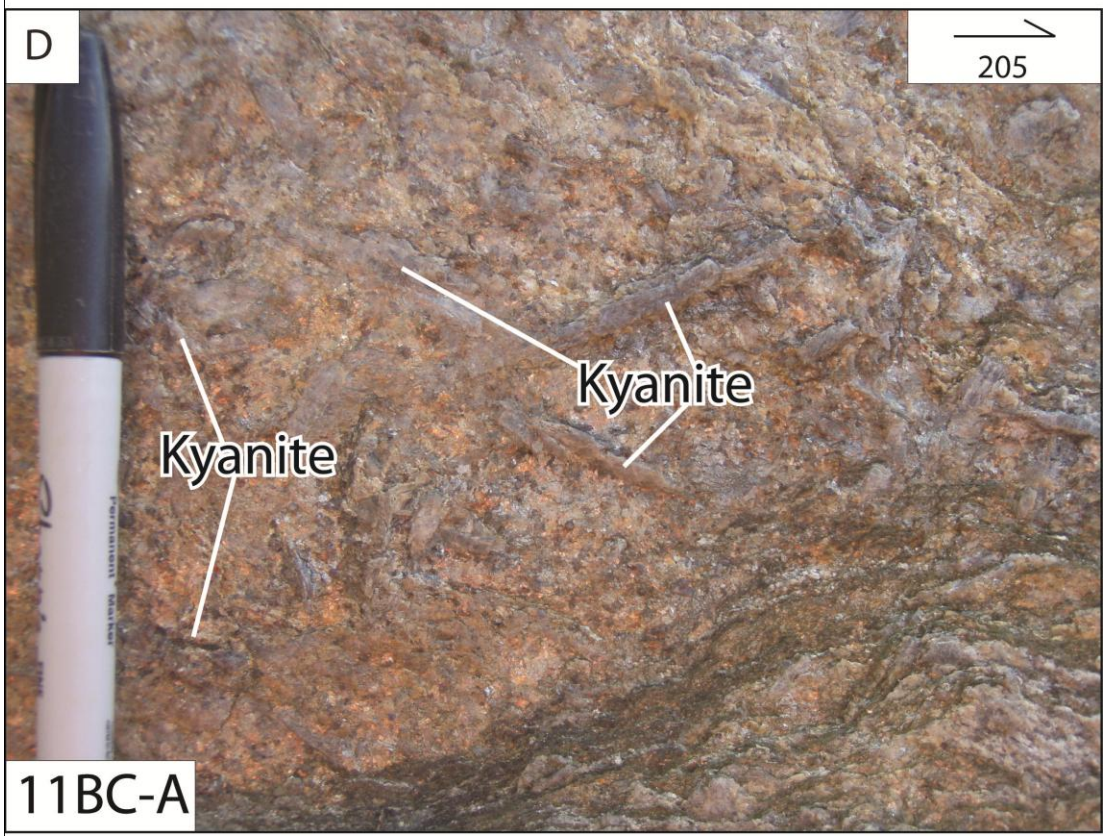
D
205
Kyanite
Kyanite
11BC-A

not directly observed. However, the two stages of garnet growth described above are consistent with the occurrence of a second-stage M_2 event. Original subhedral grain boundaries from the first growth stage are overgrown by a second stage of growth (Fig. 20a). The irregular nature of the original grain boundaries suggests dissolution of garnet occurred before the second stage of growth. Garnet zoning patterns are truncated by biotite grains that are interpreted to have grown during M_2 metamorphism since they are aligned parallel to the main foliation (Kohn and Malloy, 2004). These biotite grains commonly contain an increased amount of monazite inclusions compared to matrix grains (Fig. 20b). During their growth, monazite utilized the Y stored in garnet. X-ray maps of Y in garnets from sample 11BC-38i reveal a high-Y core and a Y-poor rim (Fig. 17b). The depleted rims are interpreted to preserve the effect of the onset of monazite nucleation in these rocks resulting from changes in mineral-forming reactions. Kohn and Malloy (2004) interpreted the monazite-forming reaction in these rocks to be coincident with the staurolite-forming reaction (reaction 1 above).

1) $Grt + Chl \pm Ms \rightarrow St + Bt$

The near absence of monazite below the staurolite isograd and the almost ubiquitous presence of monazite in samples in the staurolite zone support this interpretation.

Garnet compositional X-ray maps support the inference of a second stage M_2 metamorphic event. M_2 garnet porphyroblasts exhibit fractures that are most prominent when two grains are juxtaposed against each other. These fractures formed before M_2 since they affect zoning the pattern of the grains (Fig. 17b). Garnet from sample 11ED-8 exhibits a ~100 μm high X_{Gross} rim interpreted that developed during a late stage M_2 event (Fig. 17d). This high X_{Gross} rim is consistent with other garnet profiles from garnet grains of the western Blue Ridge (Massey and Moecher, 2005). Additionally, grain-boundary sillimanite and grain-boundary staurolite

Figure 20. Photomicrographs from the Bryson City dome. The orientation markers define the trend and the plunge of the lineation for each section where present; otherwise, the samples were cut toward the prevailing lineation of the outcrop. (A) Two-stage garnet growth indicated by overgrowth on original grain boundary. (B) Breakdown of garnet to biotite. Note the biotite grains near the garnet are parallel to S_2 and contain an increased concentration of monazite grains. Bt, biotite; Grt, garnet; Monz, monazite.

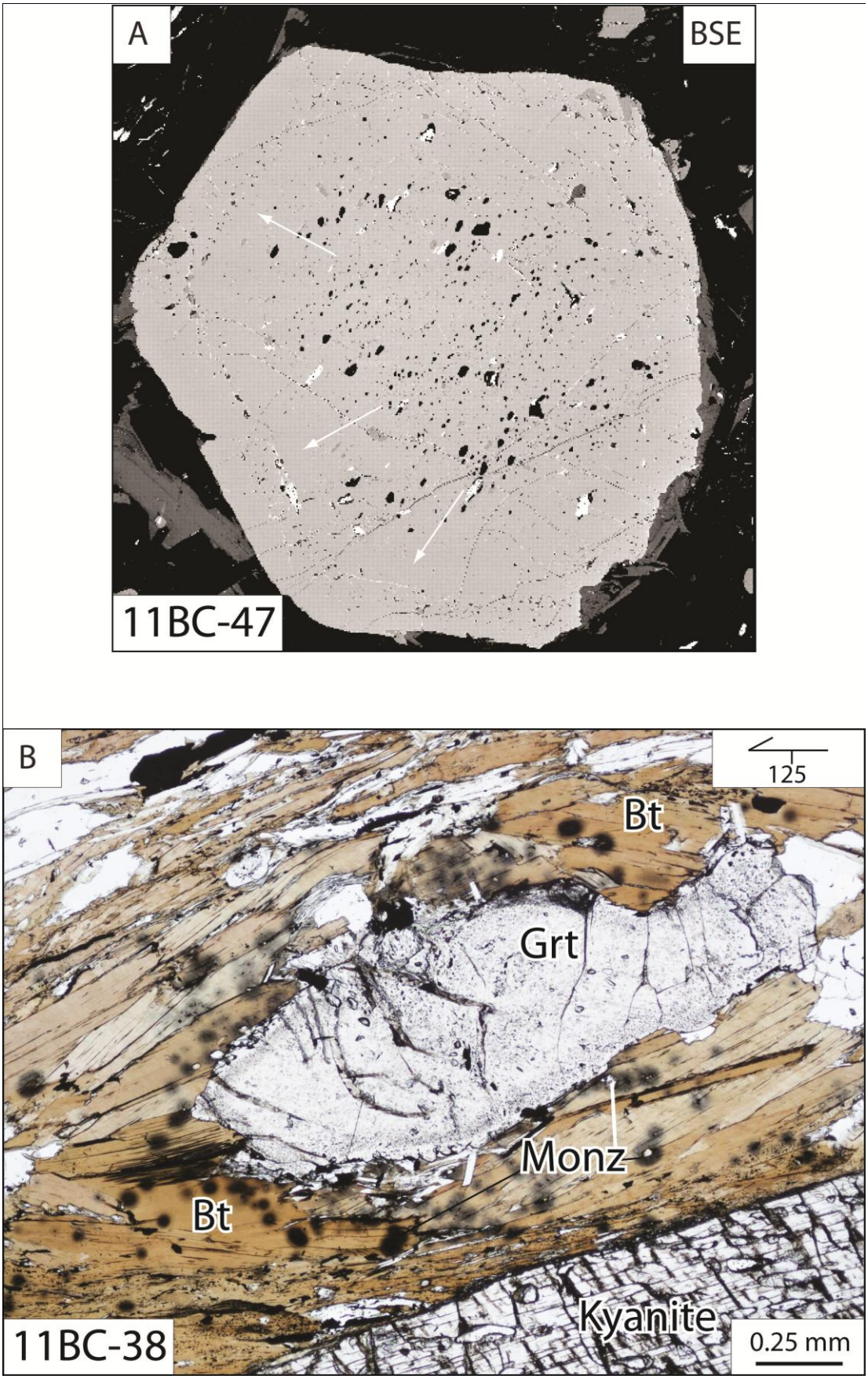
A
BSE
11BC-47
B
125
Bt
Grt
Monz
Bt
Kyanite
11BC-38
0.25 mm

described above (Chapter 3) occur in seven samples from the study area (Fig. 21a, b). This texture represents uplift and decompression and does not reflect the prograde mineral assemblage of the rocks but is rather a retrograde texture. Previous authors have attributed this growth of sillimanite to have grown during a later overprinting event (Massey and Moecher, 2005), but the presence of staurolite in a similar textures suggest it is related to M_2. Dynamically recrystallized quartz grains in both hanging wall and footwall samples exhibit GBM as the main deformation accommodating mechanism. This constrains the deformation temperature to ~500-600° C during the event.

M_3

M_3 metamorphism is related to D_3 deformation, which is commonly preserved as map-and outcrop-scale, NE-trending fold and crenulation development that increases in intensity southward. Kink deformation of muscovite grains and kyanite grains appears to be the result of D_3 deformation because the kink fold axes parallel F_3 crenulation axes (Fig. 19b). Crenulation formation in the southern portion of the field area is dominated by recrystallization and new grain growth that reflects M_3 metamorphism. Since no index minerals grew during this stage of metamorphism, the conditions of M_3 cannot be accurately determined.

M_4

M_4 is strictly a static, retrograde metamorphic event. The event is characterized by kyanite, muscovite, and feldspar alteration to randomly oriented sericite. Some samples contain kyanite grains that have been almost completely altered to sericite (Fig. 21c). Other samples exhibit biotite alteration to chlorite and replacement of garnet by chlorite and muscovite (Fig. 21d). This type of alteration is restricted to a few samples, suggesting it is a localized feature, possibly related to dike emplacement or increased fluid flow. These specific mineral alterations

Figure 21. Photomicrographs from the Ela and Bryson City domes. The orientation markers define the trend and the plunge of the lineation for each section where present; otherwise, the samples were cut toward the prevailing lineation of the outcrop. (A) Grain boundary sillimanite. (B) Grain boundary staurolite. (C) Static retrograde alteration of kyanite to white micas. (D) Retrograde alteration of biotite to chlorite. Plag, plagioclase; Bt, biotite; Ms, muscovite; Chl, chlorite, Sil, sillimanite; St, staurolite; Qtz, quartz.

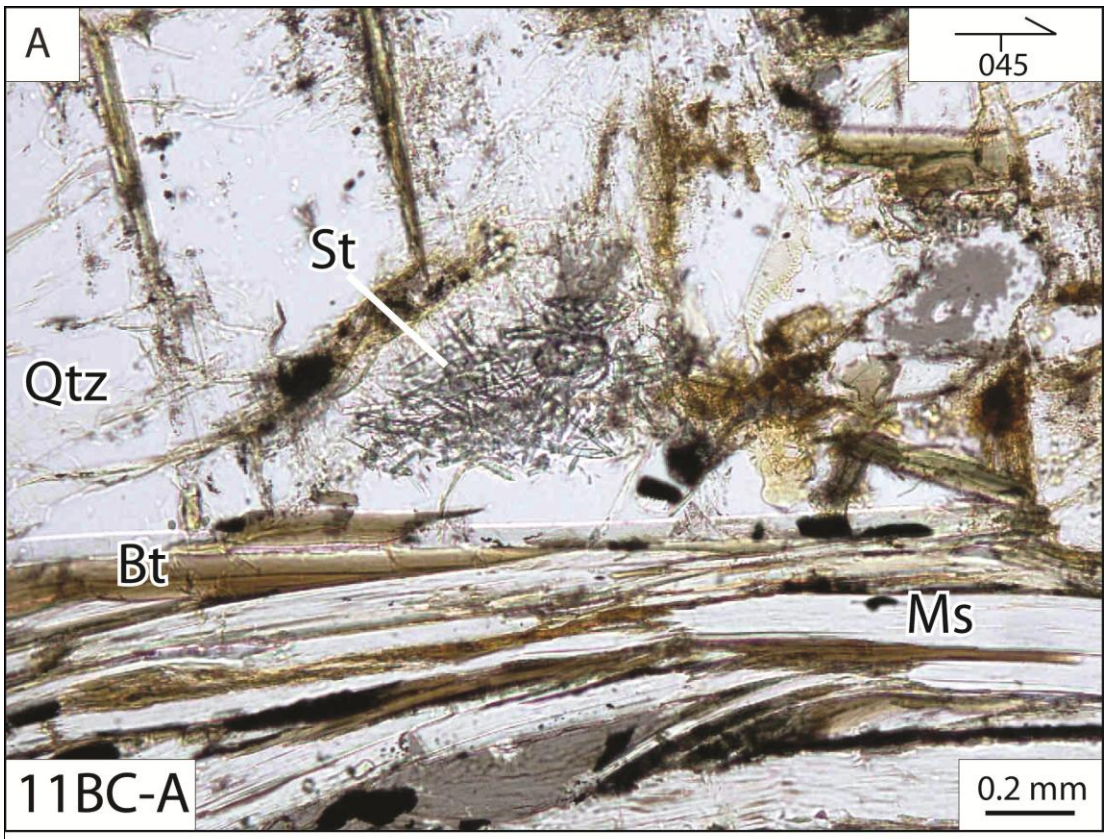
A
045
St
Qtz
Bt
Ms
11BC-A
0.2 mm

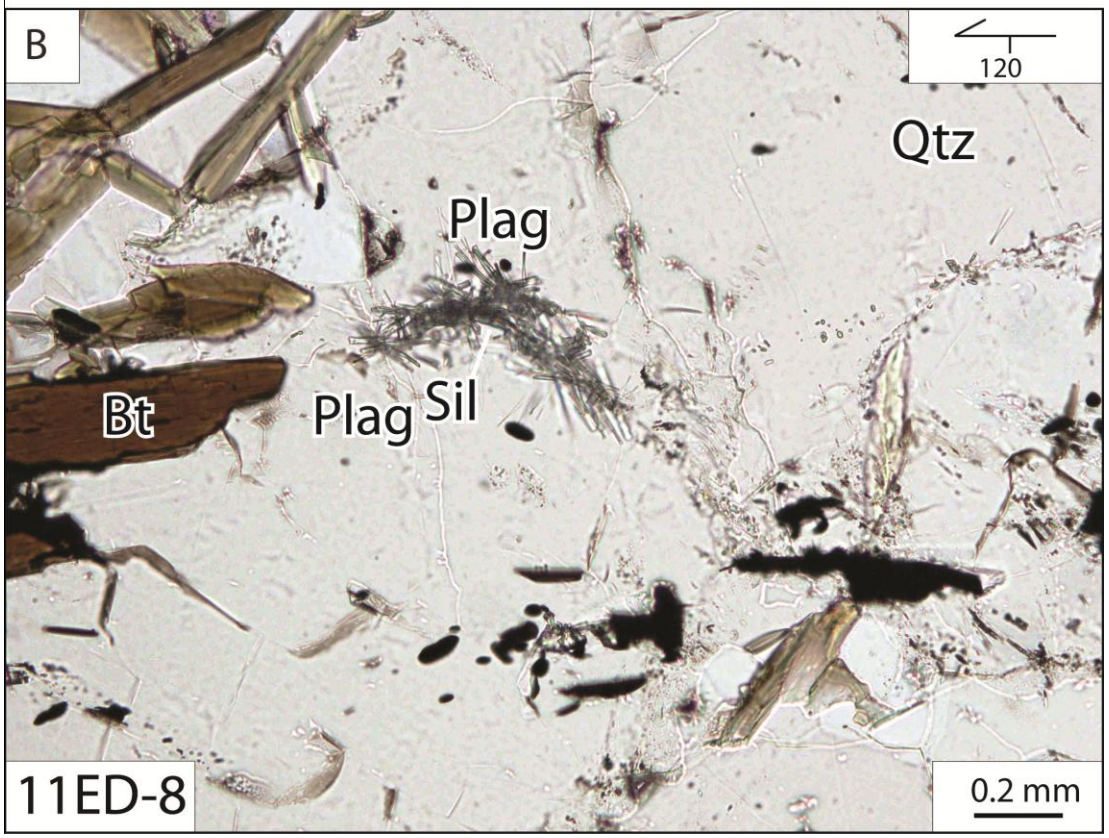
B
120
Qtz
Plag
Bt
Plag
Sil
11ED-8
0.2 mm

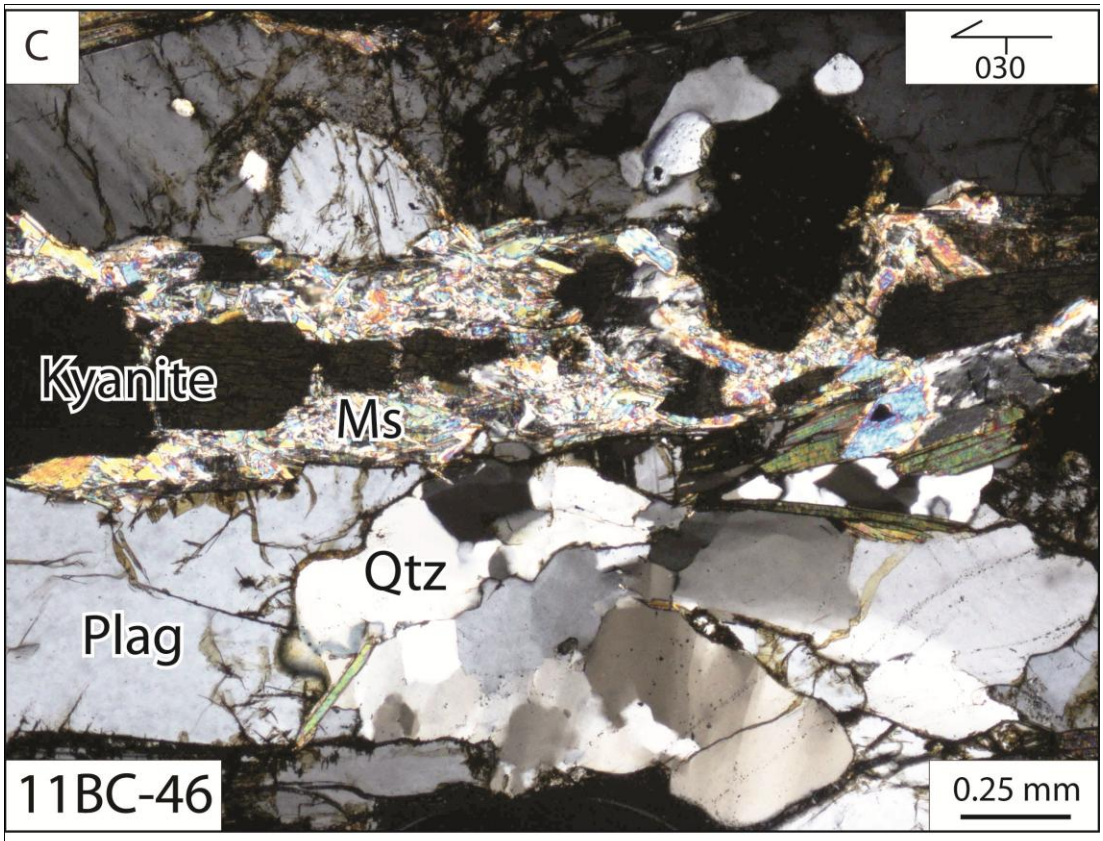
C
030
Kyanite
Ms
Qtz
Plag
11BC-46
0.25 mm

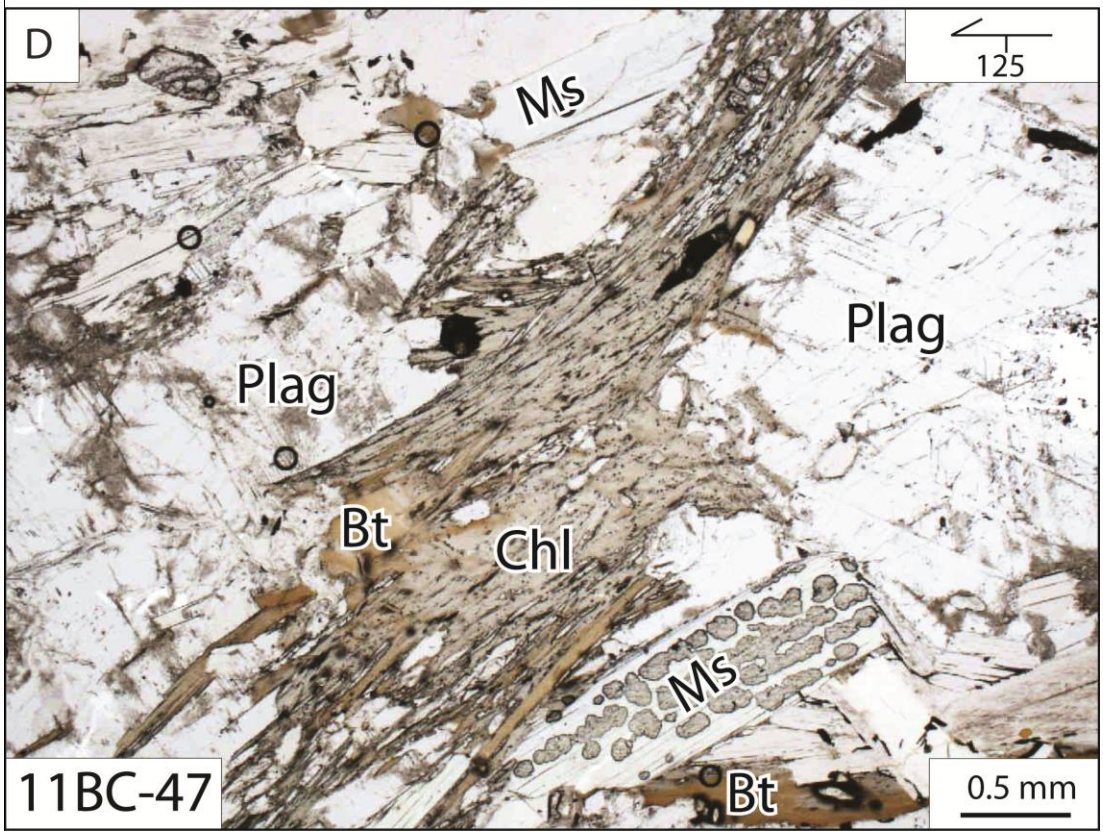
D
125
Ms
Plag
Plag
Bt
Chl
Ms
Bt
11BC-47
0.5 mm

constrain M_4 metamorphism to lower greenschist facies conditions.

CHAPTER 5

DISCUSSION AND IMPLICATIONS

The Ela and Bryson City domes, both interpreted to be the products of two generations of folding where fold axes cross at oblique angles to one another (Fig. 22), are structures with Greenville basement in the footwall and metasedimentary rocks in the hanging wall. An early generation of F_3 folds trends northeast-southwest. A later generation of folds trends northwest-southeast. Foliation in both core and cover rocks dips away from the centers of the domes. The domes are windows through the Greenbrier fault. Rocks in the fault of both domes have similar deformation styles (e.g., fold mechanisms and deformation temperatures) and similar structural features (e.g., shear sense, lineations, and strike). The three-stage deformational history, described in previous chapters for the Ela and Bryson City areas, is consistent with previous investigations of the folding history, metamorphism, fabric development, and fault development reported for the southern part of the western Blue Ridge (Hatcher , 1978; Eckert et al., 1989; Vauchez and Dallmeyer, 1989; Brumback, 1990; Quinn, 1991; Davidson, 1995; Coble, 1996; Montes, 1997; Massey and Moecher, 2005). In the map area, F_1 folds have been completely overprinted by subsequent deformational events,. Related S_1 fabric is preserved in porphyroblasts and in the fold hinges of F_2 folds. S_2 foliation, the most extensive regional foliation, formed as axial planes to F_2 isoclinal folds. D_2 deformation coincided with regional peak metamorphism (M_2). Elongate kyanite and staurolite porphyroblasts are aligned parallel to the dominate foliation (S_2). They preserve an internal foliation (S_{1i}) that is oblique to the external foliation, indicating inter- to syntectonic growth. Previous geochronology (e.g., Rodgers, 1970; Butler, 1991; Hatcher et al., 2004; Hatcher, et al., 2007;Southworth et al., 2005b) of

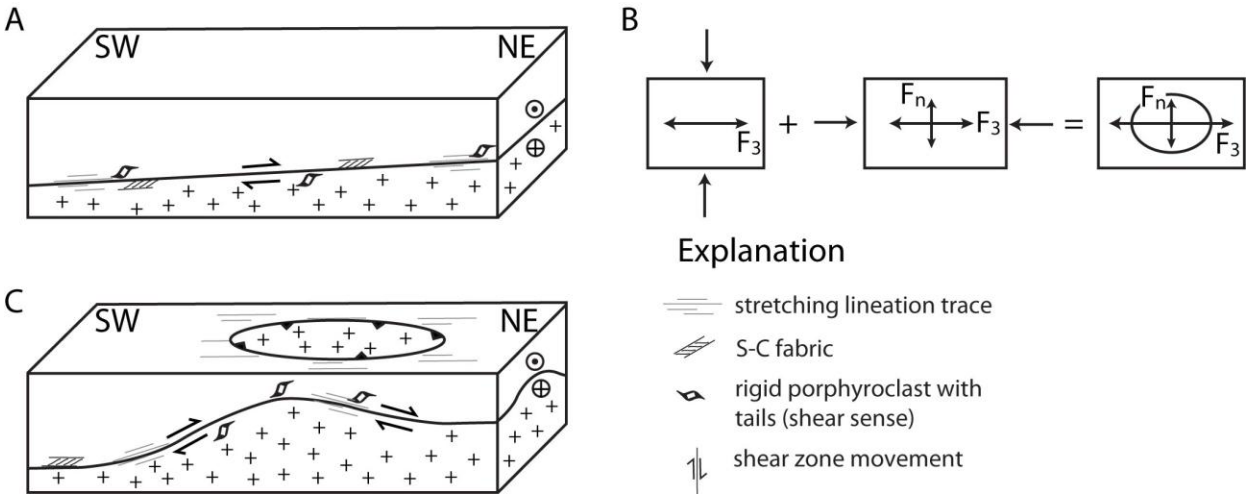

Figure 22. Schematic block diagram illustrating one possible kinematic and deformation model for the Greenbrier fault around the Ela and Bryson City domes. (A) Initial movement along the Greenbrier produced SW plunging stretching lineations and top-up-to-the-NE shear sense. (B) After movement along the Greenbrier ceased two obliquely oriented folding generations produced the domal structures. (C) After doming the, SW point of the domes display SW plunging stretching lineations and top-up-to-the-NE shear sense. The NE edges of the domes display NE plunging stretching lineations and top-down-the-NE shear sense. Not to scale.

synkinematic porphyroblasts, metamorphic zircon, and geochronology of plutonism bracket the D_2 deformation event (490 to 440 Ma) to the Taconic orogeny. F_3 open to tight folds, variably developed S_3 axial planar foliation, and crenulation cleavage overprinted D_2 fabrics. F_3 folding produced map-scale folds throughout the Great Smoky Mountains, including Ela and Bryson City domes, Alum Cave syncline, Ravensford anticlinorium, and Murphy syncline (Fig. 2). Based on the timing of folding relative to D_2 deformation, F_3 folds formed after metamorphism, potentially during Acadian or Alleghanian orogenies.

Lineations that record movement along the Greenbrier fault are unidirectional (5° → 226°). The majority of kinematic indictors exhibit top-to-the-northeast shear sense. Shear sense indicators on the north sides of the domes display top-down-to the-northeast shear sense, while

the indicators on the southern portions indicate top-up-to-the-northeast shear sense. The margins of the domes also record northeast-directed shearing that is parallel to strike. This pattern indicates post-kinematic folding of a top-to-the-northeast shear zone (Fig. 11). Although the final geometries of the domes are the result of D_3 deformation, indicated by the similar northeast-southwest trend of major F_3 folds, displacement along the Greenbrier fault predates this episode of deformation.

The dominant strain recovery mechanism for quartz in the shear zone is high temperature grain-boundary migration, indicating that movement occurred at temperatures of 500-600° C (Stipp et al., 2002). Checkerboard extinction in quartz recorded in a few samples indicates deformation at temperatures >650° C (Stipp et al., 2002). K-feldspar porphyroblasts commonly develop as mylonitic augen within the shear zone. Asymmetric strain shadows around M_2 garnets and discontinuous inclusion trails indicate movement occurred after peak mineral growth (i.e., kyanite, garnet, and staurolite). These data indicate that shearing and M_2 metamorphism occurred at similar temperatures during a late stage of the Taconic orogeny.

The parallelism of the shear zone mylonite (S_{2b}) and the main S_2 foliation (Chapter 2) could result from at least two different deformation histories. The shear fabric is either: (1) a separate event unrelated to S_2, or (2) a manifestation of localized shear in a mid-crustal shear zone during the final stages of D_2 as strain was localized along the rheologic contact. The gradation of the S_2 foliation into the mylonite zone (S_{2b}) favors the second interpretation where the Greenbrier fault is a localized shear zone in the mid-crust. The shear zone fabric (S_{2b}) transposed the S_2 foliation partially due to the rheological differences between the relatively weak metasedimentary rocks in the hanging wall and stronger gneissic rocks in the footwall. The relatively minor strain in the quartz monzonite in the footwall versus the more penetrative

mylonite of the hanging wall indicates that metapelitic rocks were less competent than quartzofeldspathic gneiss or mafic lithologies. The metapelitic rocks accommodated polyphase deformation that culminated in a localized zone of mylonite, while the gneiss is more resistant to strain and may record a different strain history. Such rheological contrasts are considered excellent potential horizons for a décollement formation (Twiss and Moores, 2007). The Greenbrier fault, exposed farther north of this study area, does not displace foliation or Taconic Barrovian isograds, indicating that the majority of movement on the fault occurred before metamorphism during the Taconic orogeny. If the Greenbrier fault around the Bryson City and Ela domes formed at this time, a portion of the fault was reactivated by ductile shearing. However, the consistent orientation of shear-sense indicators and stretching lineations implies that the shear zone is not an overprinted or reactivated portion of the fault. The mid-crustal depth of the Greenbrier around the Ela and Bryson City domes is inconstant with the Connelly and Woodward (2001) interpretations for the fault further to the north as a foreland fold fault system. However, it is possible the Greenbrier ramps up from deep-crust levels in the south to higher structures level in the north.

The majority of brittle faults in the study area are oblique to both the main foliation (S_2) and to shear fabric (S_{2b}), forming the youngest structures in the area. Brittle faulting could be related to either late-stage movement of the Greenbrier fault during exhumation or to subsequent orogenic events. Previous investigations support the latter interpretation, because the majority of the regional brittle deformation records the Alleghanian orogeny (Massey and Moecher, 2005). Pseudotachylite in the Greenbrier fault adds a new component to the previous treatment of brittle faults in the region. This investigation demonstrates that: 1) the pseudotachylite is sub-parallel to the high temperature mylonite that records top-to-the-northeast shear; 2) the foliation is not

deflected into the brittle fault surface; and 3) this thrust surface was passively folded during the Acadian orogeny. Pseudotachylite within the Greenbrier fault might record seismogenic events that occurred at deep structural positions of the Taconic orogenic wedge.

Mappable orthogneiss mylonite is limited to the north side of the Bryson City dome, although rocks of a similar type were identified on all flanks of both domes (Cameron, 1951). The formation of this zone in one portion of the field area is attributed to differences in the rheology of the rocks that were deformed. The mylonitic orthogneiss formed in the quartz monzonite, whereas migmatitic biotite paragneiss dominates the southern half of the Bryson City dome and core of the Ela dome. Cameron (1951) documented three prongs on the southwest tip of the Bryson City dome. Mapping by Cattanach and Bozdog (2010) confirmed the presence of similar map patterns on the northeast tip of the Ela dome. These prongs are the surficial expression of polyphase deformation and dome formation after movement on the shear zones. Fault-bounded domes can be uplifted by their bounding faults (Crittenden, 1980; Armstrong, 1983), but in this study area polyphase deformation is largely responsible for uplift of the domes.

The Great Smoky Group in the hanging wall of the Ela and Bryson City domes reached conditions of ~667° C and ~9.2 kbar during M_2 metamorphism. Barrovian metamorphism occurred as the crust was thickened within the Taconic orogenic wedge, following the collision of an island arc system with the Laurentian margin (Hatcher, 1987; Hatcher et al., 2007). These P-T estimates are consistent with the mapped metamorphic isograds surrounding the domes (Hadley and Goldsmith, 1963). Peak pressure estimates of ~9.2 kbar correspond to a burial depth of ~34 km (assuming a lithostatic pressure gradient of 3.7 km $kbar^{-1}$). After peak mineral growth during the Taconic up to kyanite-staurolite grade (blue area from figure 19) the rocks were decompressed through the staurolite-sillimanite stability field (green area from figure 19) as

evidenced by grain-boundary sillimanite and staurolite growth. The combination of these metamorphic conditions allows for the composing of a P-T-t-D path for the rocks surrounding the Bryson City and Ela domes (Fig. 19). An M_4 static retrograde event marks the final stage of metamorphism (Massey and Moecher, 2005).

Differences in bulk compositions and mineralogies can lead to complex and varied monazite formation during prograde metamorphism, but with proper characterization these can be a useful geochronometer for dating metamorphism of aluminous rocks in orogenic belts (e.g., DeWolf et al., 1993; Montel, 1993; Hawkins and Bowring, 1997; Foster et al., 2000; Spear and Pyle, 2010; Langille et al., 2012). Monazite growth is linked to major silicate forming reactions (e.g., Smith and Barriero, 1990; Ferry, 2000; Wing et al., 2003; Kohn and Malloy, 2004). Monazite is an accessory mineral in the metasedimentary cover rocks surrounding the Ela and Bryson City domes. Throughout the Great Smoky Mountains, monazite is nearly absent below the staurolite isograd but ubiquitous in higher grade rocks, suggesting monazite growth is related to the staurolite-in forming reaction (Kohn and Malloy, 2004). Additionally, this study and others (i.e., Kohn and Malloy, 2004) have documented textural evidence of monazite nucleation and growth (see Chapter 3) during prograde biotite growth and garnet dissolution related to the reaction:

1) $Grt + Chl \pm Ms \rightarrow St + Bt$

Further work could link the monazite-in reaction (Kohn and Malloy, 2004) and the P-T-t-D history of the rocks surrounding the Ela and Bryson City domes including: 1) comparison of garnet Y-zonation patterns with monazite growth; 2) characterization of monazite LREE zonation patterns; and 3) characterization of other LREE minerals (e.g., allanite and xenotime), which have been linked to monazite formation. Monazite geochronology could be a significant

research direction in the future.

This study has several significant implications for the thermal and kinematic history of thrust faults during the Taconic orogeny. The isoclinal F_2 folds record crustal shortening during the Taconic orogeny. Burial and heating of the orogenic wedge in the hanging wall of the Greenbrier shear zone resulted in growth of staurolite, garnet, and kyanite porphyroblasts during Barrovian metamorphism (667º C and 9.2 kbar). The timing of porphyroblast growth in the hanging wall of the domes is constrained to 480-440 Ma (Taconic) by U-Th-Pb monazite chemical ages (Moecher et al., 2003, 2004). High temperature mylonite developed during the late stages of D_2 (S_{2b}) and wrap around metamorphic porphyroblasts, indicating that it postdates Barrovian metamorphism. Stretching lineations preserved in the mylonite zone are consistent (5° → 226) and record an extension direction (X-axis of the strain ellipsoid) on the thrust fault, which is parallel to orogenic strike, prior to late-stage doming of the surface. Kinematic indicators on this surface record top-to-the-northeast sense of shear, implying a significant stage of orogen-parallel transport during the Taconic orogeny. Several studies of the southern Appalachians and Blue Ridge Province also document northeast-southwest directed ductile transport on minor and major fault systems (e.g., Cameron, 1951; Massey and Moecher, 2005; Merchat, 2009; Cattanach and Bozdog, 2010). Orogen-parallel transport has been attributed to oblique convergence during orogenic development (e.zg., Merchat, 2009). While the majority of mylonites formed at 500-600° C and mid-crustal locations (22-24 km depth; assuming 25º C/km), high-strain slip surfaces and pseudotachylite, oriented parallel to the mylonite, record seismogenic events during thrusting. The decreasing strain gradient, from the metasedimentary rocks of the hanging wall to structurally deeper positions in the immediate footwall composed of basement gneiss, indicates that strain was localized along this contact due to rheologic contrasts.

During the Acadian orogeny in the southern Appalachians, renewed crustal thickening reheated and deformed D_2 structures in the Great Smoky Mountains. Dome formation and uplift occurred from 377-340 Ma (Connelly and Dallmeyer, 1993; Southworth et al., 2005b). Temperatures reached conditions that exceeded muscovite and K-feldspar $^{40}Ar/^{39}Ar$ closure temperatures (350° C and 180° C respectively), but remained below hornblende $^{40}Ar/^{39}Ar$ closure temperature (500° C). These data provide additional support for models where the Greenbrier fault experienced movement as a mylonite zone at temperatures of 500-600° C during the Taconic orogeny.

REFERENCES CITED

Anderson, E.D., Massey, M.A., and Moecher, D.P., 2005, Disparate pressure conditions for Ky-grade metapelites and high pressure amphibolite (NOT retrograded eclogite) near the EBR-WBR terrane boundary, Dellwood Dellwood, NC: Geological Society of America., Abstract with Programs, no. 36, p. 40.

Armstrong, R.L., 1983, Mantled gneiss domes in the Albion Range, southern Idaho: Geological Society of American Bulletin, v. 49, p. 1295.

Bell, T.H., and Rubenach, M.J., 1983, Sequential porphyroblast growth and crenulation cleavage development during progressive deformation: Tectonophysics, v. 92, p. 171–194.

Bell, T.H., Hickey, K.A., and Upton, G.J.G., 1998, Distinguishing and correlating multiple phases of metamorphism across a multiply deformed region using the axes of spiral, staircase and sigmoidal inclusion trails in garnet: Journal of Metamorphic Geology, v. 16, p. 767–794.

Butler, J.R., 1991, Metamorphism, *in* Horton, J.W., Jr., and Zullo, V.A., eds., The Geology of the Carolinas—Carolina Geological Society 50th Anniversary Volume: Knoxville, University of Tennessee Press, p. 11-35.

Brumback, V.J., 1990, A metamorphic and structural transect in the central Blue Ridge, Jackson and Macon Counties, North Carolina [M.S. thesis]: University of Tennessee, Knoxville, p. 103.

Cameron, E.N., 1951, Feldspar deposits of the Bryson City district, North Carolina: North Carolina Division Mineral Resources Bulletin, v. 62, p. 1-100.

Carpenter, R.H., 1970, Metamorphic history of the Blue Ridge Province of Tennessee and North Carolina: Geological Society of America Bulletin, v. 81, p. 749–762.

Cattanach, B.L., and Bozdog, G.N., 2010, Bedrock geologic map of the Whittier 7.5 quadrangle, North Carolina: North Carolina Geological Survey Open File Map 2010-04, 1:24,000 scale.

Clemons, K.M., 2006, Petrofabric and geochemical analysis of the Great Smoky–Snowbird Group contact, western Blue Ridge, North Carolina and Tennessee [M.S. thesis]: The University of Kentucky, Lexington, p. 105.

Clemons, K.M., and Moecher, D.P., 2008, Re-interpretation of the deformation history of the Greenbrier fault, Great Smoky Mountains: Critical assessment of previous work: Southeastern Geology, v. 45, p. 203–224.

Clemons, K.M., and Moecher, D.P., 2010, Reinterpretation of the Greenbrier fault, Great Smoky Mountains: New petrofabric constraints and implications for southern Appalachian tectonics: Geological Society of American Bulletin, v. 121, p. 1108-1122.

Coble, J.F., 1996, Structural-metamorphic development of the Hayesville fault, Haywood and Jackson counties, North Carolina [Ph.D. dissertation]: University of Kentucky, Lexington, p. 180.

Connelly, J.B., and Dallmeyer, R.D., 1993, Polymetamorphic evolution of the western Blue Ridge: Evidence from $^{40}Ar/^{39}Ar$ whole-rock slate/phyllite and muscovite ages: American Journal of Science, v. 293, p. 323-359.

Connelly, J.B., and Woodward, N.B., 1992, Taconian-style thrust system in the Great Smoky Mountains, Tennessee: Geology, v. 20, p. 177-180.

Corrie, S.L. & Kohn, M.J., 2007, Resolving the timing of orogenesis in the western Blue Ridge, southern Appalachians via in situ ID-TIMS monazite geochronology: Geology, v. 35, p. 627–630.

Costello, J.O., and Hatcher, R.D., Jr., 1991, Problems of stratigraphic correlation between the Great Smoky, Snowbird, and Walden Creek Groups between the Great Smoky Mountains National Park, central east Tennessee and Ocoee Gorge, southeastern Tennessee, *in* Kish, S.A., ed., Studies of Precambrian and Paleozoic Stratigraphy in the western Blue Ridge: Carolina Geological Society Field Trip Guidebook, p. 69-77.

Crittenden, M.D.J., Coney, P.J., Davis, G.H., 1980, Cordilleran Metamorphic Core Complexes. Geological Society America Memoir 153, Boulder, CO.

Dallmeyer, R.D., 1975, $^{40}Ar/^{39}Ar$ ages of biotite and hornblende from a progressively metamorphosed basement terrane: Their bearing on the interpretation of release spectra: Geochimica et Cosmochimica Acta, v. 39, p. 1655–1669.

Davidson, G.L., 1995, The tectono-metamorphic history of a portion of the eastern Blue Ridge, Jackson County, North Carolina: [M.S. thesis] University of Tennessee, Knoxville, p. 157.

DeWolf, C., Beshaw, N., and O'Nion, R., 1993, A metamorphic history from micron-scale $^{207}Pb/^{206}Pb$ chronometry of Archean monazite: Earth and Planetary Science Letters, v. 120, p. 207–220.

Eckert, J.O., Hatcher, R.D. Jr., and Mohr, D.W., 1989, The Wayah granulite-facies metamorphic core, southwestern North Carolina: High grade culmination of Taconic metamorphism in the southern Blue Ridge: Geological Society of America Bulletin, v. 101, p. 1434–1447.

Ferry J.M., 2000, Patterns of mineral occurrence in metamorphic rocks: American Mineralogist, v. 85, p. 1573–1588.

Foster, G.L., Kinny, P., Vance, D., Prince, C. and Harris, N.B.W., 2000, The significance of monazite U-Th-Pb age data in metamorphic assemblages; a combined study of monazite and garnet chronometry: Earth and Planetary Science Letters, v. 181, p. 327–340.

Goldberg, S.A., and Dallmeyer, R.D., 1997, Chronology of Paleozoic metamorphism and deformation in the Blue Ridge thrust complex, North Carolina and Tennessee: American Journal of Science, v. 297, p. 488–526.

Hadley, J.B., and Goldsmith, R, 1963, Geology of the Eastern Great Smoky Mountains North Carolina and Tennessee: U.S. Geological Survey Professional Paper 349-B, p. B74-B95.

Hadley, J.B., and Nelson, A.E., 1971, Geologic map of the Knoxville quadrangle, North Carolina, Tennessee, and South Carolina: U.S. Geological Survey Miscellaneous Geologic Investigations Map I-654, scale 1:250,000.

Hatcher, R.D., Jr., 1978, Tectonics of the western Piedmont and Blue Ridge, southern Appalachians: Review and speculation: American Journal of Science, v. 278, p. 276–304.

Hatcher, R.D., Jr., 1987, Tectonics of the southern and central Appalachian internides: Annual Reviews of Earth and Planetary Science Letters 5, 337-362.

Hatcher, R.D., Jr., 1989, Tectonic synthesis of the U.S. Appalachians, *in* Hatcher, R.D., Jr., Thomas, W.A., and Viele, G.W., eds., The Appalachian-Ouachita orogen in the United States: Boulder, Colorado, Geological Society of America, The Geology of North America, v. F-2, p. 233-318.

Hatcher, R.D., Jr., Bream, B.R., Miller, C.F., Eckert, J.O., Jr., Fullagar, P.D., and Carrigan, C.W., 2004, Paleozoic structure of internal basement massifs, southern Appalachian Blue Ridge, incorporating new geochronologic, Nd and Sr isotopic, and geochemical data, *in* Tollo, R.P., Corriveau, L., McLelland, J., and Bartholomew, M.J., eds., Proterozoic tectonic evolution of the Grenville orogen in North America: Boulder, Colorado, Geological Society of America Memoir 197, p. 525–547.

Hatcher, R.D., Jr., Bream, B.R., Miller, C.F., Mapes, R.W., Fullagar, P.D., and Carrigan, C.W., 2004, Value of modern geochronology in understanding southern Appalachian accretionary history: Geological Society of America Abstracts with Programs, v. 37, no. 1, p. 66.

Hatcher, R.D. Jr., Bream, B.R., and Merschat, A.J., 2007, Tectonic map of the southern and central Appalachians: A tale of three orogens and a complete Wilson cycle: in Hatcher R.D. Jr., Carlson, M.P., McBride, J.M., and Martínez Catalán, J.R., eds., 4-D Framework of Continental Crust: Geologic Society of America Memoir, 200, p. 595-632.

Hatcher, R.D., Jr., 2010, The Appalachian orogen: A brief summary: in Tollo, R.P., Bartholomew, M.J., Hibbard, J.P., and Karabinos, P.M., eds., From Rodinia to Pangea:

The Lithotectonic Record of the Appalachian Region: Geological Society of America Memoir 206, p. 1–19.

Hawkins, D.. and Bowring, S., 1997, U-Pb systematic of monazite and xenotime: case studies from the Paleoproterozoic of the Grand Canyon, Arizona: Contributions to Mineralogy and Petrology, v. 127, p. 87–103.

Hirth, G., and Tullis, J., 1992, Dislocation creep regimes in quartz aggregates: Journal of Structural Geology, v. 14, p. 145-159.

Hobbs, B.E., Means, W.D., and Williams, P.K., 1976, An outline of structural geology: New York, Wiley, p. 370.

Holland, T.J.B., and Powell, R., 1998, An internally-consistent thermodynamic dataset for phases of petrological interest: Journal of Metamorphic Geology, v. 16, p. 309–344.

Huebner, M.T., and Hatcher, R.D. Jr., 2013, Polyphase reactivation history of the Towaliga Fault, Central Georgia, implications regarding the amalgamation and breakup of Pangea: The Journal of Geology, v. 121, p. 75-90.

Hurst, V. J., 1955, Stratigraphy, structure, and mineral resources of the Mineral Bluff quadrangle, Georgia: Georgia Geological Survey Bulletin v. 63, p. 137.

King, P.B., Hadley, J.B., Neuman, R.B., and Hamilton, W.B., 1958, Stratigraphy of the Ocoee Series, Great Smoky Mountains, Tennessee and North Carolina: Geological Society of America Bulletin, v. 60, p. 947-966.

King, P.B., Neuman, R.B., and Hadley, J.B., 1968, Geology of the Great Smoky Mountains National Park, Tennessee and North Carolina: U.S. Geological Survey Professional Paper 587, p. 23, and 1:125,000-scale map.

Kish, S.A., 1991, Potassium-argon dating in the western Blue Ridge of North Carolina and Tennessee, in Kish, S.A., ed., Studies of Precambrian and Paleozoic stratigraphy in the western Blue Ridge: Carolina Geological Society Field Trip Guidebook, p. 69-77.

Kish, S.A., Merschat, C.E., Mohr, D.W., and Wiener, L.S., 1975, Guide to the Geology of the Blue Ridge South of the Great Smoky Mountains, North Carolina: Carolina Geological Society Field Trip Guidebook, p. 49.

Kohn, M.J, and Malloy, M.A., 2004, Formation of monazite via prograde metamorphic reactions among common silicates: Implications for age determinations: Geochimica et Cosmochimica Acta, v. 68, p. 101-113.

Kohn, M.J., and Spear, F.S., 2000, Retrograde net transfer reaction insurance for pressure-temperature estimates: Geology, v. 28, p. 1127–1130.

Kruhl, J.H., 1996, Prim- and basal-plane parallel subgrain boundaries in quartz; a microstructural geothermobarmeter: Journal of Metamorphic Geology, v. 14, p. 581-589.

Langille, J.M., Jessup, M.J., Cottle, J.M., Lederer, G., and Ahmad, J., 2012, Timing of metamorphism, melting and exhumation of the Leo Pargil dome, northwest India: Journal of Metamorphic Geology., v. 30, p. 769.

Law, R.D., 1987, Heterogeneous deformation and quartz crystallographic fabric transitions: natural examples from the Moine Thrust zone at the stack of Glencoul, northern Assynt: Journal of Structural. Geology, v. 9, p. 819–833.

Lister, G.S., and Hobbs, B.E., 1980, The simulation of fabric development during plastic deformation and its application to quartzite: the influence of deformation history: Journal of Structural Geology, v. 2 (3), p. 355-370.

Lister, G.S., and Snoke, A.W., 1984, S-C mylonites: Journal of Structural Geology, v. 6, p. 617-638.

Lister, G.S. and Williams, P.P., 1979, Fabric development in shear zones: theoretical controls and observed phenomena: Journal of Structural Geology, v. 1, p. 283–298.

Massey, M.A., and Moecher, D.P., 2005, Deformation and metamorphic history of the western Blue Ridge–eastern Blue Ridge terrane boundary, southern Appalachian orogen: Tectonics v. 24, p. 18.

Merschat, A.J., 2009, Assembling the Blue Ridge and Inner Piedmont: Insights into the nacre and timing of terrane accretion in the southern Appalachian orogeny from geologic mapping, stratigraphy, kinematic analysis, petrology, geochemistry, and modern geochronology [Ph. D. dissertation]: Knoxville, Tennessee, University of Tennessee, p. 455.

Merschat, A.J., Hatcher, R.D., Jr., and Davis, T.L., 2005, The northern Inner Peidmont southern Appalachinans USA: Kinematics of transpression and SW-directed mid-crustal flow: Journal of Structural Geology, v. 27, p. 1252-1281.

Moecher, D.P., Tracy, R.J., and Anderson, E.D., 2003, Taconican metamorphism in eastern Great Smoky Mountains inferred from U-Th-Pb monazite chemical ages: Geological Society of America, Abstract with Programs, v. 10, p. 4.

Moecher, D.P., Massey, M.A., and Tracy, R.J., 2004, Timing and pattern of metamorphism in the western and central Blue Ridge, TN and NC: Status and outstanding problems: Carolina Geological Society Annual Field Trip Guide Book, p. 57-66.

Moecher, D.P., Hietpas, J., Samson, S. and Chakrborty, S., 2011, Insights into southern Appalachian tectonics from ages of detrital monazite and zircon in modern alluvium: Geosphere, v. 7, p. 494-512.

Montel, J., 1993, A model for monazite/melt equilibrium and application to the generation of granitic magmas: Chemical Geology, v. 110, p. 127–146.

Montes, C., 1997, The Greenbrier and Hayesville faults in central-western North Carolina: [M.S. thesis] University of Tennessee, Knoxville, p. 145.

Mohr, D.W., and Newton, R.C., 1983, Kyanite-Staurolite metamorphism in sulfidic schist of the Anakeesta Formation, Great Smoky Mountains, North Carolina: American Journal of Science, v. 283, p. 97-134.

Passchier, C.W. and Trouw, A.J., 2005, Microtectonics, 2nd edition: Springer-Verlag Berlin, Heidelburg, New York Publishers, p. 366.

Powell, R., Holland, T.J., and Worley, B., 1998, Calculating phase diagrams with THERMOCALC: methods and examples: Journal of Metamorphic Geology, v. 16.

Quinn, M.J., 1991, Two lithotectonic boundaries in western North Carolina: Geologic interpretation of a region surrounding Sylva, Jackson County: [M.S. thesis], University of Tennessee, Knoxville, p. 223.

Rankin, D.W., 1975, The continental margin of eastern North American in the southern Appalachians; The opening and closing of the proto-Atlantic ocean: American Journal of Science, v. 275-A, p. 298-336.

Ramsay, J.G., 1962, Interference patterns produced by the superposition of folds of similar type: The Journal of Geology, v. 70, p. 466-481.

Rast, N., and Kohles, K. M., 1986, The origin of the Ocoee SuperGroup: American Journal of Science, v. 286, p. 593-616.

Rodgers, J., 1970, The tectonics of the Appalachians: New York, Wiley-Interscience, p. 271.

Simpson, C., De Paor, D.G., 1993, Strain and kinematic analysis in general shear zones: Journal of Structural Geology, v. 15 (1), p. 1-20.

Smith, H.A., and Barreiro, B., 1990, Monazite U-Pb dating of staurolite grade metamorphism in pelitic schists: Contributions to Mineralogy and Petrology, v. 105, p. 602–615.

Southworth, S., Schultz, A., and Denenny, D., 2005a, Geologic Map and Report of the Great Smoky Mountains National Park Region, Tennessee and North Carolina: U.S. Geological Survey Open File Report 2005-1225, p. 22-24, 71-73.

Southworth, S., Aleinikoff, J.N., Kunk, M.J., Naeser, C.W., and Naeser, N.D., 2005b , Geochronology of the Great Smoky Mountains Nation Park region, TN/NC, with correlation to the rocks and orogenic events of the Appalachian Blue Ridge, in Hatcher, R.D., Jr., and Merschat, A.J., eds., Blue Ridge Geology Geotraverse East of the Great Smoky Mountains National Park, western North Carolina: North Carolina Geological Survey, Carolina Geological Society Annual Field Trip Guidebook, p. 45-56.

Southworth, S., Schultz, A., Kunk, M.J., Aleinkoff, J.N., Clemons, K.M., Naeser, N.D., Naeser, C.W., and Denenny, D., 2006, The Polygenetic Greenbrier fault, Great Smoky Mountains TN/NC: Geological Society of American, Abstract with Programs, v. 38, p. 66.

Spear, F.S., 1991, On the interpretation of peak metamorphic temperatures in light of garnet diffusion during cooling: Journal of Metamorphic Geology v. 9, p. 379-388.

Spear, F.S., 1993, Metamorphic phase equilibria and pressure-temperature-time paths: Mineralogical Society of America Monograph, p. 799.

Spear, F.S., Kohn, M.J., and Cheney, J.T., 1999, *P-T* paths from anatectic pelites: Contributions to Mineralogy and Petrology, v. 134, p. 17–32.

Spear, F., and Pyle, J., 2010, Theoretical modeling of monazite growth in a low-Ca metapelite: Chemical Geology, v. 273, p. 111–119.

Stipp, M., Stünitz, H., Heilbronner, R., and Schmid, S.M., 2002, The eastern Tonale fault zone: A "natural laboratory" for crystal plastic deformation of quartz over a temperature range from 250°C to 700°C: Journal of Structural Geology. v. 24, p. 1861–1884.

Thigpen, J.R., and Hatcher, R.D., Jr., 2009, Geologic Map of the western Blue Ridge and Portions of the Eastern Blue Ridge and Valley and Ridge Provinces in Southeast Tennessee, Southwest North Carolina, and Northern Georgia: The Geological Society of America, 1:200,000 scale.

Thomas, W.A., 1991, The Appalachian-Ouachita rifted margin of southeastern North America: Geological Society of America Bulletin, v. 103, p. 415–431.

Tracy, R.J., 1982, Compositional zoning and inclusions in metamorphic minerals, in Ferry, J.M., eds., Characterization of metamorphism through mineral equilibria, rev. mineral: Mineralogical Society of America, v. 10, p. 355 – 397.

Tracy, R.J., Robinson, P., and Thompson, A.B., 1976, Garnet composition and zoning in the determination of temperature and pressure of metamorphism, central Massachusetts: American Mineral, v. 61, p. 762-775.

Vauchez, A.R., and Dallmeyer, R.D., 1989, Polyphase tectonic evolution of the Hayesville fault, Georgia–North Carolina: Geological Society of America, Abstract with Programs, v. 21, p. 63.

Wehr, F., and Glover, L. III, 1985, Stratigraphy and tectonics of the Virginia-North Carolina Blue Ridge: Evolution of a late Proterozoic-early Paleozoic hinge zone: Geological Society of America Bulletin, v. 96, p. 285 –295.

Wing, B.N., Ferry, J.M., and Harrison, T.M., 2003, Prograde destruction and formation of monazite and allanite during contact and regional metamorphism of pelites: Petrology and geochronology: Contributions to Mineralogy and Petrology, v. 145**,** p. 228–250.

Williams, H., 1985, Paleozoic miogeoclines and suspect terranes of the North Atlantic Region: Cordilleran comparisons, In Howel, D.G., eds, Tectonostratigraphic terranes of the Circum-Pacific region: CircumPacific Council for Energy and Mineral Resources, Earth Science Series, n. 1, p. 71-75.

Woodward, N., Connelly, J., Walters, R., and Lewis, J., 1991, Tectonic evolution of the Great Smoky Mountains, In Kish, S.A., eds, Studies of Precambrian and Paleozoic Stratigraphy in the western Blue Ridge: Carolina Geological Society Annual Field Trip Guide, p. 55-68.

Yin, A., 2004, Gneiss domes and gneiss dome systems, in Whitney, D.L., Teyssier, C., and Siddoway, C.S., eds., Gneiss domes in orogeny: Boulder, Colorado, Geological Society of America Special Paper, v. 380, p. 14.

Yardley, B.W.D., 1977, The nature and significance of the mechanism of sillimanite growth in the Connemara schists, Ireland: Contributions to Mineralogy and Petrology, v. 65, p. 53–58.

APPENDIX I

ELECTRON MICROPROBE DATA FROM THE UNIVERSITY OF TENNESSEE USED FOR PRESSURE AND TEMPERATURE CALCULATIONS

11BC-A

Biotite	SiO2	TiO2	Al2O3	Cr2O3	Fe203	MgO	CaO	MnO	FeO	Na2O	K2O	Total
	35.93	1.61	18.22	0.02	0.00	10.79	0.01	0.02	17.81	0.11	9.00	93.50
	31.76	1.07	19.74	0.02	0.00	12.82	0.01	0.03	20.94	0.04	5.36	91.80
	34.45	1.15	18.69	0.01	0.00	11.77	0.05	0.03	19.10	0.09	7.18	92.52
	36.39	1.00	18.89	0.02	0.00	11.15	0.05	0.03	18.14	0.14	8.74	94.57
	35.89	1.35	18.34	0.00	0.00	10.66	0.00	0.01	18.48	0.20	7.92	92.86
	35.41	1.54	18.42	0.02	0.00	10.53	0.01	0.03	18.35	0.15	8.78	93.25
	36.36	1.30	18.49	0.01	0.00	10.92	0.04	0.04	18.19	0.17	8.71	94.23
	35.27	2.23	18.41	0.04	0.00	9.92	0.00	0.00	18.18	0.20	9.07	93.31
	35.39	1.86	18.53	0.02	0.00	10.12	0.01	0.02	18.06	0.15	9.03	93.21
	35.36	1.79	18.26	0.00	0.00	10.23	0.01	0.01	18.27	0.18	9.02	93.14
	35.74	1.53	19.03	0.01	0.00	10.44	0.02	0.00	18.00	0.16	9.03	93.97
	35.56	1.56	18.35	0.03	0.00	10.43	0.00	0.02	18.85	0.17	8.80	93.77
	35.17	1.90	18.08	0.03	0.00	10.36	0.01	0.01	19.52	0.13	8.33	93.53
	36.19	1.42	18.47	0.00	0.00	10.71	0.01	0.02	18.53	0.18	9.12	94.66
	35.81	1.54	18.58	0.03	0.00	10.56	0.01	0.03	18.48	0.15	9.13	94.31
	36.28	1.33	18.65	0.01	0.00	10.86	0.02	0.03	18.26	0.17	8.90	94.51
	35.95	1.45	18.98	0.04	0.00	10.32	0.06	0.05	17.60	0.11	8.32	92.87
	35.33	1.57	18.45	0.02	0.00	10.31	0.04	0.01	18.39	0.15	8.59	92.86
	35.81	1.17	18.47	0.02	0.00	10.82	0.06	0.02	18.39	0.13	8.35	93.25
Average	35.48	1.49	18.58	0.02	0.00	10.72	0.02	0.02	18.50	0.15	8.49	93.48

Si	Ti	Al	Cr	Fe^{+3}	Mg	Ca	Mn	Fe^{+2}	Na	K	Total
5.51	0.19	3.30	0.00	0.00	2.47	0.00	0.00	2.29	0.03	1.76	19.55
4.99	0.13	3.65	0.00	0.00	3.00	0.00	0.00	2.75	0.01	1.07	19.61
5.34	0.13	3.41	0.00	0.00	2.72	0.00	0.00	2.48	0.03	1.42	19.54
5.51	0.11	3.37	0.00	0.00	2.52	0.00	0.00	2.30	0.04	1.69	19.55
5.53	0.16	3.33	0.00	0.00	2.45	0.00	0.00	2.38	0.06	1.56	19.46
5.46	0.18	3.35	0.00	0.00	2.42	0.00	0.00	2.37	0.05	1.73	19.57
5.53	0.15	3.32	0.00	0.00	2.48	0.00	0.00	2.31	0.05	1.69	19.54
5.45	0.26	3.35	0.00	0.00	2.29	0.00	0.00	2.35	0.06	1.79	19.54
5.46	0.22	3.37	0.00	0.00	2.33	0.00	0.00	2.33	0.05	1.78	19.55
5.47	0.21	3.33	0.00	0.00	2.36	0.00	0.00	2.37	0.05	1.78	19.57
5.46	0.18	3.43	0.00	0.00	2.38	0.00	0.00	2.30	0.05	1.76	19.55
5.47	0.18	3.33	0.00	0.00	2.39	0.00	0.00	2.42	0.05	1.73	19.58
5.43	0.22	3.29	0.00	0.00	2.39	0.00	0.00	2.52	0.04	1.64	19.54
5.50	0.16	3.31	0.00	0.00	2.43	0.00	0.00	2.36	0.05	1.77	19.59
5.47	0.18	3.35	0.00	0.00	2.41	0.00	0.00	2.36	0.04	1.78	19.59
5.51	0.15	3.34	0.00	0.00	2.46	0.00	0.00	2.32	0.05	1.73	19.56
5.52	0.17	3.43	0.00	0.00	2.36	0.00	0.00	2.26	0.03	1.63	19.43
5.47	0.18	3.37	0.00	0.00	2.38	0.00	0.00	2.38	0.05	1.70	19.53
5.50	0.14	3.35	0.00	0.00	2.48	0.00	0.00	2.36	0.04	1.64	19.52
5.45	0.17	3.37	0.00	0.00	2.46	0.00	0.00	2.38	0.04	1.66	19.55

Muscovite	SiO2	TiO2	Al2O3	Cr2O3	Fe203	MgO	CaO	MnO	FeO	Na2O	K2O	Total
	45.57	0.88	35.08	0.02	0.00	0.65	0.01	0.02	1.19	0.93	9.38	93.72
	45.77	0.89	34.50	0.03	0.00	0.83	0.01	0.02	1.45	0.79	9.31	93.59
	46.10	0.95	34.45	0.03	0.00	0.91	0.00	0.02	1.25	0.73	9.62	94.06
	45.71	0.84	35.12	0.00	0.00	0.90	0.01	0.00	1.45	0.68	9.40	94.10
	46.55	0.69	34.13	0.01	0.00	1.10	0.00	0.01	1.26	0.74	9.67	94.17
	45.89	0.93	34.71	0.01	0.00	0.78	0.02	0.02	1.21	0.74	9.42	93.72
	46.11	0.98	35.13	0.04	0.00	0.84	0.00	0.00	1.29	0.69	9.60	94.68
	45.71	1.01	34.83	0.02	0.00	0.83	0.00	0.01	1.28	0.72	9.32	93.72
	45.62	0.94	35.04	0.06	0.00	0.71	0.02	0.00	1.10	0.61	9.28	93.39
	46.21	0.90	34.98	0.02	0.00	0.84	0.01	0.00	1.12	0.59	9.53	94.19
	46.21	0.78	34.27	0.01	0.00	1.04	0.03	0.02	1.16	0.56	9.33	93.41
	46.21	0.81	34.12	0.01	0.00	0.97	0.00	0.01	1.29	0.75	9.63	93.80
	46.64	0.81	34.21	0.02	0.00	1.08	0.02	0.02	1.28	0.57	9.40	94.05
Average	46.02	0.88	34.66	0.02	0.00	0.88	0.01	0.01	1.26	0.70	9.45	93.89

Si	Ti	Al	Cr	Fe^{+3}	Mg	Ca	Mn	Fe^{+2}	Na	K	Total
6.14	0.09	5.57	0.00	0.00	0.13	0.00	0.00	0.13	0.24	1.61	17.92
6.18	0.09	5.49	0.00	0.00	0.17	0.00	0.00	0.16	0.21	1.60	17.90
6.19	0.10	5.45	0.00	0.00	0.18	0.00	0.00	0.14	0.19	1.65	17.91
6.13	0.09	5.55	0.00	0.00	0.18	0.00	0.00	0.16	0.18	1.61	17.90
6.24	0.07	5.39	0.00	0.00	0.22	0.00	0.00	0.14	0.19	1.65	17.92
6.18	0.09	5.51	0.00	0.00	0.16	0.00	0.00	0.14	0.19	1.62	17.88
6.15	0.10	5.52	0.00	0.00	0.17	0.00	0.00	0.14	0.18	1.63	17.90
6.15	0.10	5.52	0.00	0.00	0.17	0.00	0.00	0.14	0.19	1.60	17.88
6.15	0.10	5.57	0.00	0.00	0.14	0.00	0.00	0.12	0.16	1.60	17.85
6.18	0.09	5.52	0.00	0.00	0.17	0.00	0.00	0.13	0.15	1.63	17.86
6.23	0.08	5.44	0.00	0.00	0.21	0.00	0.00	0.13	0.15	1.61	17.85
6.22	0.08	5.42	0.00	0.00	0.20	0.00	0.00	0.15	0.20	1.65	17.91
6.25	0.08	5.40	0.00	0.00	0.22	0.00	0.00	0.14	0.15	1.61	17.85
6.18	0.09	5.49	0.00	0.00	0.18	0.00	0.00	0.14	0.18	1.62	17.88

Plagioclase	SiO2	TiO2	Al2O3	Cr2O3	Fe203	MgO	CaO	MnO	FeO	Na2O	K2O	Total
	61.81	0.00	23.61	0.00	0.00	0.00	5.60	0.00	0.06	8.03	0.10	99.20

Si	Ti	Al	Cr	Fe^{+3}	Mg	Ca	Mn	Fe^{+2}	Na	K	Total
2.76	0.00	1.24	0.00	0.00	0.00	0.27	0.00	0.00	0.70	0.01	4.97

Garnet	SiO2	TiO2	Al2O3	Cr2O3	Fe203	MgO	CaO	MnO	FeO	Na2O	K2O	Total
	36.75	0.02	21.00	0.00	0.03	4.04	2.52	0.99	34.19	0.00	0.00	99.52

Si	Ti	Al	Cr	Fe^{+3}	Mg	Ca	Mn	Fe^{+2}	Na	K	Total
2.96	0.00	2.00	0.00	0.00	0.49	0.22	0.07	2.31	0.00	0.00	8.04

Staurolite	SiO2	TiO2	Al2O3	Cr2O3	Fe203	MgO	CaO	MnO	FeO	Na2O	K2O	Total
	28.28	0.02	54.23	0.00	0.00	1.44	0.01	0.06	9.81	0.00	0.00	93.85
	28.08	0.02	54.32	0.00	0.00	1.38	0.01	0.07	9.95	0.00	0.00	93.83
	28.51	0.01	54.51	0.00	0.00	1.32	0.02	0.04	9.13	0.00	0.00	93.53
Average	28.29	0.02	54.36	0.00	0.00	1.38	0.01	0.06	9.63	0.00	0.00	93.74

Si	Ti	Al	Cr	Fe^{+3}	Mg	Ca	Mn	Fe^{+2}	Na	K	Total
3.93	0.00	8.89	0.00	0.00	0.30	0.00	0.01	1.14	0.00	0.00	14.27
3.91	0.00	8.92	0.00	0.00	0.29	0.00	0.01	1.16	0.00	0.00	14.29
3.96	0.00	8.92	0.00	0.00	0.27	0.00	0.00	1.06	0.00	0.00	14.22
3.93	0.00	8.91	0.00	0.00	0.29	0.00	0.01	1.12	0.00	0.00	14.26

11BC-38m Data used in matrix garent P-T calculation

Biotite	SiO2	TiO2	Al2O3	Cr2O3	Fe203	MgO	CaO	MnO	FeO	Na2O	K2O	Total
	36.01	1.35	19.24	0.00	0.00	12.26	0.00	0.08	16.51	0.24	8.66	94.36
	36.41	1.32	19.04	0.00	0.00	12.47	0.00	0.03	16.89	0.27	8.85	95.29
	36.38	1.44	18.88	0.00	0.00	12.42	0.00	0.04	16.86	0.30	8.89	95.21
	36.58	1.53	19.09	0.00	0.00	12.29	0.05	0.03	16.57	0.30	8.82	95.27
	36.10	1.53	19.60	0.00	0.00	11.97	0.01	0.03	16.08	0.36	9.03	94.71
	36.15	1.69	19.65	0.00	0.00	12.07	0.02	0.03	16.11	0.32	9.05	95.10
	36.39	1.63	19.56	0.00	0.00	12.16	0.11	0.01	16.18	0.32	8.83	95.18
	36.19	1.68	19.12	0.00	0.00	12.36	0.04	0.04	16.09	0.30	8.69	94.53
	36.54	1.32	19.40	0.00	0.00	12.42	0.03	0.03	16.68	0.27	8.57	95.25
	36.61	1.67	20.06	0.00	0.00	12.01	0.01	0.03	16.33	0.31	8.73	95.77
	36.20	1.80	19.61	0.00	0.00	11.99	0.11	0.04	16.66	0.32	8.77	95.49
	36.02	1.57	19.11	0.00	0.00	11.76	0.00	0.04	17.14	0.31	8.55	94.48
	35.53	1.62	19.20	0.00	0.00	11.57	0.04	0.05	16.48	0.26	8.99	93.73
	36.33	1.54	19.46	0.00	0.00	12.03	0.01	0.02	16.58	0.34	8.70	95.01
	36.49	1.59	19.43	0.00	0.00	12.15	0.00	0.04	16.58	0.30	8.64	95.22
	36.51	1.62	19.09	0.00	0.00	12.07	0.10	0.00	17.16	0.29	8.79	95.64
	36.51	1.55	19.22	0.00	0.00	12.13	0.00	0.04	16.96	0.28	8.80	95.50
	36.14	1.99	19.11	0.00	0.00	11.62	0.05	0.06	16.11	0.37	8.32	93.78
	36.26	1.72	19.37	0.00	0.00	11.89	0.09	0.06	16.93	0.30	8.77	95.38
	36.01	1.73	19.25	0.00	0.00	11.64	0.07	0.02	16.94	0.31	8.85	94.82
	36.23	1.85	19.31	0.00	0.00	11.87	0.00	0.05	17.16	0.32	8.75	95.54
	36.23	1.89	19.58	0.00	0.00	11.64	0.00	0.03	17.11	0.38	8.91	95.77
	36.27	1.91	19.13	0.00	0.00	11.89	0.00	0.03	17.30	0.26	8.76	95.55
	36.18	2.05	19.11	0.00	0.00	11.72	0.01	0.03	17.21	0.27	8.90	95.49

Si	Ti	Al	Cr	Fe^{+3}	Mg	Ca	Mn	Fe^{+2}	Na	K	Total
5.43	0.15	3.42	0.00	0.00	2.76	0.00	0.01	2.08	0.07	1.67	19.58
5.45	0.15	3.36	0.00	0.00	2.78	0.00	0.00	2.11	0.08	1.69	19.61
5.45	0.16	3.33	0.00	0.00	2.77	0.00	0.01	2.11	0.09	1.70	19.62
5.46	0.17	3.36	0.00	0.00	2.74	0.01	0.00	2.07	0.09	1.68	19.57
5.42	0.17	3.47	0.00	0.00	2.68	0.00	0.00	2.02	0.10	1.73	19.59
5.40	0.19	3.46	0.00	0.00	2.69	0.00	0.00	2.01	0.09	1.73	19.59
5.43	0.18	3.44	0.00	0.00	2.70	0.02	0.00	2.02	0.09	1.68	19.56
5.43	0.19	3.38	0.00	0.00	2.77	0.01	0.01	2.02	0.09	1.66	19.56
5.45	0.15	3.41	0.00	0.00	2.76	0.00	0.00	2.08	0.08	1.63	19.56
5.42	0.19	3.50	0.00	0.00	2.65	0.00	0.00	2.02	0.09	1.65	19.52
5.39	0.20	3.44	0.00	0.00	2.66	0.02	0.01	2.08	0.09	1.67	19.56
5.43	0.18	3.40	0.00	0.00	2.64	0.00	0.01	2.16	0.09	1.65	19.56
5.41	0.19	3.44	0.00	0.00	2.63	0.01	0.01	2.10	0.08	1.75	19.60
5.43	0.17	3.43	0.00	0.00	2.68	0.00	0.00	2.08	0.10	1.66	19.56
5.44	0.18	3.42	0.00	0.00	2.70	0.00	0.01	2.07	0.09	1.64	19.54
5.44	0.18	3.36	0.00	0.00	2.68	0.02	0.00	2.14	0.09	1.67	19.58
5.45	0.17	3.38	0.00	0.00	2.70	0.00	0.01	2.12	0.08	1.67	19.57
5.46	0.23	3.40	0.00	0.00	2.62	0.01	0.01	2.04	0.11	1.60	19.47
5.42	0.19	3.41	0.00	0.00	2.65	0.02	0.01	2.12	0.09	1.67	19.56
5.42	0.20	3.41	0.00	0.00	2.61	0.01	0.00	2.13	0.09	1.70	19.57
5.41	0.21	3.40	0.00	0.00	2.64	0.00	0.01	2.14	0.09	1.67	19.57
5.40	0.21	3.44	0.00	0.00	2.59	0.00	0.00	2.13	0.11	1.69	19.57
5.42	0.21	3.37	0.00	0.00	2.65	0.00	0.00	2.16	0.08	1.67	19.56
5.41	0.23	3.37	0.00	0.00	2.61	0.00	0.00	2.15	0.08	1.70	19.56

	36.06	1.62	19.29	0.00	0.00	11.74	0.05	0.05	17.32	0.24	8.62	94.99
Average	36.25	1.65	19.32	0.00	0.00	12.01	0.03	0.04	16.72	0.30	8.77	95.08

	5.42	0.18	3.42	0.00	0.00	2.63	0.01	0.01	2.18	0.07	1.65	19.56
Average	5.43	0.19	3.41	0.00	0.00	2.68	0.01	0.00	2.09	0.09	1.67	19.56

Muscovite	SiO2	TiO2	Al2O3	Cr2O3	Fe203	MgO	CaO	MnO	FeO	Na2O	K2O	Total
	45.96	0.48	36.29	0.00	0.00	0.70	0.06	0.00	1.04	1.94	8.63	95.11
	46.19	0.51	36.45	0.00	0.00	0.62	0.00	0.01	0.80	1.96	8.52	95.07
	46.10	0.64	36.60	0.00	0.00	0.68	0.00	0.00	0.96	1.81	8.75	95.54
	46.22	0.45	36.73	0.00	0.00	0.77	0.08	0.00	0.93	1.65	9.12	95.95
	46.21	0.62	36.54	0.00	0.00	0.74	0.02	0.01	1.01	1.52	9.01	95.68
	45.87	0.34	37.16	0.00	0.00	0.52	0.00	0.00	0.88	1.77	8.79	95.32
	46.26	1.27	36.00	0.00	0.00	0.87	0.00	0.01	0.93	1.37	9.13	95.83
	46.52	0.78	35.24	0.00	0.00	0.97	0.00	0.00	1.00	1.41	9.12	95.05
Average	46.17	0.64	36.38	0.00	0.00	0.73	0.02	0.00	0.94	1.68	8.88	95.45

Muscovite	Si	Ti	Al	Cr	Fe^{+3}	Mg	Ca	Mn	Fe^{+2}	Na	K	Total
	6.09	0.05	5.66	0.00	0.00	0.14	0.01	0.00	0.12	0.50	1.46	18.01
	6.10	0.05	5.68	0.00	0.00	0.12	0.00	0.00	0.09	0.50	1.44	17.98
	6.07	0.06	5.68	0.00	0.00	0.13	0.00	0.00	0.11	0.46	1.47	17.99
	6.07	0.05	5.69	0.00	0.00	0.15	0.01	0.00	0.10	0.42	1.53	18.02
	6.08	0.06	5.67	0.00	0.00	0.15	0.00	0.00	0.11	0.39	1.51	17.97
	6.05	0.03	5.78	0.00	0.00	0.10	0.00	0.00	0.10	0.45	1.48	17.99
	6.08	0.13	5.58	0.00	0.00	0.17	0.00	0.00	0.10	0.35	1.53	17.94
	6.17	0.08	5.50	0.00	0.00	0.19	0.00	0.00	0.11	0.36	1.54	17.96
Average	6.09	0.06	5.65	0.00	0.00	0.14	0.00	0.00	0.10	0.43	1.49	17.98

Plagioclase	SiO2	TiO2	Al2O3	Cr2O3	Fe203	MgO	CaO	MnO	FeO	Na2O	K2O	Total
	66.92		20.86	0.09	0.00	0.00	1.56	0.00	0.25	10.64	0.00	100.32

Plagioclase	Si	Ti	Al	Cr	Fe^{+3}	Mg	Ca	Mn	Fe^{+2}	Na	K	Total
	2.93	0.00	1.08	0.00	0.00	0.00	0.07	0.00	0.01	0.90	0.00	4.99

Garnet	SiO2	TiO2	Al2O3	Cr2O3	Fe203	MgO	CaO	MnO	FeO	Na2O	K20	Total
	37.35	0.01	21.13	0.00	0.00	3.47	2.19	1.51	35.27	0.01	0.00	100.95

Garnet	Si	Ti	Al	Cr	Fe^{+3}	Mg	Ca	Mn	Fe^{+2}	Na	K	Total
	2.98	0.00	1.99	0.00	0.00	0.41	0.19	0.10	2.35	0.00	0.00	8.03

Staurolite	SiO2	TiO2	Al2O3	Cr2O3	Fe203	MgO	CaO	MnO	FeO	Na2O	K2O	Total
	27.98	0.75	53.58	0.00	0.00	1.87	0.00	0.13	13.47	0.01	0.04	97.81
	27.83	0.74	53.45	0.00	0.00	1.80	0.00	0.15	13.81	0.01	0.18	97.96
	27.81	0.69	53.98	0.00	0.00	1.94	0.01	0.13	13.04	0.02	0.03	97.64
Average	27.87	0.72	53.67	0.00	0.00	1.87	0.00	0.14	13.44	0.01	0.08	97.80

Staurolite	Si	Ti	Al	Cr	Fe^{+3}	Mg	Ca	Mn	Fe^{+2}	Na	K	Total
	3.71	0.07	8.37	0.00	0.00	0.37	0.00	0.01	1.49	0.00	0.01	18.04
	3.69	0.07	8.36	0.00	0.00	0.36	0.00	0.02	1.53	0.00	0.03	18.07
	3.69	0.07	8.43	0.00	0.00	0.38	0.00	0.02	1.45	0.00	0.01	18.04
Average	3.70	0.07	8.39	0.00	0.00	0.37	0.00	0.02	1.49	0.00	0.01	18.05

11BC-38i Data used included garnet P-T calculation

Biotite	SiO2	TiO2	Al2O3	Cr2O3	Fe203	MgO	CaO	MnO	FeO	Na2O	K2O	Total
	36.01	1.35	19.24	0.00	0.00	12.26	0.00	0.08	16.51	0.24	8.66	94.36
	36.41	1.32	19.04	0.00	0.00	12.47	0.00	0.03	16.89	0.27	8.85	95.29
	36.38	1.44	18.88	0.00	0.00	12.42	0.00	0.04	16.86	0.30	8.89	95.21
	36.58	1.53	19.09	0.00	0.00	12.29	0.05	0.03	16.57	0.30	8.82	95.27
	36.10	1.53	19.60	0.00	0.00	11.97	0.01	0.03	16.08	0.36	9.03	94.71
	36.15	1.69	19.65	0.00	0.00	12.07	0.02	0.03	16.11	0.32	9.05	95.10
	36.39	1.63	19.56	0.00	0.00	12.16	0.11	0.01	16.18	0.32	8.83	95.18
	36.19	1.68	19.12	0.00	0.00	12.36	0.04	0.04	16.09	0.30	8.69	94.53
Average	36.28	1.52	19.27	0.00	0.00	12.25	0.03	0.04	16.41	0.30	8.85	94.96

Biotite	Si	Ti	Al	Cr	Fe^{+3}	Mg	Ca	Mn	Fe^{+2}	Na	K	Total
	5.43	0.15	3.42	0.00	0.00	2.76	0.00	0.01	2.08	0.07	1.67	19.58
	5.45	0.15	3.36	0.00	0.00	2.78	0.00	0.00	2.11	0.08	1.69	19.61
	5.45	0.16	3.33	0.00	0.00	2.77	0.00	0.01	2.11	0.09	1.70	19.62
	5.46	0.17	3.36	0.00	0.00	2.74	0.01	0.00	2.07	0.09	1.68	19.57
	5.42	0.17	3.47	0.00	0.00	2.68	0.00	0.00	2.02	0.10	1.73	19.59
	5.40	0.19	3.46	0.00	0.00	2.69	0.00	0.00	2.01	0.09	1.73	19.59
	5.43	0.18	3.44	0.00	0.00	2.70	0.02	0.00	2.02	0.09	1.68	19.56
	5.43	0.19	3.38	0.00	0.00	2.77	0.01	0.01	2.02	0.09	1.66	19.56
Average	5.43	0.17	3.40	0.00	0.00	2.74	0.00	0.00	2.06	0.09	1.69	19.58

Muscovite	SiO2	TiO2	Al2O3	Cr2O3	Fe203	MgO	CaO	MnO	FeO	Na2O	K2O	Total
	45.96	0.48	36.29	0.00	0.00	0.70	0.06	0.00	1.04	1.94	8.63	95.11
	46.19	0.51	36.45	0.00	0.00	0.62	0.00	0.01	0.80	1.96	8.52	95.07
Average	46.08	0.50	36.37	0.00	0.00	0.66	0.03	0.01	0.92	1.95	8.58	95.09

Si	Ti	Al	Cr	Fe^{+3}	Mg	Ca	Mn	Fe^{+2}	Na	K	Total
6.09	0.05	5.66	0.00	0.00	0.14	0.01	0.00	0.12	0.50	1.46	18.01
6.10	0.05	5.68	0.00	0.00	0.12	0.00	0.00	0.09	0.50	1.44	17.98
6.09	0.05	5.67	0.00	0.00	0.13	0.00	0.00	0.10	0.50	1.45	18.00

Plagioclase	SiO2	TiO2	Al2O3	Cr2O3	Fe203	MgO	CaO	MnO	FeO	Na2O	K2O	Total
	66.79	0.00	20.62	0.00	0.00	0.00	1.21	0.00	0.14	10.95	0.01	99.72

Si	Ti	Al	Cr	Fe^{+3}	Mg	Ca	Mn	Fe^{+2}	Na	K	Total
2.94	0.00	1.07	0.00	0.00	0.00	0.06	0.00	0.01	0.93	0.00	5.00

Garnet	SiO2	TiO2	Al2O3	Cr2O3	Fe203	MgO	CaO	MnO	FeO	Na2O	K20	Total
	37.35	0.01	21.13	0.00	0.00	3.47	2.19	1.51	35.27	0.01	0.00	100.95

Si	Ti	Al	Cr	Fe^{+3}	Mg	Ca	Mn	Fe^{+2}	Na	K	Total
2.98	0.00	1.99	0.00	0.00	0.41	0.19	0.10	2.35	0.00	0.00	8.03

Staurolite	SiO2	TiO2	Al2O3	Cr2O3	Fe203	MgO	CaO	MnO	FeO	Na2O	K2O	Total
	27.98	0.75	53.58	0.00	0.00	1.87	0.00	0.13	13.47	0.01	0.04	97.81
	27.83	0.74	53.45	0.00	0.00	1.80	0.00	0.15	13.81	0.01	0.18	97.96
	27.81	0.69	53.98	0.00	0.00	1.94	0.01	0.13	13.04	0.02	0.03	97.64
Average	27.87	0.72	53.67	0.00	0.00	1.87	0.00	0.14	13.44	0.01	0.08	97.80

Si	Ti	Al	Cr	Fe^{+3}	Mg	Ca	Mn	Fe^{+2}	Na	K	Total
3.71	0.07	8.37	0.00	0.00	0.37	0.00	0.01	1.49	0.00	0.01	18.04
3.69	0.07	8.36	0.00	0.00	0.36	0.00	0.02	1.53	0.00	0.03	18.07
3.69	0.07	8.43	0.00	0.00	0.38	0.00	0.02	1.45	0.00	0.01	18.04
3.70	0.07	8.39	0.00	0.00	0.37	0.00	0.02	1.49	0.00	0.01	18.05

APPENDIX II

FIELD DATA (2011 and 2012)

Appendix II

Collected during the 2011 and 2012 field seasons

Sample	Location	Latitude	Longitude	Strike	Dip (S_3)	Plunge	Trend	Strike	Dip (S_3)	Rock type	Axial Surface
11BC-A	Bryson City dome	35.4692	-83.4296	265	23		045			grt schist	
11BC-B	Bryson City dome	35.4465	-83.4641	215	14	30	020			augen orthogneiss	
11RML-1	Bryson City dome	35.4412	-83.4307	005	83		115			augen orthogneiss	
11RML-2	Bryson City dome	35.4412	-83.4307	005	83	N/A				qtz-feld orthogneiss	
11BC-1	Bryson City dome	35.4477	-83.4692	220	70	5	226	020	65	schist	
11BC-2	Bryson City dome	35.4473	-83.4661	225	85	5	235			metagraywacke	
11BC-3A	Bryson City dome	35.4468	-83.4656	212	81	11	242			schist	
11BC-3B	Bryson City dome	35.4468	-83.4656	220	85	N/A				metagraywacke	
11BC-4A	Bryson City dome	35.4465	-83.4654	217	85	17	210	035	72	schist	
11BC-4B	Bryson City dome	35.4465	-83.4654	217	85	17	237			metagraywacke	
11BC-5	Bryson City dome	35.4465	-83.4648	210	76	21	225			augen orthogneiss	
11BC-6	Bryson City dome	35.4464	-83.4645	200	47	N/A				augen orthogneiss	
11BC-7	Bryson City dome	35.4464	-83.4645	190	61	N/A				augen orthogneiss	
11BC-8	Bryson City dome	35.4465	-83.4641	220	79	20	230			augen orthogneiss	
11BC-9	Bryson City dome	35.4466	-83.4638	230	73	30	250			augen orthogneiss	
11BC-10	Bryson City dome	35.4466	-83.4638	055	90	15	230			augen orthogneiss	
11BC-11	Bryson City dome	25 ft east of 11BC-12		070	35	25	215			augen orthogneiss	
11BC-12	Bryson City dome	35.3884	-83.4927	054	18	N/A				augen orthogneiss	
11BC-13	Bryson City dome	35.3881	-83.4958	005	35	25	030			metagraywacke	
11BC-14	Bryson City dome	35.3880	-83.4959	020	46	N/A				metagraywacke	
11BC-15	Bryson City dome	35.3880	-83.4974	019	73	16	023			metagraywacke	
11BC-16	Bryson City dome			024	80	15	025			metagraywacke	
11BC-17	Bryson City dome	35.4303	-83.4797	082	43	23	115			grt schist	
11BC-18	Bryson City dome			008	45	23	165			schist	
11BC-19	Bryson City dome			010	56	N/A				metagraywacke	
11BC-20	Bryson City dome			001	62	N/A				metagraywacke	
11BC-21	Bryson City dome			015	40	N/A				metagraywacke	
11BC-22	Bryson City dome	35.3919	-83.4869	003	76	46	165			schist	
11BC-23	Bryson City dome			001	76	N/A				augen orthogneiss	
11BC-24	Bryson City dome	35.3879	-83.4755	070	60	N/A				metagraywacke	
11BC-25	Bryson City dome	35.3844	-83.4753	080	50	50	110			grt schist	(F_2) 095/20SE
11BC-26	Bryson City dome	35.4642	-83.4332	285	32	27	010			bt orthogneiss	
11BC-27	Bryson City dome	35.4644	-83.4327	285	26	N/A				bt orthogneiss	
11BC-28a	Bryson City dome	35.4645	-83.4328	305	27	10	092			schist	
11BC-28b	Bryson City dome	35.4645	-83.4328	290	20	8	090			schist	
11BC-29	Bryson City dome	35.4656	-83.4304	292	31	23	062			schist	
11BC-30	Bryson City dome	35.4652	-83.4332	310	19	15	030			schist	
11BC-31	Bryson City dome	35.4655	-83.4345	330	14	N/A				schist	
11BC-32	Bryson City dome	35.4281	-83.4525	054	76	33	060			bt orthogneiss	
11BC-33	Bryson City dome	35.4251	-83.4535	240	75	N/A				bt orthogneiss	

11BC-34	Bryson City dome	35.4262	-83.4675	013	9	N/A				bt orthogneiss
11BC-35	Bryson City dome	35.4271	-83.4689	215	74	N/A	095			bt orthogneiss
11BC-36	Bryson City dome	35.4278	-83.4704	025	68	36	185			bt orthogneiss
11BC-37	Bryson City dome	35.4292	-83.4735	050	80	28	215			bt orthogneiss
11BC-38	Bryson City dome	35.4405	-83.4805	035	80	N/A				st ky schist
11BC-39	Bryson City dome	35.4405	-83.4805	040	65	N/A				st ky schist
11BC-40	Bryson City dome	35.4648	-83.4333	002	16	10	034			augen orthogneiss
11BC-41	Bryson City dome	35.4648	-83.4333	350	11	11	080			augen orthogneiss
11BC-42	Bryson City dome	35.4648	-83.4333	315	16	11	009			metagraywacke
11BC-43	Bryson City dome	35.4648	-83.4333	357	31	31	087			metagraywacke
11BC-44	Bryson City dome	35.4648	-83.4333	300	22	22	017			augen orthogneiss
11BC-45	Bryson City dome	35.4431	-83.4731	043	71	9	030	210	31	st ky schist
11BC-46	Bryson City dome	35.4300	-83.4776	209	72	N/A				ky schist
11BC-47	Bryson City dome	35.4135	-83.4477	045	54	N/A				ky schist
11ED-1	Ela dome	35.4307	-83.3983	011	37	19	059			grt schist
11ED-2	Ela dome	35.4307	-83.3989	039	50	35	184			mylonite paragneiss
11ED-3	Ela dome	35.4307	-83.3984	039	35	19	060			grt schist
11ED-4A	Ela dome	35.4306	-83.3989	055	23	5	054			schist
11ED-4B	Ela dome	35.4306	-83.3989	055	23	5	054			metagraywacke
11ED-5	Ela dome	35.4308	-83.3984	055	34	N/A		090	19	bt gneiss
11ED-6	Ela dome	35.4285	-83.4006	032	30	20	070			grt schist
11ED-7	Ela dome	35.4289	-83.4006	020	43	7	055			schist
11ED-8	Ela dome	35.4292	-83.4002	041	54	40	120	010	45	grt schist
11ED-9	Ela dome	35.4295	-83.4000	020	55	32	053			grt schist
11ED-10	Ela dome	35.4709	-83.3873	227	65	3	219			metagraywacke
11ED-11	Ela dome	35.4715	-83.3877	230	85	29	053			grt schist
11Ed-12	Ela dome	35.4459	-83.3766	065	56	8	230			schist
11Ed-15	Ela dome	35.4458	-83.3763	055	32	15	210			schist
11Ed-16	Ela dome	35.4458	-83.3761	035	53	23	195			schist
11Ed-17	Ela dome	35.4455	-83.3758	050	49	24	213			schist
11Ed-18	Ela dome	35.4422	-83.3826	020	24	11	065			grt schist
11Ed-19	Ela dome	35.4430	-83.3827	110	45	32	270			bt paragneiss
11ED-20	Ela dome	35.4435	-83.3899	100	32	N/A				bt paragneiss
Stop #										
RML-1	Bryson City dome	35.4440	-83.4353	265	50	N/A				bt orthogneiss
RML-2	Bryson City dome	35.4412	-83.4475	020	90	35	200			bt orthogneiss
RML-3	Bryson City dome	35.4419	-83.4280	005	60	N/A				metagraywacke
RML-4	Bryson City dome	35.4465	-83.4654	N/A		N/A				cover-core contact
RML-5	Bryson City dome	35.3883	-83.4928	090	15	N/A				bt orthogneiss
RML-6	Bryson City dome	35.3878	-83.4954	float		N/A				metagraywacke
RML-7	Bryson City dome			020	40	N/A				metagraywacke
RML-8	Bryson City dome			045	84	N/A		039	56	metagraywacke
RML-9	Bryson City dome			069	29	N/A				bt orthogneiss

RML-10	Bryson City dome					N/A				bt orthogneiss	(F_2) 004/51E
RML-11	Bryson City dome			055	58	N/A				bt orthogneiss	
RML-12	Bryson City dome	35.4594	-83.4321	170	38	25	290			augen orthogneiss	
RML-13	Bryson City dome	35.4651	-83.4292	035	19	N/A				metagraywacke	
RML-14	Bryson City dome	35.4648	-83.4318	315	9	N/A				metagraywacke	
RML-15	Bryson City dome			295	15	N/A				metagraywacke	
RML-16	Bryson City dome	35.4639	-83.4337	317	32	N/A				augen orthogneiss	
RML-17	Bryson City dome			320	19	N/A				augen orthogneiss	
RML-18	Bryson City dome	35.4300	-83.4001	045	50	N/A				augen orthogneiss	
RML-19	Ela dome	35.4291	-83.4007			N/A				metagraywacke	(F_2) 028/33SE
RML-21	Bryson City dome	35.4338	-83.4396	200	51	N/A				bt paragneiss	
RML-22	Bryson City dome	35.4339	-83.4312	320	85	N/A				metagraywacke	(F_2) 320/85NE
RML-23	Ela dome	35.4706	-83.3870	225	85	N/A				schist	
RML-24	Ela dome	35.4713	-83.3875	210	83	N/A				grt schist	
RML-25	Ela dome	35.4348	-83.3949	005	52	N/A				cover-core contact	
RML-26	Ela dome	35.4348	-83.3946	017	60	N/A				metagraywacke	(F_3) 190/40W
RML-28	Ela dome	35.4458	-83.3763			N/A				metagraywacke	(F_3) 200/55W
RML-29	Ela dome	35.4457	-83.3760			N/A				metagraywacke	
RML-30	Ela dome	35.4434	-83.3830	310	75	N/A				bt paragneiss	
RML-31	Ela dome	35.4412	-83.4308	064	31	27	183			bt paragneiss	
RML-32	Ela dome			071	34	N/A				cover-core contact	
RML-33	Ela dome	35.4486	-83.4377	061	34	32	185			augen orthogneiss	
RML-34	Ela dome	35.4642	-83.4332	038	75	12	042	335	21	bt orthogneiss	
RML-35	Bryson City dome	35.4471	-83.4731	035	20	35	020			augen orthogneiss	
RML-36	Bryson City dome	35.4478	-83.4692	030	80	21	040	245	41	metagraywacke	
RML-37	Bryson City dome	35.3878	-83.4756	050	57	4	225			schist	
RML-38	Bryson City dome			025	74	14	050	035	30	schist	
RML-39	Bryson City dome	35.4311	-83.4142	040	47	40	047	040	47	schist	(F_3) 030/50SE
RML-40	Bryson City dome	35.4306	-83.4137	012	43	10	000	012	43	schist	(F_3) 012/43SE
RML-41	Bryson City dome	35.4348	-83.3948	350	50	10	350	350	50	grt schist	
RML-42	Bryson City dome	35.4457	-83.3763	053	35	53	035	205	47	metagraywacke	(F_3) 205/47NW
RML-43	Bryson City dome	35.4632	-83.3515	021	44	9	193			bt orthogneiss	
RML-44	Bryson City dome	35.4724	-83.3893	215	75	10	039			schist	

Abbreviations: bt, biotite; ms, muscovite; grt, garnet; ky, kyanite; st, staurolite

APPENDIX III

THIN SECTIONS

Appendix III

Ela and Bryson City domes petrographic and microstructural analysis

Collected during the 2011 and 2012 field seasons

Sample	Lat.	Long.	Strik	(S_2) I	Plu	Cut d	trike	(S_3)	Rock type	Major Mineral	Assc mineral	SS	SS indicator	Def. T °C[b]
Bryson City dome														
11BC-A	35.4692	-83.4296	265	23		45			grt schist	qtz, bt, ms, plag, grt, ky	sta grh, tour, ap, monz, zr, op	t-NE	sig/C'/	500-600
11BC-B	35.4465	-83.4641	215	14	30	20			augen ortho	qtz, bt, ms, plag, ksp	ep, chl, cal, sph, myr	t-NE	meso sig/sig/	500-600
11BC-1	35.4477	-83.4692	220	70	5	226	20	65	schist	qtz, bt, ms, plag	tour, ap, zr, opaque	t-NE	fold/sig/S-C/C'/fish	500-600
11BC-2	35.4473	-83.4661	225	85	5	235			metagraywache	qtz, bt, ms, plag, ksp	tour, ap, sph, zr, op, myr	t-NE	feld sigma	500-600
11BC-3A	35.4468	-83.4656	212	81	11	242			shist	qtz, bt, ms, plag, grt	grh, tour, ap, monz, zr, op	t-NE	fish/sigma/C'	500-600
11BC-3B	35.4468	-83.4656	220	85		240			metagraywache	qtz, bt, ms, plag, grt	silla, ap, monz, zr, opaque	t-NE	sigma/	500-600
11BC-4A	35.4465	-83.4654	217	85	17	210	35	72	schist	qtz, bt, ms, plag	grh, ap, monz, zr, opaque		fold	500-600
11BC-4B	35.4465	-83.4654	217	85	17	237			metagraywache	qzt, bt, ms, plag, grt	ap, monz, zr, opaque			500-600
11BC-5	35.4465	-83.4648	210	76	21	225			augen ortho	qtz, bt, ms, plag, ksp	ep, myr			500-600
11BC-6	35.4464	-83.4645	200	47		220			augen ortho	qtz, bt, ms, plag, ksp	ep, myr, perth	t-NE		500-600
11BC-7	35.4464	-83.4645	190	61		220			augen ortho	qtz, bt, ms, plag, ksp	ep, myr	t-NE		500-600
11BC-8	35.4465	-83.4641	220	79	20	230			augen ortho	qtz, bt, ms, plag, ksp	ep, myr	t-NE		500-600
11BC-9	35.4466	-83.4638	230	73	30	250			augen ortho	qtz, bt, ms, plag, ksp	ep, myr, sph	t-NE	C'	500-600
11BC-10	35.4466	-83.4638	55	90	15	230			augen ortho	qtz, bt, ms, plag, ksp	ep, myr, sph, perth	t-NE	S-C, sigma	500-600
11BC-17	35.4303	-83.4797	82	43	23	115			grt schist	qtz, bt, ms, plag, grt, st	ap, monz, zr, op			500-600
11BC-32	35.4281	-83.4525	54	76	33	60			bt ortho	qtz, bt, ms, plag, ksp	ep, myr, sph			500-600
11BC-33	35.4251	-83.4535	240			300			bt ortho	qtz, bt, ms, plag, ksp	ep, myr, sph			500-600
11BC-34	35.4262	-83.4675	13	9		163			bt ortho	qtz, bt, ms, plag, ksp	ep, myr, sph			500-600
11BC-35	35.4271	-83.4689	215	74		95			bt ortho	qtz, bt, ms, plag, ksp	ep, myr, sph			500-600
11BC-36	35.4278	-83.4704	25	68	36	185			bt ortho	qtz, bt, ms, plag, ksp	ep, myr, sph			500-600
11BC-37	35.4292	-83.4735	50	80	28	215			bt ortho	qtz, bt, ms, plag, ksp	ep, myr, sph			500-600
11BC-38	35.4405	-83.4805	35	80		125			st ky schist	qtz, bt, ms, plag, grt, ky, st	grh, silla, ap, monz, zr, op			500-600
11BC-45	35.4431	-83.4731	43	71	9	30	210	31	st ky schist	qtz, bt, ms, plag, grt, ky, st	grh, silla, ap, monz, zr, op			500-600
11BC-46	35.4300	-83.4776	209	72					ky schist	qtz, bt, ms, plag, grt, ky	tour, ap, zr, rutile, op			500-600
11BC-47	35.4135	-83.4477	45	54					ky schist	qtz, bt, ms, plag, grt, ky	ap, zr, rutile, op			500-600
Ela dome														
11ED-1	35.4307	-83.3983	11	37	19	59			grt schist	qtz, bt, ms, plag, grt	ap, silla, monz, zr, op			500-600
11ED-2	35.4307	-83.3989	39	50	35	184			myl. paragneiss	qtz, bt, ms, plag, grt, ksp	ap, ep, myr, sph	t-S	S-C	500-600
11ED-3	35.4307	-83.3984	39	35	19	60			grt schist	qtz, bt, ms, plag, grt	ap, silla, monz, zr, op		sigma	500-600
11ED-4A	35.4306	-83.3989	55	23	5	54			schist	qtz, bt, ms, plag	ap, monz, op	t-NE		500-600
11ED-4B	35.4306	-83.3989	55	23	5	54			metagraywache	qtz, bt, ms, plag	ap, monz, op	t-NE	S-C, C', mica fish	500-600
11ED-5	35.4308	-83.3984	55	34		115	90	19	bt gneiss	qtz, bt, ms, plag, grt, ksp	ap, ep, myr, sph, hrn			500-600
11ED-6	35.4285	-83.4006	32	30	20	70			grt schist	qtz, bt, ms, plag, grt	ap, monz, zr, op			500-600
11ED-7	35.4289	-83.4006	20	43	7	55			schist	qtz, bt, ms, plag	ap, monz, op	t-NE	plag sigma	500-600
11ED-8	35.4292	-83.4002	41	54	40	60	10	45	grt schist	qtz, bt, ms, plag, grt	ap, monz, zr, op			500-600
11ED-9	35.4295	-83.4000	20	55	32	53			grt schist	qtz, bt, ms, plag, grt	ap, monz, op	t-NE		500-600
11Ed-18	35.4422	-83.3826	20	24	11	65			grt schist	qtz, bt, ms, plag, grt	ap, monz, op			500-600
11Ed-19	35.4430	-83.3827	110	45	32	270			bt paragneiss	qtz, bt, ms, plag, ksp	ap, ep, myr, sph			500-600

11ED-20	35.4435	-83.3899	100	32	bt paragneiss	qtz, bt, ms, plag, ksp	ap, ep, myr, sph	500-600

Abbreviations: qtz, quartz; bt, biotite; ms, mucsovite; plag, plagioclase; grt, garnet; ky, kyanite; st, staurolite; grh, graphite; tour, tourmaline; ap, apatite; monz, monzazite; zr, zircon; ep, epidote; chl, chlorite; myr, myremkite;

[a] occurs at the grain boundary of plagioclase

[b] all samples display GBM as the dominant quartz deformation mechanism

Vita

Remington Matthew Leger was born December 9th, 1985, in Metairie, Louisiana to Eldridge Joseph Leger and Eliza Mineo Leger. He graduated from Fontainebleau High School in the spring of 2005 and was accepted to Louisiana State University the following fall. During the Spring 2008 semester he was a member of a 6-week NSF Antarctica Research Expedition to the Ross Sea, focused on determining when the last glacial maximum occurred. During Remy's last two semesters at LSU he conducted an undergraduate research project under Dr. Alexander Webb entitled "Metamorphic Field Gradients across the Himachal Himalaya, Northwest India: Implications for the Emplacement of the Himalayan Crystalline Core." After graduation, he spent a semester as a research assistant under Dr. Webb while completing and publishing his undergraduate research. He began his Masters of Science at the University of Tennessee, Knoxville, in August 2010. After graduation he began his career as a geologist with Schlumberger in Houston, Texas.